VISCOUS HYDRODYNAMIC INSTABILITY THEORY OF THE PEAK AND MINIMUM POOL BOILING HEAT FLUXES

BY

VIJAY K. DHIR

DEPARTMENT OF
MECHANICAL ENGINEERING

UKY BU100

NOVEMBER 1972

GRAVITY BOILING PROJECT
NASA GRANT NGR 18-001-035

COLLEGE OF ENGINEERING
UNIVERSITY OF KENTUCKY

UKY BU100

NOVEMBER 1972

VISCOUS HYDRODYNAMIC INSTABILITY THEORY OF THE PEAK AND MINIMUM POOL BOILING HEAT FLUXES

BY

VIJAY K. DHIR, RESEARCH ASSOCIATE

BOILING AND PHASE-CHANGE LABORATORY

DEPARTMENT OF MECHANICAL ENGINEERING
UNIVERSITY OF KENTUCKY
LEXINGTON, KENTUCKY

GRAVITY BOILING PROJECT, NASA GRANT NGR/18-001-035

PRINCIPAL INVESTIGATOR, JOHN H. LIENHARD

ABSTRACT

Liquid viscosity has been included in the Bellman-Pennington theory of the Taylor wave in a liquid vapor interface. Predictions of the "most susceptible" wavelength, and of the wave frequency, are made as a function of a liquid viscosity parameter and the Bond number.

The stability of a gas jet in a viscous liquid has been studied and the ensuing result is used to predict the peak heat flux on large horizontal heaters.

Experimental measurements of the dominant Taylor wave and its growth rate are made during the film boiling of cyclohexanol on cylindrical heaters. The results bear out the predictions quite well. The thickness of the vapor blanket surrounding a cylindrical heater has been measured and a correlation suggested. The effect of large fluxes of vapor volume on the dominant wavelength has also been noted.

The peak heat flux is observed on relatively large flat plate heaters both at earth normal gravity and at higher gravities for boiled liquids that are nearly inviscid (e.g. acetone, benzene, methanol isopropanol and water) and for boiled liquids that are significantly viscous (e.g. cyclohexanol). The peak heat flux is also measured when cyclohexanol is boiling on cylindrical heaters. Theoretical

results of the peak heat flux are compared with the experimental data.

The effect of finite geometry of flat plate heaters on the peak heat flux is also discussed.

PREFACE

The present study is the last in-house report of a long range program aimed at learning how gravity and geometry interact to influence the hydrodynamic mechanisms that dictate the peak and minimum boiling heat fluxes. This general program has been supported since 1967 by NASA grant NGR/18-001-035, under the direction of Professor John H. Lienhard, Mechanical Engineering Department at the University of Kentucky. Mr. Thomas H. Cochran of the NASA Lewis Research Center has served as Project Manager. The text of this report is the text of Vijay K. Dhir's dissertation for the Ph.D. degree in Mechanical Engineering, with J.H. Lienhard as dissertation director.

We wish to thank several people for their help with this work. Messrs. E.B. Yates, E.R. Hoover, and W. Reed were immensely helpful with the apparatus described here. In addition to Mr. D.M. Riherd and Mr. D.E. Davis, whose significant contributions to the experimental program we mention in the report, we also are grateful to Mr. W.G. Dogget and Mr. K.S. Thind for their help with experiments. We also wish to thank Mrs. Bonnie Turner and Mrs. Pauline Chappell for typing the final manuscript with unusual care and skill.

V. K. Dhir and J.H. Lienhard
Lexington, Kentucky 1972

TABLE OF CONTENTS

PRECEDING PAGE BLANK NOT FILMED

APPENDIX

LIST OF ILLUSTRATIONS

I. INTRODUCTION

Brief History of Previous Studies.

Nukiyama [1][1], in 1934, observed the stable regions of the now well-known heat flux versus temperature difference curve for pool boiling. He identified these regions as nucleate boiling and film boiling respectively. Nukiyama was also able to locate the two extremes of this curve, i.e. the peak and minimum boiling heat fluxes. Drew and Muller [2] subsequently observed the intermediate region which is now called the region of transitional boiling.

Since then, extensive studies have been made of the various regimes of Nukiyama's boiling curve. These studies have been mainly motivated by the association of the boiling process with much larger heat transfer coefficients than those occurring in other processes. In this chapter we will briefly review the evolution of the hydrodynamic theory as applied to the peak and minimum heat flux on flat plates and cylindrical heaters.

In the late forties, Kutateladze [3] suggested that the transition from nucleate to film boiling was purely a hydrodynamic

[1]Numbers in square brackets represent entries in Reference section.

phenomenon. Based on similarity considerations related to the equations of motion and energy, he identified two dimensionless groups[2]:

$$\frac{q_{max}}{\rho_g h_{fg} U_g} \quad \text{and} \quad \frac{\sigma(\rho_f - \rho_g)g}{U_g^4 \rho_g^2} \tag{1}$$

where q_{max} is the peak heat flux and U_g is the velocity of the gas in vapor jets. Combining these two groups he gave a very successful correlation for the peak heat flux:

$$\left(q_{max}\right)_{inviscid} = 0.16\sqrt{\rho_g}\, h_{fg}\left[\sigma g(\rho_f - \rho_g)\right]^{1/4} \tag{2}$$

Kutateladze did not suggest any restrictions as to the heater geometries that equation (2) should describe.

Borishanski [4] correlated peak heat flux data obtained by various authors for circular heaters and horizontal strips. In a personal communication[3], Borishanski recalled that the data he used in forming the correlation were generally free from induced convection effects. His modified equation, similar to equation (2), with the effect of liquid viscosity included, was:

$$q_{max_F} = (0.13 + 4.0N^{-0.4})\left\{\sqrt{\rho_g}\, h_{fg}\left[\sigma g(\rho_f - \rho_g)\right]^{1/4}\right\} \tag{3}$$

---

[2]Symbols commonly used are explained in the section on nomenclature.

[3]Conversation with J.H. Lienhard in Minsk, U.S.S.R, May 17, 1972.

where

$$N \equiv \frac{\rho_f \sigma}{\mu_f^2}\left[\frac{\sigma}{g(\rho_f - \rho_g)}\right]^{1/2} \tag{4}$$

Costello et al. [5] showed that the peak heat flux could be strongly affected by induced convection. Subsequently, Lienhard and Keeling [6] correlated their peak heat flux data for ribbons subjected to induced flow from the sides on a $\sqrt{NL'}$ axis. In their case, L' was the characteristic width of the ribbon:

$$L' \equiv L\sqrt{g(\rho_f - \rho_g)/\sigma} \tag{5}$$

In 1958, Zuber and Tribus [7] explained that the transition from nucleate to film boiling was a consequence of hydrodynamic instability. The peak heat flux occurred when vapor jets became Helmholtz unstable and hence collapsed; thereby obstructing the flow of liquid toward the heater. By making certain assumptions regarding the spacing of the jets, their diameter, and the wavelength at which the vapor jets became unstable, Zuber obtained an expression for the peak heat flux from a horizontal surface:

$$q_{max_Z} = \frac{\pi}{24}\sqrt{\rho_g}\, h_{fg}\left[\sigma g(\rho_f - \rho_g)\right]^{1/4} \tag{6}$$

Equation (6) applies as long as the system pressure is not close to the critical pressure. We have not amplified the derivation of equation (6) here as its development will form a part of our dis-

cussion in Chapter IV.

Cichelli and Bonilla [8], Berenson [9], and Costello et al. [5] measured the peak heat flux on flat plate heaters in the absence of any induced flow from the sides. The limited data of the first two authors for clean surfaces seem to bear out equation (6) with a little change in the constant[4], $\frac{\pi}{24}$. However, Costello's data for distilled water are much lower than predicted by equation (6). Thus, more data must be obtained for flat plate heaters with different liquids and at various gravities before one can judge whether or not equation (6) really represents the peak heat flux on horizontal surfaces. Part of the present effort will be aimed at doing this.

In 1964 Bobrovich, Gogonin and Kutateladze [10] and in 1965 Lienhard and Watanabe [11] independently showed that diverse peak heat flux data on cylinders of various radii and at different gravities could be correlated by:

$$q_{max} = q_{max_Z} \cdot f(R') \tag{7}$$

where $f(R')$ is an undetermined function of R' and

$$R' \equiv R\sqrt{g(\rho_f - \rho_g)/\sigma} \tag{8}$$

Equation (8) may be taken as a dimensionless parameter combin-

---

[4]This is explained in detail in Chapter IV.

ing the size of the heater and the gravity acting on the system.

Later, in 1970, Lienhard and Sun [12] proposed a hydrodynamic theory of boiling for cylindrical heaters and gave the following equation which was verified by about 900 q_{max} data over a wide range of heater size, liquids, pressures, and gravities:

$$(q_{max})_{inviscid} = q_{max_Z} \cdot [0.89 + 2.27 \exp(-3.44\sqrt{R'})] \qquad (9)$$

for $R' \geq 0.15$. This study conclusively proved that $q_{max} \sim g^{1/4}$ for $R' \geq 3.5$ for all gravities. However, for small R', the peak heat flux depended on gravity not only as it appeared in q_{max_Z} but also through the functional dependence upon the dimensionless radius, R'. Thus the disagreement arising out of Costello and Adam's [13] observation that the peak heat flux did not depend on one-fourth power of gravity at lower gravities was resolved.

Zuber also realized that the steady cyclic release of bubbles at discrete locations in film boiling was nothing but a classical example of Taylor Instability. He argued that at the minimum heat flux, the spacing of the bubble releasing nodes lie between 'most susceptible" and "critical" Taylor wavelengths and that the average rate of penetration of vapor region into liquid was slower than that predicted by Taylor instability. Zuber assumed that the bubble diameter at the departure was half of the dominant wavelength and that the bubble grew linearly in accordance with

Taylor instability theory up to a height equal to 40 percent of wavelength. He based his arguments on the experimental observations of Lewis [15] and Allred and Blount [16]. Zuber averaged the growth rate during linear growth and for the bubble frequency obtained:

$$f_b = \frac{1}{\lambda_d} \overline{\frac{d\eta}{dt}}$$

where

$$\overline{\frac{d\eta}{dt}} = \frac{1}{0.4\lambda} \int_0^{0.4\lambda} \frac{d\eta}{dt}\, d\eta = 0.2\, \omega_d \lambda_d \quad \text{for } \lambda = \lambda_d$$

Thus, for the minimum heat flux on flat surfaces he obtained:

$$(q_{min_F})_{inviscid} = 0.177\, \rho_g h_{fg} \sqrt[4]{\sigma g(\rho_f - \rho_g)/(\rho_f + \rho_g)^2} \qquad (10)$$

Berenson [9] subsequently made several observations of the minimum heat flux on flat plates. He argued that Zuber should have time-averaged the growth rate rather than averaging over η. A considerable portion of wave growth may be nonlinear, hence a complete growth history is needed to form a proper time average. Berenson himself could not form the average because of the limited information available to him. However, he suggested that the experimental constant in equation (10) should be 0.09 instead of 0.177.

In 1963, Lienhard and Wong [17] incorporated the effect of transverse curvature of the interface in the instability theory.

They were thus successful in predicting "most susceptible" Taylor wavelength to be expected in film boiling on horizontal cylinders. Based on arguments similar to Zuber's they obtained the following expression for the minimum heat flux:

$$(q_{min})_{inviscid} = (q_{min_F})_{inviscid} \cdot \left[\frac{1.289}{R'^2(2R'^2+1)}\right]^{1/4} \qquad (11)$$

where q_{min_F} is given by equation (10) with the constant changed to Berenson's value. Their experimental observation for alcohols and the data of Kovalev [18] for water confirmed the trend given by equation (11), but the data of the two authors define different constants in equation (11). The difference was due to the way the wire was mounted during the experimental observations. The end mountings can have a significant cooling effect on the wire and may cause an early collapse of film boiling at the ends.

In 1967, Baumeister and Hamill [19] made a theoretical prediction of the heat transfer coefficient for film boiling from horizontal wires. They solved the equations of motion and energy and optimized the heat transfer from the wire. Their rough model of the film boiling process also enabled them to predict the vapor blanket thickness around the cylindrical heater.

Later, in 1969, Lienhard and Sun [20] measured wavelengths during film boiling on horizontal cylinders. Their experiments

included a wide range of liquids, wire sizes and gravities. For a particular dimensionless radius, R', their data for wavelengths showed a significant variability. However, it was found that all the wavelengths were consistent with frequencies within ± 10 percent of the maximum frequency.

The present study will concentrate both on the "infinite" flat plate and cylindrical heaters. The induced convection situation will be avoided in the first case by limiting the configuration of the boiling vessel to that of a flat plate with vertical side walls to approximate an infinite flat plate. In the second case, the geometry itself is such that the induced flow is free to pass by without interfering with the bubble flow path.

Present Objectives.

Nearly all the work done so far on boiling heat transfer ignores one of the important liquid transport properties, i.e. viscosity. This assumption may be valid at pressures that are not extremely low for almost all the Newtonian liquids usually used in boiling. Still, one would like to know the contribution of viscosity, if any. In this context we have the following goals in mind:

1) Taylor Wave Behavior.

(a) Extend Bellman and Pennington's [14] Theory to determine the effect of liquid viscosity on the "most susceptible" wavelength and the corresponding frequency.

(b) Make experimental observations of the dominant unstable wavelength in film boiling on cylindrical heaters to pick up the effect of liquid viscosity, and make observations of the rate of growth of the unstable disturbance.

Since, for the commonly available liquids, viscosity decreases exponentially with temperature, the observations in part (b) will be made at very low pressures. Thus we would like to know:

(c) The effect, if any, of large volume fluxes in stretching the dominant unstable wavelength.

2) Heat Fluxes.

(a) Use above obtained expressions for Taylor wavelength and the wave frequency to discuss the minimum heat flux on an "infinite" flat plate and a cylindrical heater.

(b) Attempt to predict how the peak heat flux varies with viscosity in both these geometries.

(c) Put Zuber's equation (6) to a rigorous test by measuring the peak heat flux on an "infinite" flat plate heater at various gravities with different liquids being boiled. If

equation (6) does not represent the data for peak heat flux on an "infinite" flat plate, suggest a new theoretical model consistent with the observations.

(d) Observe the peak heat flux on an "infinite" flat plate and a cylindrical heater, when the boiled liquids are viscous. Relate the data to item 2b.

II. DERIVATION OF EXPRESSIONS FOR WAVELENGTH AND MINIMUM POOL BOILING HEAT FLUX IN VISCOUS LIQUIDS

In 1950, G.I. Taylor [22] discussed the instability of the horizontal interface between two ideal incompressible fluids of infinite depth. He showed that irregularities at the interface tended to grow if the acceleration was directed from the less dense to the more dense medium. Bellman and Pennington [14] extended his problem and showed how to take into account the interfacial surface tension and fluid viscosity. They gave closed form expressions only for the "most susceptible" wavelength (i.e., the wavelength for which the growth rate for a small disturbance at the interface is maximum) and the corresponding frequency. They obtained solutions for the situation in which only the surface tension at the interface was considered, but they were unable to do so in the more general case in which both the liquid viscosity and interfacial surface tension were considered.

We shall begin with formulation of the instability problem similar to that made by Bellman and Pennington; we shall then incorporate the pressure contribution of curvature of a cylindrical surface as was done by Lienhard and Wong [17] for the inviscid

case. Thus we shall attempt to obtain numerical values of the "most susceptible" frequency and corresponding wavelength as a function of liquid viscosity, as well as radius of curvature of the cylindrical heater. This evaluation in turn will be used to predict the minimum heat flux.

Hydrodynamic Analysis.

Before dwelling on the instability theory it is appropriate to state the various assumptions we are going to make:

1) The fluids are incompressible.

2) The fluids are Newtonian.

3) The fluid depths are large as compared to wavelength. This is not exactly valid for the vapor blanket thickness in film boiling, but we shall show later that the above assumption is not unrealistic.

4) The liquid is above a gaseous phase, such that the acceleration at the interface is always directed from the lighter to the heavier fluid. We assume this is so, because this is the situation encountered in all film boiling cases we will treat.

5) Nonlinear effects are negligible.

Figure 1a shows the interface between two incompressible viscous fluids of infinite depth. The linearized equations govern-

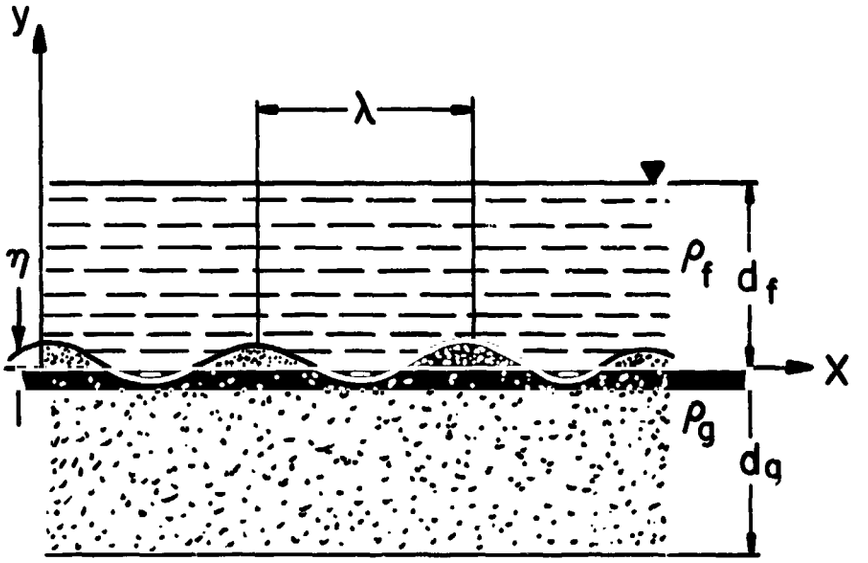

Fig. 1a Interface between two incompressible viscous fluids of infinite depth.

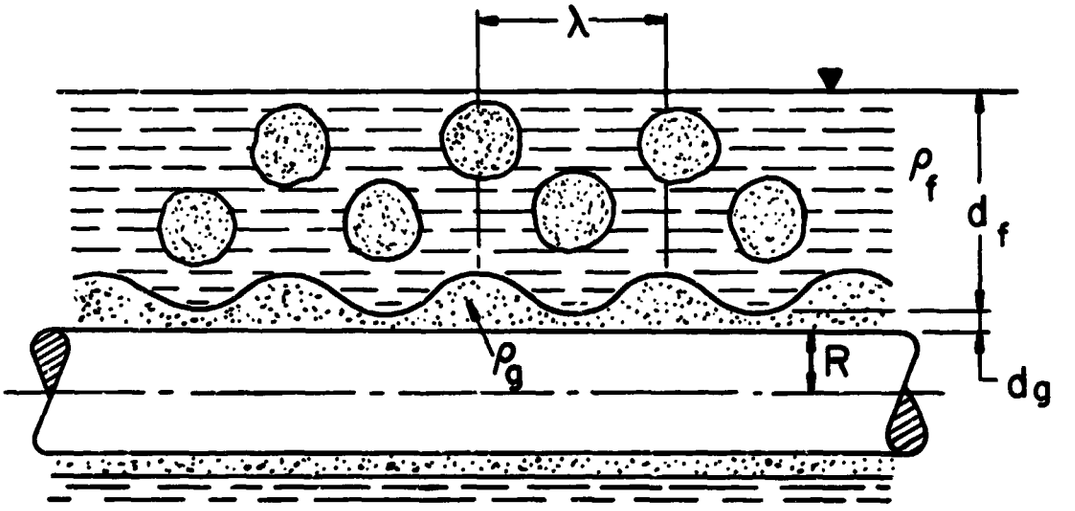

Fig. 1b Schematic diagram of a typical configuration of film boiling on cylinders.

ing the motion are:

$$u_x + v_y = 0 \tag{12}$$

$$u_t = -\frac{1}{\rho} p_x + \frac{\mu}{\rho}(u_{xx} + u_{yy}) \tag{13}$$

$$v_t = -\frac{1}{\rho} p_y - g + \frac{\mu}{\rho}(v_{xx} + v_{yy}) \tag{14}$$

These equations are satisfied by

$$u = -\varphi_x - \psi_y \tag{15}$$

$$v = -\varphi_y + \psi_x \tag{16}$$

and

$$p = p_o - \rho g y + \rho \varphi_t \tag{17}$$

provided that

$$\varphi_{xx} + \varphi_{yy} = 0 \tag{18}$$

and

$$\frac{\mu}{\rho}(\psi_{xx} + \psi_{yy}) = \psi_t \tag{19}$$

where u and v are the velocities in the x and y directions, respectively; p is the static pressure; p_o is the total pressure, and ρ is the density of the fluid.

Let us take, for the liquid phase:

$$\varphi_f = A_f e^{-ky+\omega t} \cos kx \tag{20}$$

$$\psi_f = B_f e^{-m_f y+\omega t} \sin kx \tag{21}$$

$$p_f = p_o - \rho_f g y + \rho_f (\varphi_f)_t \tag{22}$$

where k is the wave number, ω is the frequency, and:

$$m_f^2 = k^2 + \rho_f \omega / \mu_f \tag{23}$$

Similarly for the gaseous phase:

$$\varphi_g = A_g e^{ky+\omega t} \cos kx \tag{24}$$

$$\psi_g = B_g e^{m_g y+\omega t} \sin kx \tag{25}$$

$$p_g = p_o - \rho_g g y + \rho_g (\varphi_g)_t \tag{26}$$

and

$$m_g^2 = k^2 + \rho_g \omega / \mu_g \tag{27}$$

The real part of m_f or m_g has to be positive so the velocity remains finite as y becomes large.

Considering that waves of height $y = \eta(x,t)$ are propagated, we obtain for the linearized kinematic condition at the interface:

$$\eta_t = v_f \tag{28}$$

or

$$\eta = \eta_o e^{\omega t} \cos kx \tag{29}$$

where

$$\eta_o = -\frac{k(A_f + B_f)}{\omega} \tag{30}$$

The boundary conditions at the interface, <u>i.e.</u>, at $y=\eta$, are:

$$u_f = u_g \tag{31}$$

$$v_f = v_g \tag{32}$$

$$-p_f + 2\mu_f (v_f)_y = -p_g + 2\mu_g (v_g)_y - \sigma\eta_{xx} \tag{33}$$

$$\mu_f[(v_f)_x + (u_f)_y] = \mu_g[(v_g)_x + (u_g)_y] \tag{34}$$

The substitution of equations (20) through (22); (24) through (26) and (29) in equations (31) to (34) gives four linear and homogeneous equations in the four constants, A_f, B_f, A_g, and B_g:

$$kA_f + m_f B_f - kA_g + m_g B_g = 0 \tag{35}$$

$$A_f + B_f + A_g - B_g = 0 \tag{36}$$

$$\left[\frac{g(\rho_f - \rho_g)k}{\omega} - \frac{\sigma k^3}{\omega} - \rho_f \omega - 2\mu_f k^2\right] A_f + \left[\frac{g(\rho_f - \rho_g)k}{\omega} - \frac{\sigma k^3}{\omega} - 2\mu_f k m_f\right] B_f$$

$$+ [\rho_g \omega + 2\mu_g k^2] A_g - [2\mu_g k m_g] B_g = 0 \tag{37}$$

and

$$2\mu_f k^2 A_f + \mu_f (k^2 + m_f^2) B_f + 2\mu_g k^2 A_g - \mu_g (k^2 + m_g^2) B_g = 0 \tag{38}$$

The above equations have a non-trivial solution if and only if the determinant of the coefficient matrix is zero, i.e.:

$$\begin{vmatrix} k & m_f & -k & m_g \\ 1 & 1 & 1 & -1 \\ \left\{\frac{g(\rho_f-\rho_g)k}{\omega} - \frac{\sigma k^3}{\omega}\right\} & \left\{\frac{g(\rho_f-\rho_g)k}{\omega} - \frac{\sigma k^3}{\omega}\right\} & \rho_g\omega + 2\mu_g k^2 & -2\mu_g k m_g \\ \left\{-\rho_f\omega - 2\mu_f k^2\right\} & \left\{-2\mu_f k m_f\right\} & & \\ 2\mu_f k^2 & \mu_f(k^2+m_f^2) & 2\mu_g k^2 & -\mu_g(k^2+m_g^2) \end{vmatrix} = 0 \qquad (39)$$

Equation (39) should be valid only when the fluid depths are infinite and there is no curvature in the transverse direction at the interface. In film boiling on horizontal cylinders the depth of the vapor blanket is finite and there is a curvature in the transverse direction. A typical configuration is shown in Figure 1b.

Recently, Hsieh [23] analyzed the inviscid instability problem in the presence of heat and mass transfer. His analysis also incorporated a finite depth of fluids. Commenting on his work as applied to film boiling, we [24] showed that there was no effect of finite vapor blanket on the "most susceptible" wavelength, while the effect on the corresponding frequency was to

decrease it by a small amount.

As proposed earlier by Lienhard and Wong [17], a two dimensional model can be used for cylindrical geometries. The effect of transverse curvature is treated in the form of an additional oscillating pressure difference component across the interface, as shown in Figure 2.

The expression for the transverse pressure may be written as:

$$\Delta p_{tr} = \frac{\sigma}{2R^2(1+d_g/R)^2}\,\eta \qquad (40)$$

where d_g is the depth of the vapor blanket over the wire.

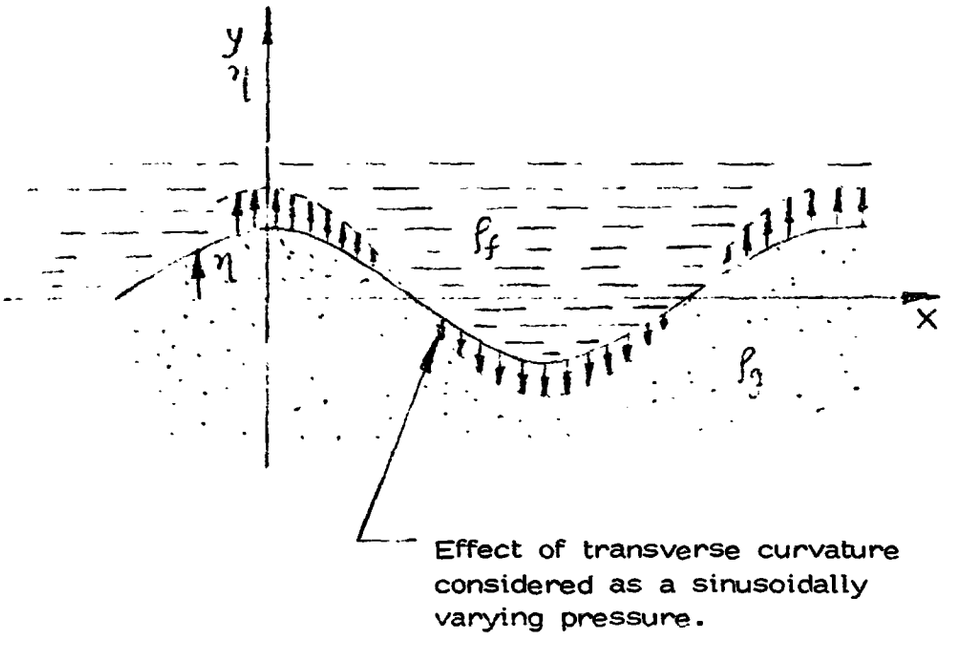

Figure 2. Contribution of transverse curvature on a two dimensional wave.

If we define a corrected radius, $R_c \equiv R[1+d_g/R]$, we can write equation (33) as:

$$-p_f + 2\mu_f(v_f)_y = -p_g + 2\mu_g(v_g)_y - \sigma\eta_{xx} - \frac{\sigma}{2R_c^2}\eta \qquad (33a)$$

Consequently equation (36) becomes

$$\begin{vmatrix} k & m_f & -k & m_g \\ 1 & 1 & 1 & -1 \\ \left\{\frac{g(\rho_f-\rho_g)k}{\omega} - \frac{\sigma k^3}{\omega}\right\} & \left\{\frac{g(\rho_f-\rho_g)k}{\omega} - \frac{\sigma k^3}{\omega}\right\} & (\rho_g\omega + 2\mu_g k^2) & -2\mu_g k m_g \\ \left\{-\rho_f\omega - 2\mu_f k^2 + \frac{\sigma k}{2R_c^2\omega}\right\} & \left\{-2\mu_f k m_f + \frac{\sigma k}{2R_c^2\omega}\right\} & & \\ 2\mu_f k^2 & \mu_f(k^2 + m_f^2) & 2\mu_g k^2 & -\mu_g(k^2+m_g^2) \end{vmatrix} = 0 \qquad (39a)$$

The evaluation of the determinant equation, (39a), gives:

$$\left[-g(\rho_f-\rho_g)k + \sigma k^3 - \frac{\sigma k}{2R_c^2} + (\rho_f+\rho_g)\omega^2\right]\left[\mu_f(k+m_f)+\mu_g(k+m_g)\right]$$

$$+ 4\omega k[\mu_f k + \mu_g m_g][\mu_g k + \mu_f m_f] = 0 \qquad (39b)$$

Our next step is to put equation (39b) in a more usable form, so that it can be explicitly solved for frequency and wave number, or wavelength. The vapor viscosity μ_g is much less than μ_f so it may be neglected in comparison to liquid viscosity. Thus we may write, for the frequency, ω,

$$\omega = f(\rho_f+\rho_g,\ \rho_f-\rho_g,\ \mu_f,\ \sigma,\ k,\ g,\ R_c) \qquad (41)$$

This expression relates eight quantities which are expressible in three dimensions. Using the Buckingham Pi-Theorem, we can recast this problem in terms of five dimensionless groups. For these groups we choose:

(i) a dimensionless frequency

$$\Omega \equiv \omega\left[\frac{\sigma}{g^3(\rho_f-\rho_g)}\right]^{1/4} \qquad (42)$$

(ii) a dimensionless wave number

$$K \equiv k\left[\frac{\sigma}{g(\rho_f-\rho_g)}\right]^{1/2} \qquad (43a)$$

or a dimensionless wavelength, Λ, defined as

$$\Lambda = 1/(\sqrt{3}\, K) \tag{43b}$$

(iii) a dimensionless liquid viscosity parameter

$$M \equiv \frac{\rho_f \sigma^{3/4}}{\mu_f g^{1/4} (\rho_f - \rho_g)^{3/4}} \tag{44}$$

The square of this group is very nearly the Borishanski number, N, as defined in equation (4).

(iv) a dimensionless density

$$\Gamma \equiv \frac{\rho_f - \rho_g}{\rho_f + \rho_g} \tag{45}$$

(v) a non-dimensional cylinder radius

$$R_c' \equiv R_c \left[\frac{g(\rho_f - \rho_g)}{\sigma}\right]^{1/2} \tag{46}$$

This number is related to the Bond number, Bo, by $Bo \equiv R_c'^{\,2}$.

Using these dimensionless numbers, we may write equation (39b) as

$$1 - K^2 + \frac{1}{2Bo} - \frac{\Omega^2}{\Gamma K} + \frac{K}{(K^2+\Omega M)^{1/2}} - \frac{K^3}{(K^2+\Omega M)^{1/2}}$$

$$- \frac{\Omega^2}{\Gamma(K^2+\Omega M)^{1/2}} - \frac{4\Omega K}{M\Gamma} + \frac{K}{2Bo(K^2+\Omega M)^{1/2}} = 0 \qquad (47)$$

Equation (47) gives a relation between frequency and wave number for an unstable disturbance (corresponding to Ω positive and real), when the interfacial surface tension, transverse curvature and liquid viscosity are taken into account.

From equation (47) it is clear that when the wave propagation velocity is zero, there is no effect of liquid viscosity on the critical wavelength. Also, when $M \to \infty$ (i.e., the liquid is inviscid) equation (47) reduces to the same equation as obtained by Lienhard and Wong [16] for the inviscid case.

We are interested in the "most susceptible" frequency, or the frequency for which growth rate of the disturbance is maximum (i.e., the one for which $\frac{d\Omega}{dk} = 0$). Differentiating equation (47) with respect to k and setting $\frac{d\Omega}{dk} = 0$, gives

$$-2K + \frac{\Omega^2}{\Gamma K^2} + \frac{1}{(K^2+\Omega M)^{1/2}} - \frac{K^2}{(K^2+\Omega M)^{3/2}} - \frac{3K^2}{(K^2+\Omega M)^{1/2}}$$

$$+ \frac{K^4}{(K^2+\Omega M)^{3/2}} + \frac{\Omega^2 K}{\Gamma(K^2+\Omega M)^{3/2}} - \frac{4\Omega}{M\Gamma} + \frac{1}{2Bo(K^2+\Omega M)^{1/2}}$$

$$- \frac{K^2}{2Bo(K^2+\Omega M)^{3/2}} = 0 \qquad (48)$$

Thus we have two nonlinear equations (47) and (48) in two unknowns, Ω and K. The two equations were solved numerically on an IBM/360 computer using a subroutine: XFNLES, which solves a system of nonlinear equations. This subroutine is available in the Numerical Analysis Library [25] for the S/360. Γ was taken to be 0.9995 ($\simeq$1) in the calculations.

The "most susceptible" frequency and corresponding wavelength are plotted in Figures 3 and 4, respectively, as a function of the viscosity parameter M and Bond number, Bo. As evident from these figures, the effect of liquid viscosity is to increase the wavelength and to decrease the corresponding frequency. Figures 5 and 6 show the effect of Bond number and liquid viscosity separately on the frequency wavelength relationship equation (47). Transverse curvature of the cylindrical heater reduces the "most susceptible" wavelength and increases the frequency. Figure 6 shows that apart from increasing the wavelength, viscosity also

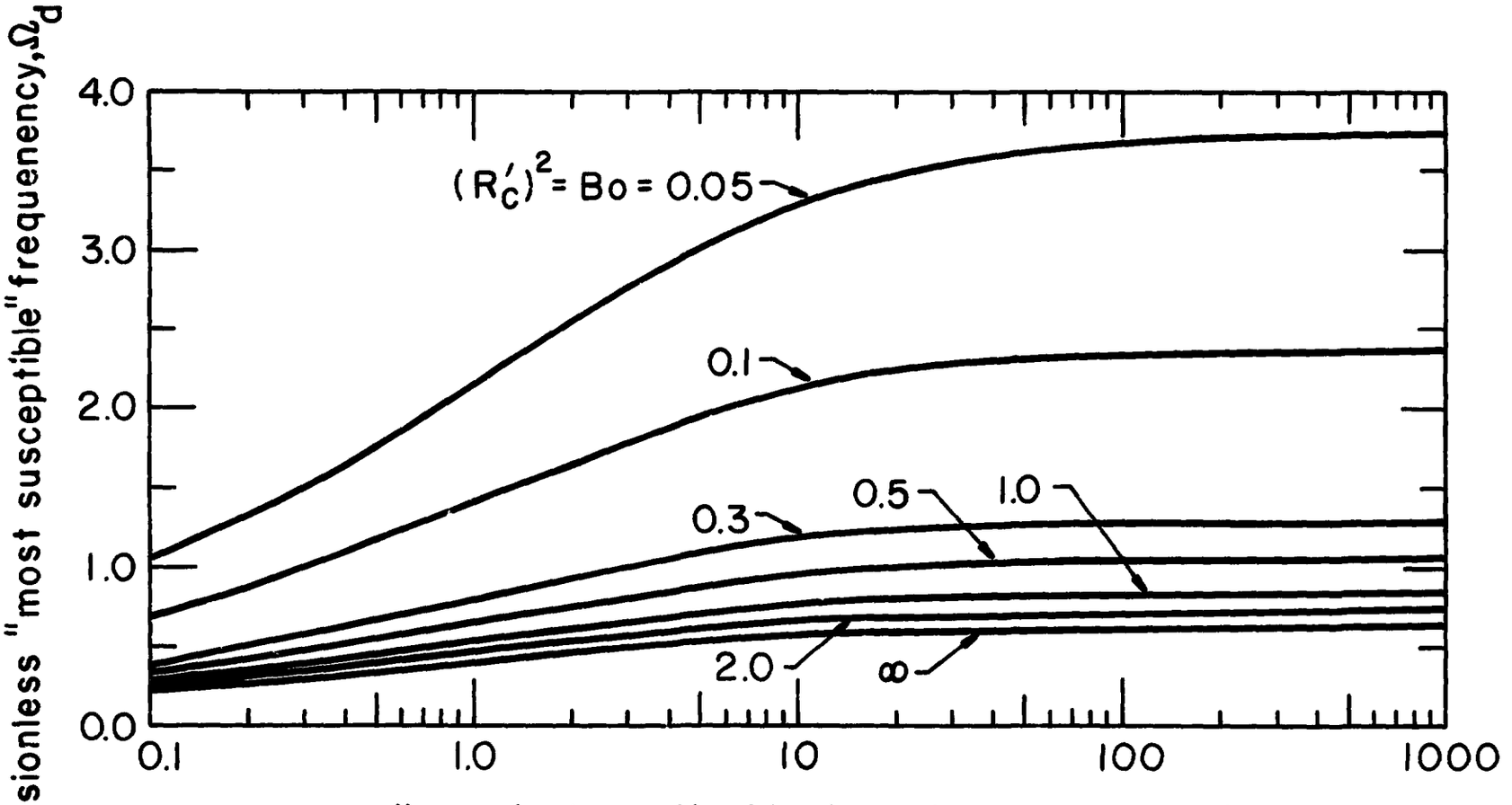

Fig. 3 Variation of Ω_d with M for various Bond numbers

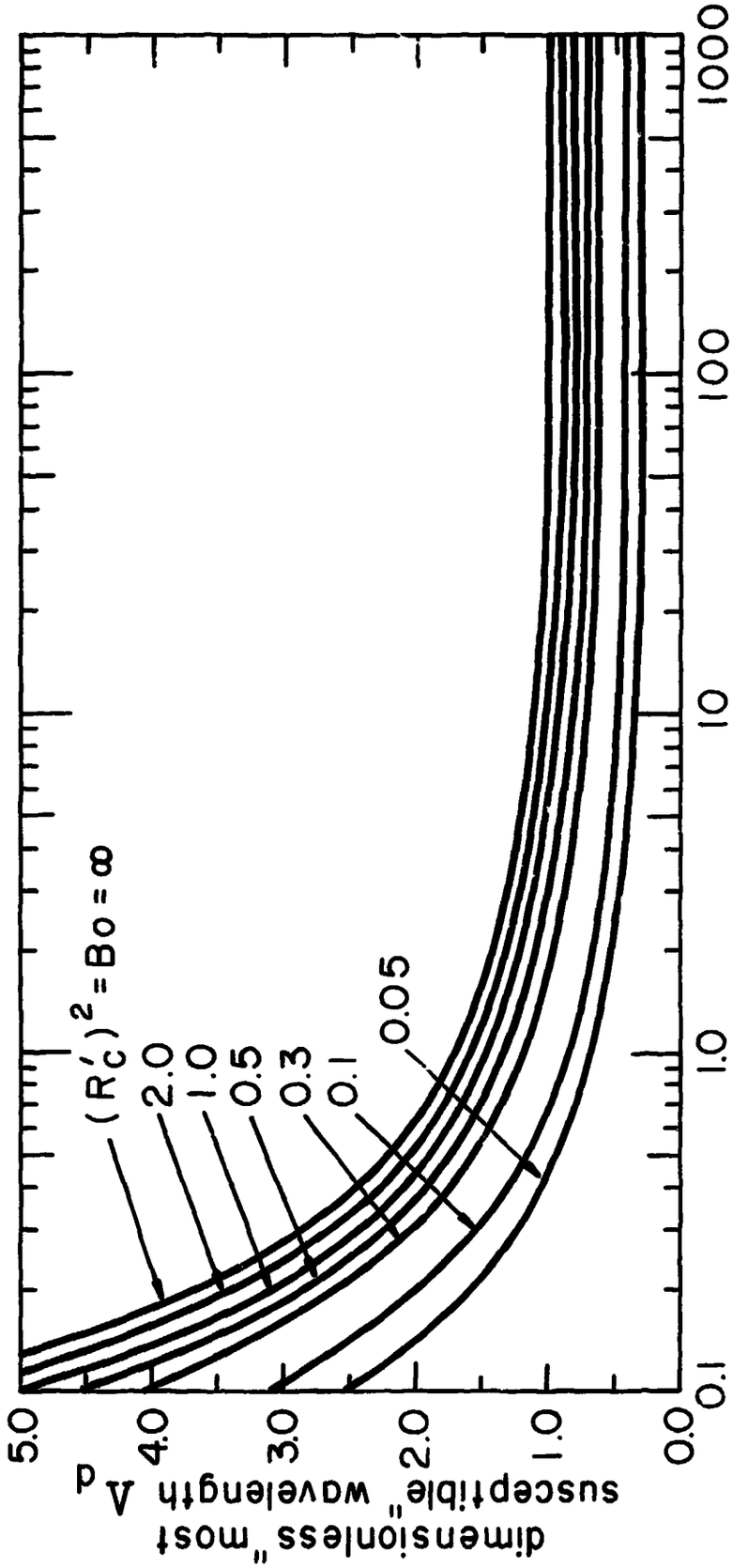

Fig. 4 Variation of Λ_d with M for various Bond numbers

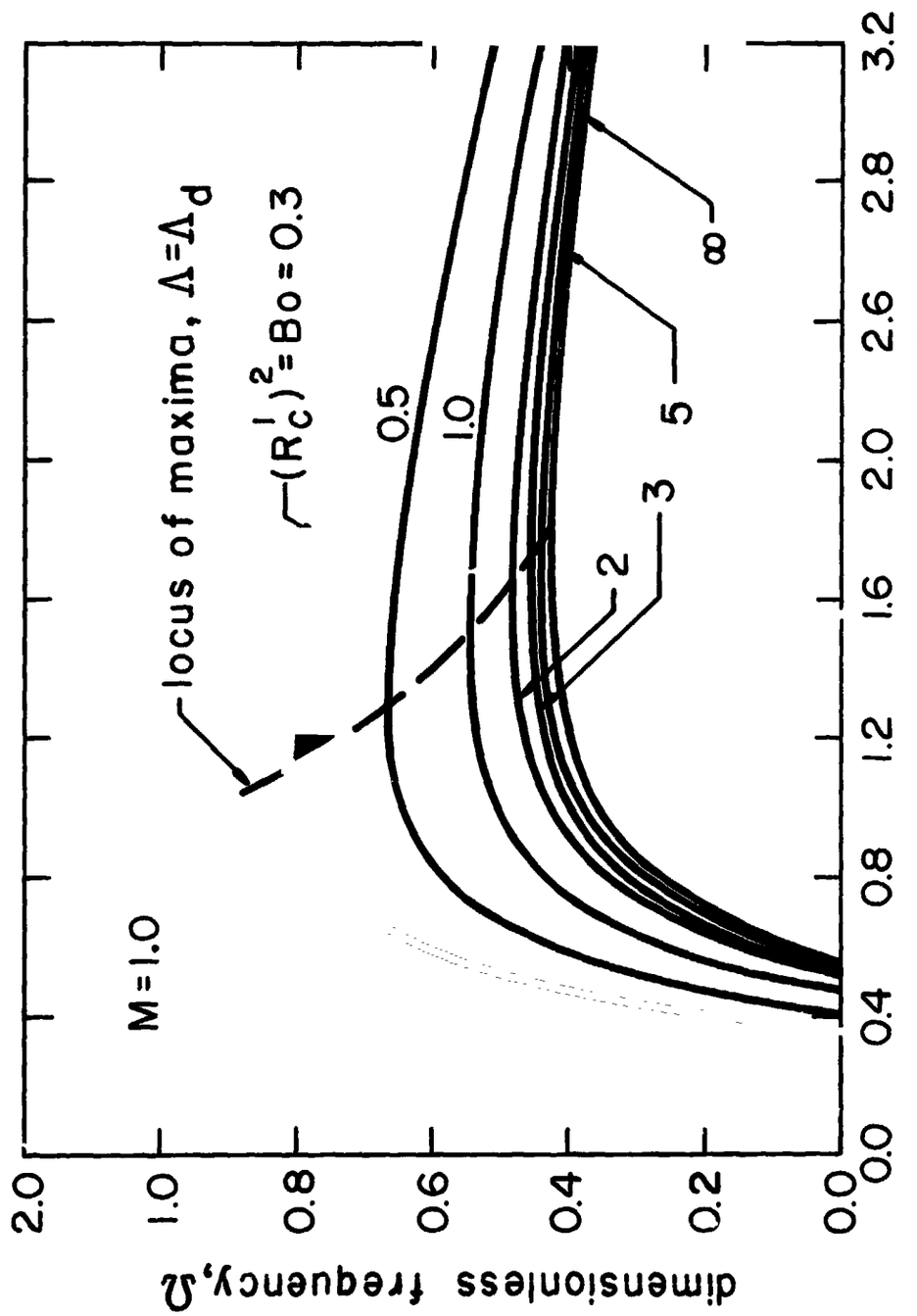

Fig. 5 Effect of radius on dispersion relation for cylinders

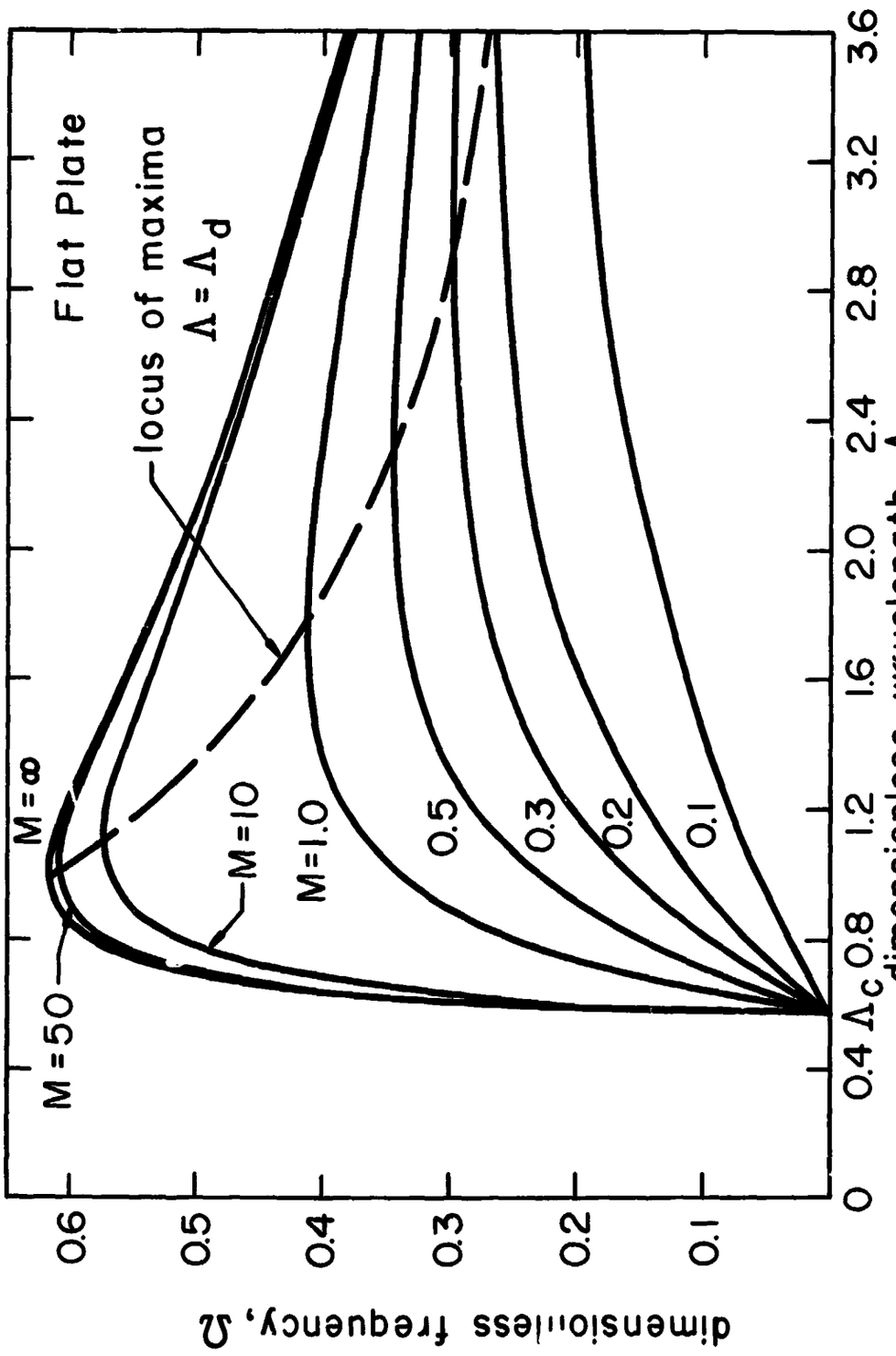

Fig. 6 Effect of viscosity on dispersion relation for a flat plate

tends to increase the region of near neutral stability slightly. By "region of near neutral stability" we mean the range of wavelengths that can exist within, say, 10 percent of the maximum frequency.

Minimum Heat Flux on a Flat Plate.

We can make a prediction of the minimum heat flux by making an energy balance at the surface of the heater.

$$q_{min_F} = \left[\frac{\text{latent heat transport}}{\text{unit volume}}\right]\left[\frac{\text{number of bubbles}}{\text{unit time}}\right]$$

$$\left[\text{volume of a bubble}\right]\left[\frac{1}{\text{area of the heater}}\right] \qquad (49)$$

or

$$q_{min_F} = \left[\rho_g h_{fg}\right]\left[4 b\omega_d\right]\left[\frac{4}{3}\pi\left(\frac{\lambda_d}{4}\right)^3\right]\left[\frac{1}{\lambda_d^2}\right] \qquad (50)$$

where we have assumed that the dominant wavelength is the "most susceptible" one, and the departing bubble diameter is half of it. Lienhard and Wong have shown experimentally that this is true within a certain range. In the above expression for q_{min_F}, the bubble release frequency, f_b, has been assumed to be $b\omega_d$, where b is an experimental constant. Here again we do not yet include the effect of viscosity on b. Experimental observations will subsequently shed more light on the validity of these assumptions. Equation (50) may be written as

$$q_{min_F} = \frac{\pi}{12} b \rho_g h_{fg} \Omega_d \Lambda_d \left[\frac{\sigma g}{\rho_f - \rho_g}\right]^{1/4} \tag{51}$$

Dividing equation (51) by equation (10) we get

$$Q_{min_F} = \frac{q_{min_F}}{(q_{min_F})_{inviscid}} = 1.608 \Omega_d \Lambda_d / \Gamma^{1/2} \tag{52}$$

Minimum Heat Flux on a Cylindrical Heater.

Following arguments similar to those for the flat plate we may write an expression for the minimum heat flux on cylinders:

$$q_{min} = [\rho_g h_{fg}][2 b \omega_d][\frac{4}{3} \pi (\frac{\lambda_d}{4})^3][1/2 \pi R \lambda_d] \tag{53}$$

This may be rewritten as

$$q_{min} = \frac{b}{48} \frac{\rho_g h_{fg}}{R} \Omega_d \Lambda_d^2 \left[\frac{\sigma}{g(\rho_f - \rho_g)}\right]^{3/4} g^{1/2} \tag{54}$$

Lienhard and Wong gave an expression for the inviscid case as

$$(q_{min})_{inviscid} = \frac{b}{48} \frac{1}{3^{3/4}} \frac{\rho_g h_{fg}}{R} \left[\frac{2g(\rho_f - \rho_g)}{\rho_f + \rho_g} + \frac{\sigma}{(\rho_f + \rho_g) R^2}\right]^{1/2}$$

$$\times \left[\frac{g(\rho_f - \rho_g)}{\sigma} + \frac{1}{2R^2}\right]^{-3/4} \tag{55}$$

Dividing equation (54) by equation (55) we get

$$Q_{min} = \frac{q_{min}}{(q_{min})_{inviscid}} = 1.585 \frac{\Omega_d \Lambda_d^2}{\Gamma^{1/2}} [1 + 1/2\ 3o]^{1/4} \qquad (56)$$

Thus, knowing Ω_d and Λ_d as functions of the liquid viscosity parameter, M, and the Bond number, Bo, one can predict the minimum pool boiling heat flux. As M is decreased, Ω_d and Λ_d vary such that the dimensionless heat flux, $q_{min}/(q_{min})_{inviscid} > 1$. We shall return to question this particular result on pages 70-71.

Conclusions.

1. The effect of liquid viscosity is to decrease the "most susceptible" frequency and to increase the corresponding wavelength.

2. The effect of transverse curvature of the interface is to shorten the "most susceptible" wavelength and to increase the corresponding frequency.

3. There is no effect of liquid viscosity on critical wavelength.

4. The region of neutral stability (i.e., the region close to the "most susceptible" frequency) increases slightly with liquid viscosity.

III. EXPERIMENTAL OBSERVATIONS OF THE DOMINANT UNSTABLE WAVELENGTH AND ITS GROWTH RATE DURING THE FILM BOILING OF VISCOUS LIQUIDS

An experimental program was carried out to observe the wavelength, its rate of growth, and the thickness of the vapor blanket surrounding the wire heater during film boiling in viscous liquids. Since the viscosity of most of the liquids is fairly low when they boil at normal pressures, the experiments had to be performed at very low pressures. With the limitations of attaining maximum vacuum in the existing boiling apparatus in mind, a survey of various available chemicals was made. It was found that Cyclohexanol $CH_2(CH_2)_4$ CHOOH and Ethylene Glycol $CH_3(CHOH)$ CH_2OH were best suited for the purpose. However, nearly all the experiments reported here were performed with cyclohexanol as the boiling liquid. Various physical properties of cyclohexanol are plotted in Appendix B.

A. Description of the Experiment.

1. Experimental Apparatus.

A test capsule 8.9 cm wide, 8.9 cm high and 17.8 cm long, with glass windows in the 8.9 by 17.8 cm walls, was used in all

of the experiments. The capsule was made of brass and insulated on the sides with 0.63 cm thick styrofoam sheet. An electric preheater and 0.63 cm diameter brass holders to support the test heaters were fitted to the capsule. Nichrome wires were used as test heaters and copper hooks were attached to their ends so they could be mounted in the brass holders. The hooks were attached in such a manner so as to minimize the end effects. A 2.54 cm marker was mounted on the bottom of the capsule to provide a reference dimension for the reduction of photographic data.

Figure 7 shows a schematic diagram of the apparatus. AC power was employed in most of the experiments. The power supply to the wire was calculated from the measured current and voltage in the wire. A mercury manometer or a vacuum gage was used to note pressure inside the capsule. This pressure was corrected to take into account the head of liquid above the wire. An identical apparatus was used by Sun and Lienhard to make similar measurements. Full details are given in reference [20].

2. Procedure.

A nichrome wire approximately 10 cm long was cleaned with soap and hot water to remove any grease or oily matter and then was rinsed with the test liquid. The wire surface was

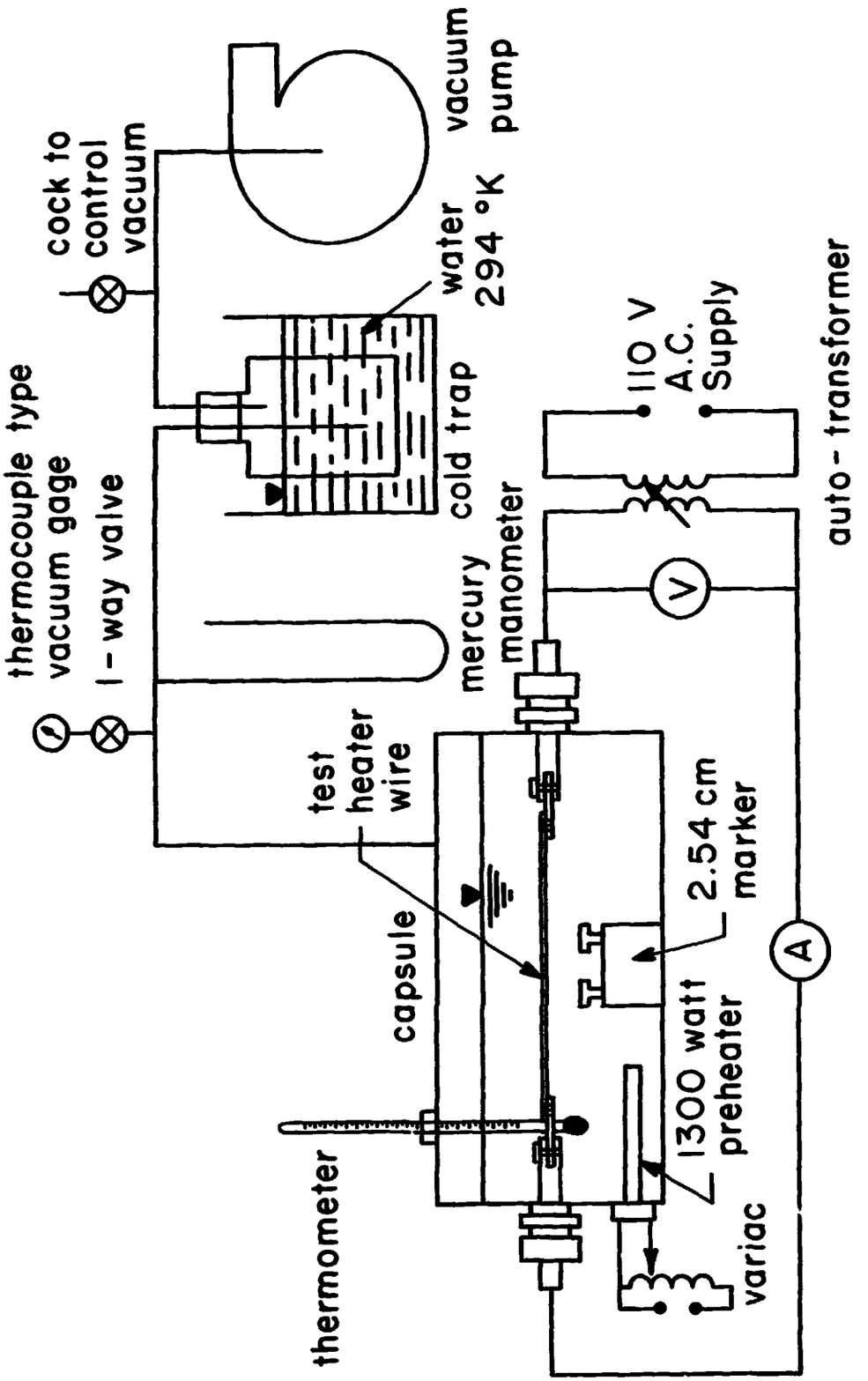

Fig. 7. Schematic diagram of the apparatus.

smooth and had a cold-rolled finish (as supplied by the manufacturer). The wire was mounted in the brass holders and the glass windows were positioned. The capsule was filled with reagent grade test liquid to a level of about 2.5 cm above the wire. The vacuum pump was started and the preheater was turned on to heat the liquid to saturation temperature. The preheater was turned off before energizing the wire. This was done to avoid any effects of convective currents and electric fields.

The current in the wire was steadily increased until the peak heat flux was reached and the transition from nucleate to film boiling was observed. Thereafter the current was reduced until film boiling started to disappear at the ends. This insured that the heat flux was close to minimum. Still pictures of the film boiling phenomenon were taken and observations of the temperature and pressure were also made. The heat flux was again increased in steps. At each step a photograph was taken and other corresponding observations were made. This procedure was continued until the heat flux was such that the wire started glowing or the bubble merger mechanism was evident. By "bubble merger" we mean that two neighboring bubbles growing in the first half of the cycle come into contact with the adjoining bubble from the second half of the cycle. Again the heat flux was decreased in steps and the process repeated.

This procedure was repeated for wires of different sizes and various pressures. Each time a new wire was used, the liquid in the capsule was also replaced. In some cases high speed movies were made, to facilitate study of the growth rate of the disturbance, with a Hycam motion picture camera at a speed of 500 frames per second and an exposure time of 1/1250 second.

3. Data reduction.

Photographic information was used to make three different kinds of observations. We describe them under three separate subtitles:

Wavelength measurements. -- Still pictures were printed with a 2.54 cm marker as a reference dimension; the wavelengths at various heat fluxes were measured. Care was taken to avoid situations where bubble merger or deformation of the wave pattern had taken place. This deformation may be caused by drift in the phase angle along the wire or by oscillations generated through the movement of the outgoing bubbles. The probable error in the measurements of the shortest wavelengths was only about ± 4.5 percent. The error was less for larger wavelengths.

Vapor blanket thickness measurements. -- In film boiling, a vapor blanket of finite thickness always surrounds the heater and there is no liquid contact with the surface of the heater. The instability of the upper boundary of this vapor blanket causes a

steady release of bubbles. For the application of the theory developed in the previous chapter we must obtain the corrected radius of the heater wire by adding the minimum blanket thickness to R.

To observe the vapor blanket thickness, representative pictures of film boiling were enlarged. The minimum diameter of the vapor blanket surrounding the wire was measured, using the 2.54 cm marker again as a reference. This was done to avoid any refraction effects that might creep in if the wire diameter were chosen as a reference. Furthermore, the wire diameter could not be seen clearly through the vapor blanket. The wire diameter was subtracted from this measurement to give twice the vapor blanket thickness. In other words, we anticipated that vapor surrounded the wire equally on the top and the bottom. Sometimes a cusp appeared on the blanket in the wake of a departing bubble, and we have ignored it.

Measurements of growth rate of disturbance. -- Hycam movies were viewed on a microfilm viewer. At first, a preliminary survey was made to sort out those bubbles which grew undisturbed by other adjoining bubbles. Starting with a frame in which a bubble had just broken away from the interface, the height of the interface was measured from the lowest boundary of the vapor blanket. Later, the minimum diameter of the vapor

blanket tube surrounding the wire was subtracted from each of the above observations to give the amplitude of the wave.

The minimum height of the interface was used as a reference dimension for obtaining dimensionless amplitude. It may become more clear if one recalls equation (29) for the amplitude of the wave. At a particular value of x, say x=0, one may write

$$\eta = \eta_o \exp(\omega t) \tag{58}$$

or

$$\frac{\eta}{\eta_o} = \exp[\Omega(1.612\, \omega_{d_F} t)] \tag{59}$$

or

$$\ln\left(\frac{\eta}{\eta_o}\right) = \Omega(1.612\, \omega_{d_F} t) \tag{60}$$

where η_o is the minimum depth, d_g, of vapor blanket and ω_{d_F} is the "most susceptible" frequency for the disturbance in the inviscid fluid in the absence of any geometrical effects of the heater. In all cases the dimensionless amplitude, η/η_o, was plotted against dimensionless time, $(1.612\, \omega_{d_F} t)$, on semilogarithmic graph paper. The slope of the curve at any instant gave the dimensionless frequency, Ω. The probable error in the observation of the linear growth rate was ± 10 percent.

Now we would like to compare the experimental observations of wavelength and frequency with the theoretical predictions. Be-

fore we do this it is necessary to present some sort of correlation for vapor blanket thickness, because the wire radius has to be corrected for it.

B. Discussion of Results.

1. Vapor Blanket Thickness Correlation.

Baumeister and Hamill [19], while analyzing heat transfer from wires in film boiling, developed an expression for vapor blanket thickness. Their theoretical model for the film boiling configuration was a fairly approximate one; a sequence of spherical domes connected by annular passages. Neglecting inertia, they solved the equations of motion and energy with the assumption that heat transfer rate is maximum.

For the heat transfer coefficient for film boiling on wires they got:

$$h_w = 0.23\left[\frac{k_g^3 h_{fg}^* g(\rho_f-\rho_g)\rho_g}{\mu_g \Delta T \sqrt{\frac{\sigma}{g(\rho_f-\rho_g)}}}\right]^{1/4} \cdot \left[\left(\frac{1}{2R'}\right)^3 + 2.25\left(\frac{1}{2R'}\right)\left(1+\Delta\right)^2\right]^{1/4} \qquad (61)$$

where $\Delta \equiv d_g/R$. All the physical properties of the vapor in the above equation are evaluated at the mean film temperature, i.e., at $T=T_{sat} + \Delta T/2$. The latent heat of vaporization has been cor-

rected to take into account any sensible heat required to heat the vapor above its saturation temperature. Assuming a parabolic velocity profile and mean film temperature for vapor in the vapor blanket, Breen and Westwater [26] gave a corrected expression for h_{fg}:

$$h^*_{fg} = h_{fg}\left[1 + \frac{0.34\, c_v \Delta T}{h_{fg}}\right]^2$$

Baumeister and Hamill changed the constant in equation (61) from 0.23 to 0.35 for small wires ($R' \leq 0.05$) to take into account any heat transfer from the domes. This constant was further corrected to 0.485 for larger wires ($R' \geq 0.05$) to fit the experimental data. Essentially, the constant in equation (61) was fixed from experimental results. This was necessary owing to their necessarily simplified model of the film boiling process.

Their theoretical expression for the vapor blanket thickness was

$$\Delta = \exp\left\{4.35\left[\frac{k_g \mu_g \Delta T}{h^*_{fg} 2R \rho_g \sigma}\right]^{1/4}\left[\frac{1}{1+9R'^2(1+\Delta)^2}\right]^{1/4}\right\} - 1 \qquad (62)$$

where the term in the second square bracket is close to unity for small values of R' and Δ.

If heat flux, q, is taken to be an independent variable; the temperature difference, ΔT, between the heater wall and the surrounding liquid can be written as

$$\Delta T = \frac{q}{h_w}$$

Using this expression for ΔT and equation (61) in equation (62) gives

$$\Delta = \exp\left\{7.05\left[\frac{q\mu_g}{h^*_{fg}\rho_g\sigma}\right]^{1/3}\left[\frac{1}{1 + 9R'^2(1+\Delta)^2}\right]^{1/3}\right\} - 1 \qquad (63)$$

The group $\mu_g/h^*_{fg}\rho_g$ is a weak function of temperature. We took ΔT=425K, which is typical of the film boiling situation, and plotted the present data for cyclohexanol, as well as some old data of Sun for acetone [21] against equation (63). The predictions were too high and did not correlate the data well for various dimensionless radii. This suggests that we should take another look at the various factors influencing vapor blanket thickness.

The vapor blanket thickness will primarily depend on seven independent variables, q, ρ_g, h^*_{fg}, $g(\rho_f-\rho_g)$, σ, μ_g and R. The heat flux q is imagined to be transferred by conduction and used fully in the phase transformation. The eight variables, including vapor blanket thickness, d_g, can be written in four dimensions: joule, kg, meter, and sec. Thus, in accordance with Buckingham Pi Theorem, we expect the problem to be reducible to a relation among four dimensionless groups. For these we choose:

a) The dimensionless vapor blanket thickness, Δ.

b) The Bond number, Bo, or ratio of buoyant to surface tension forces.

c) A ratio of viscous to surface tension forces,

$$B \equiv \frac{q\mu_g}{\rho_g h^*_{fg} \sigma} \quad . \tag{64}$$

d) A ratio of inertial to viscous forces--a kind of Reynolds number based on the vapor velocity,

$$Re \equiv \frac{qR\Delta}{\mu_g h^*_{fg}} \quad . \tag{65}$$

Baumeister and Hamill's equation (63) involves the first three groups but the fourth group is missing because they neglected inertial terms in their equation of motion. Their assumption is realistic as long as either the wire radius, or the heat flux, or the vapor blanket thickness is small; but the ratio of inertial to viscous forces may be of the same order of magnitude when the heat flux is high or the vapor blanket thickness is large.

Radiation losses can also form a significant portion of the total heat transfer from a wire in film boiling. We employed nichrome wires in all the experiments performed. The total hemispherical emittance for slightly oxidized nichrome at a temperature of 750K has been given by Touloukian [27] as 0.65. Thus the radiative heat flux may be written as:

$$q_r = 0.65\,\sigma\,(T_w^4 - T_s^4) \qquad (66)$$

For $\Delta T \simeq 425K$, which is quite representative for our own vapor blanket thickness, equation (66) gives

$$q_r = 0.132 \times 10^5 \text{ watts/meter}^2 \qquad (67)$$

This heat flux may form as much as 10-20 percent of the total heat flux, and is absorbed by the liquid. To know the depth of penetration of the radiant heat flux, absorptive properties of liquid cyclohexanol are needed. However, this information is not available in the existing literature. Water [28] is a good absorber of infrared radiation. Values of the absorption or extinction coefficient for water as listed in reference [29] indicate that all the radiant energy is absorbed in a very thin layer of liquid. We presume that this is probably true for cyclohexanol also. The radiant energy is absorbed by the liquid adjoining the interface and is utilized in generating additional amounts of vapor.

Depending upon the total amount of vapor generated, the vapor blanket thickness and vapor velocity in the vapor blanket, will adjust themselves in such a way as to optimize the process. The Reynolds number, Re, as defined in equation (65) gives a relation between vapor velocity and the vapor blanket thickness, hence it is an important correlation parameter.

In Figure 8, we have plotted 21 data points for vapor blank-

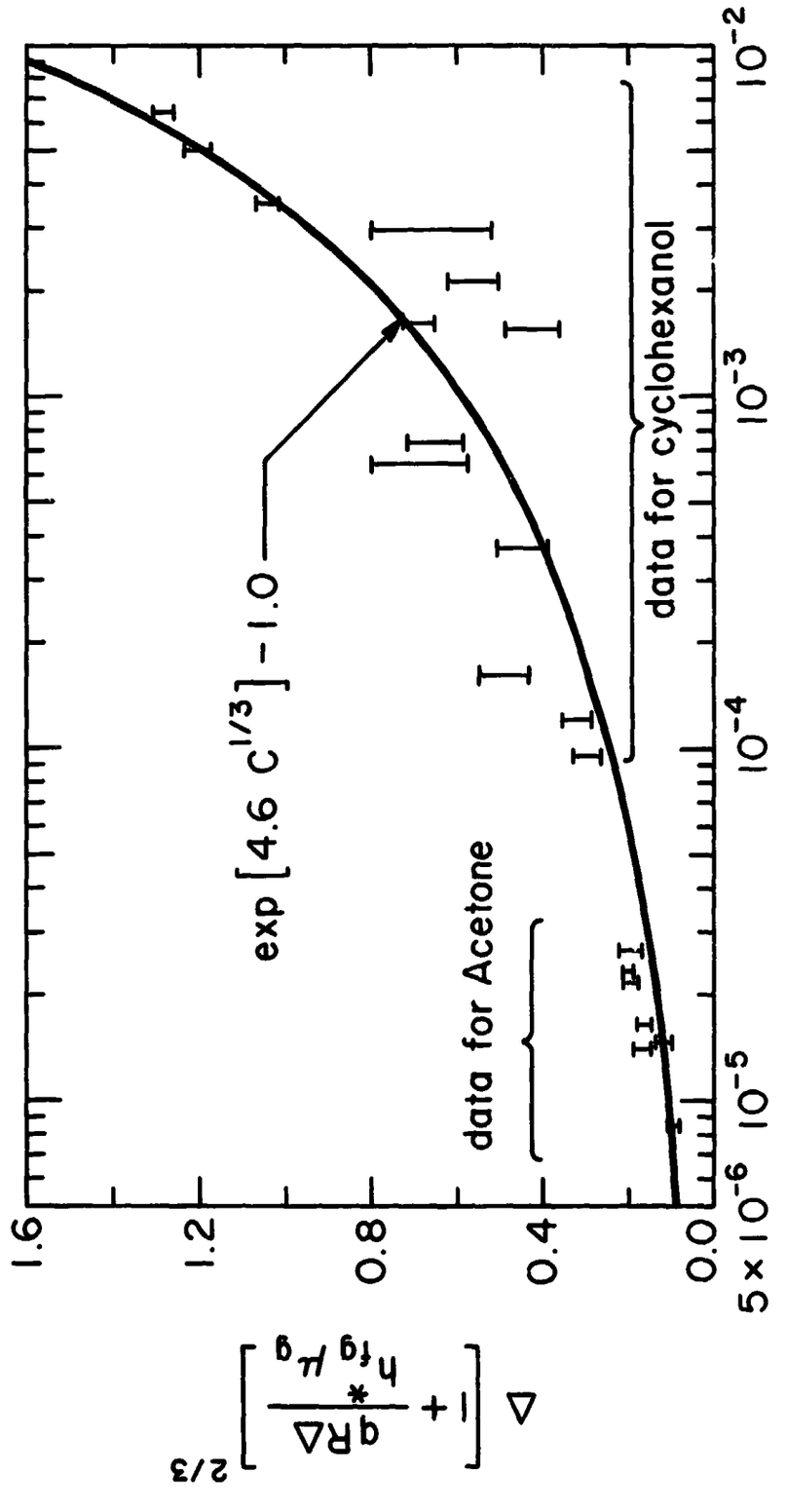

Fig. 8 Correlation for vapor blanket thickness.

et thickness on wires in the range $0.11 \leq R' \leq 0.65$ during the film boiling of acetone and cyclohexanol. While the abscissa is the same as Baumeister and Hamill's, the vapor blanket thickness has been correlated with the Reynolds number as an additional parameter. This correction has been obtained by trial and error procedure and as yet, no theoretical reason is offered for taking the exponent in the inertia correction term to be 2/3. It may also be mentioned that in forming the vapor blanket thickness correlation, all of the vapor properties have been evaluated at the mean film temperature.

In all the observations the group, $qR\Delta/\mu_g h^*_{fg}$, varied approximately from 0.2 to 2.5. Smaller values of this group usually occur near the left hand side of the figure. The data scatter represents minimum and maximum measurements of vapor blanket thickness. The accuracy of these measurements is ±10 percent. The data seem to be correlated well by the solid line whose governing equation is:

$$\Delta = \frac{\left\{4.60\left[\frac{q\mu_g}{\rho_g h^*_{fg}\sigma}\right]^{1/3}\left[\frac{1}{1+9R'^2(1+\Delta)^2}\right]^{1/3}\right\} - 1}{\left[1+\frac{qR\Delta}{\mu_g h^*_{fg}}\right]^{2/3}} \qquad (68)$$

The constant, 4.60, in equation (68) would correspond to a value of 0.32 instead of 0.23 for the constant in front of equation (61).

2. Comparison of Theoretical Predictions of the Wavelength with Experiment.

Observed wavelengths for cyclohexanol boiling at a temperature of 302.5K, corresponding to absolute pressure of 0.296 kPa, are displayed in Figure 9. The value of the liquid viscosity parameter, M, is close to 5. The theoretical prediction for the viscous case is shown in a solid line. The dotted line marks the inviscid predictions. The wire radius has been corrected to R_c to take into account the thickness of the vapor blanket surrounding it.

Although wavelengths were measured for various heat fluxes, those displayed in Figure 9 correspond to the lowest heat flux. This is done to avoid the longer wavelengths which may be favored at higher heat fluxes. We will discuss this point later in the text. The data show a wide variability, but the lowest points in the range of the data scatter do embrace the theoretical predictions which assume that the dominant wavelength is the "most susceptible" one. The inviscid predictions would have suggested wavelengths about 28 percent too short.

Figure 10 shows photographs of film boiling for two of the data points in Figure 9. Although there is slight phase difference across the length of the wire, the Taylor wave is very well developed. The bubble release pattern is good. The process is

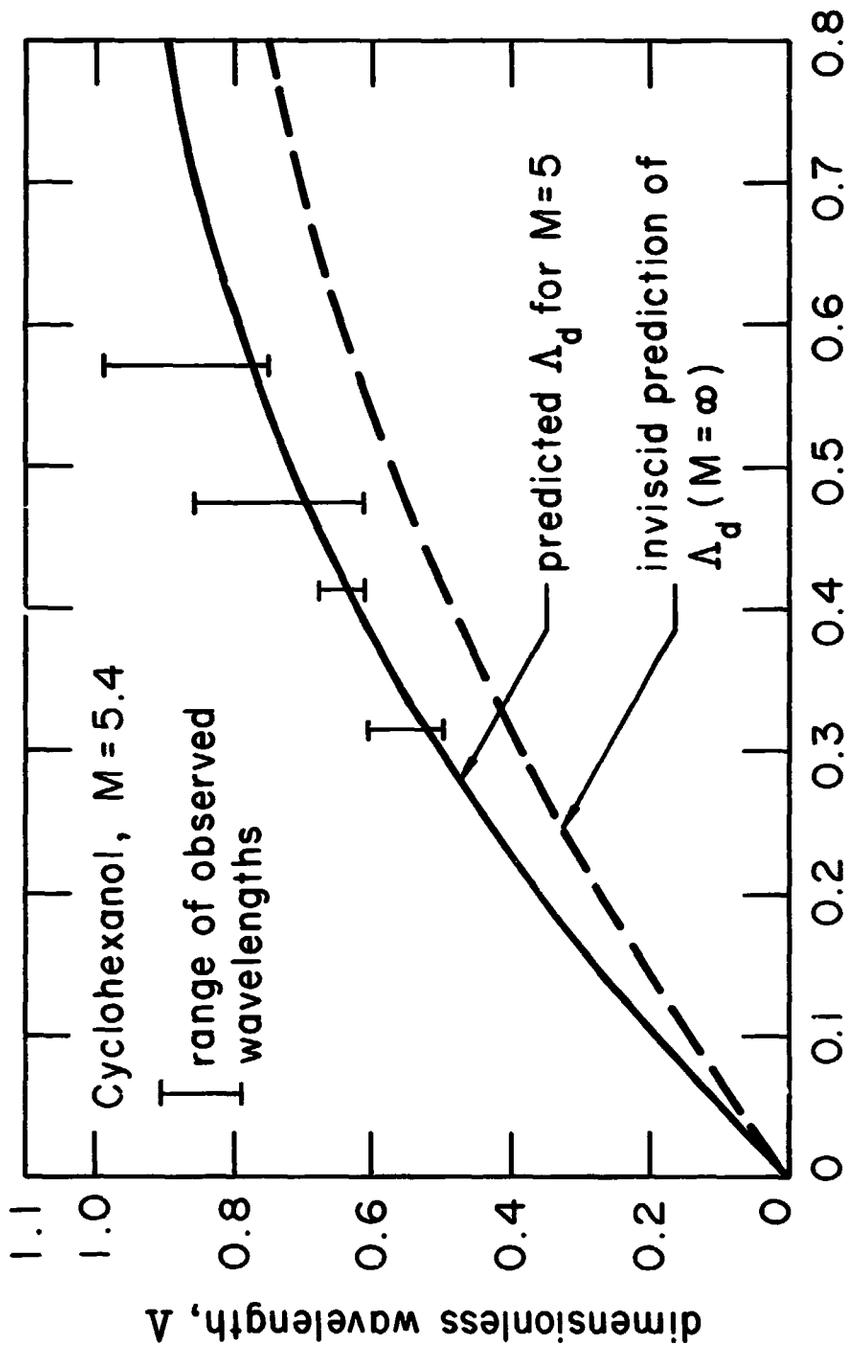

Fig. 9 Wavelengths on horizontal cylinders.

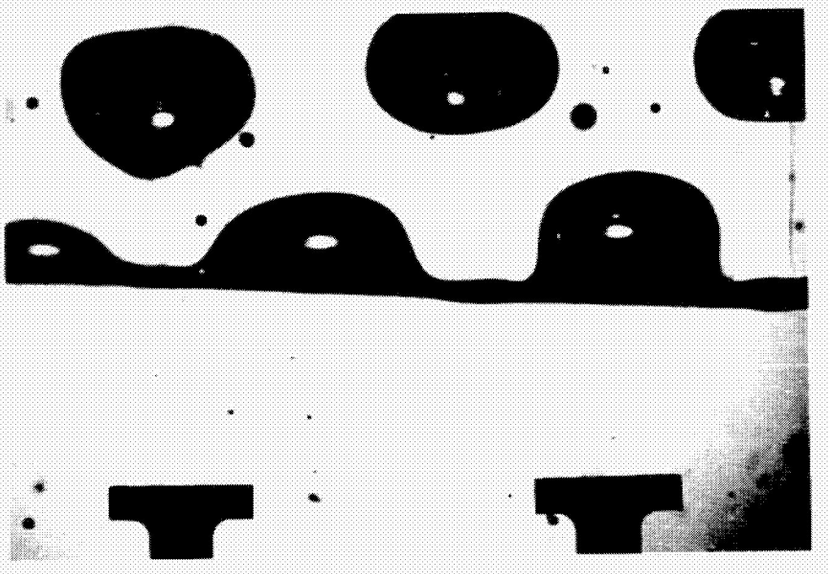

R' = 0.23 R'_c = 0.33

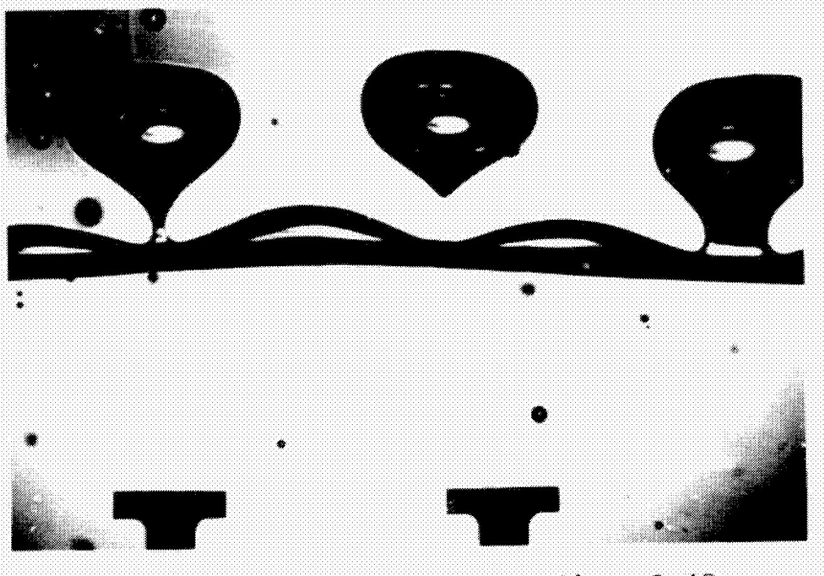

R' = 0.34 R'_c = 0.43

Fig. 10. Film Boiling of Cyclohexanol. M = 5.4

slower and viscosity seems to have dampened the small interfacial disturbances which may be observed in less viscous liquids.

Wavelength data for M=16 are plotted in Figure 11. Here the absolute pressure is 1.06 kPa and the saturation temperature is 329K. In this case, observed wavelengths are higher and the data again show wide variability. This variability in data could be explained from the dispersion relation shown in Figure 5. Near the maximum frequency there is a wide region of near-neutral stability. Thus, for frequencies slightly less than the maximum, a large range of wavelengths close to λ_d is possible.

3. Wave Growth Rate Analysis.

Figures 12, 13 and 14 display plots of dimensionless wave amplitude versus time on semi-logarithmic coordinates in an increasing order of R'. In all cases, the liquid viscosity parameter, M, for cyclohexanol is 16. The data contained in these figures are for two to three randomly-picked, regularly-growing waves during 5 to 10 seconds of motion pictures of film boiling.

All the figures reveal that bubbles grow linearly during the first 12 percent or so of growth. This is the period during which we would expect our theoretical predictions of the frequency to be valid. Occasionally during the early growth of a bubble, an oscillation of the interface was observed. This was probably caused

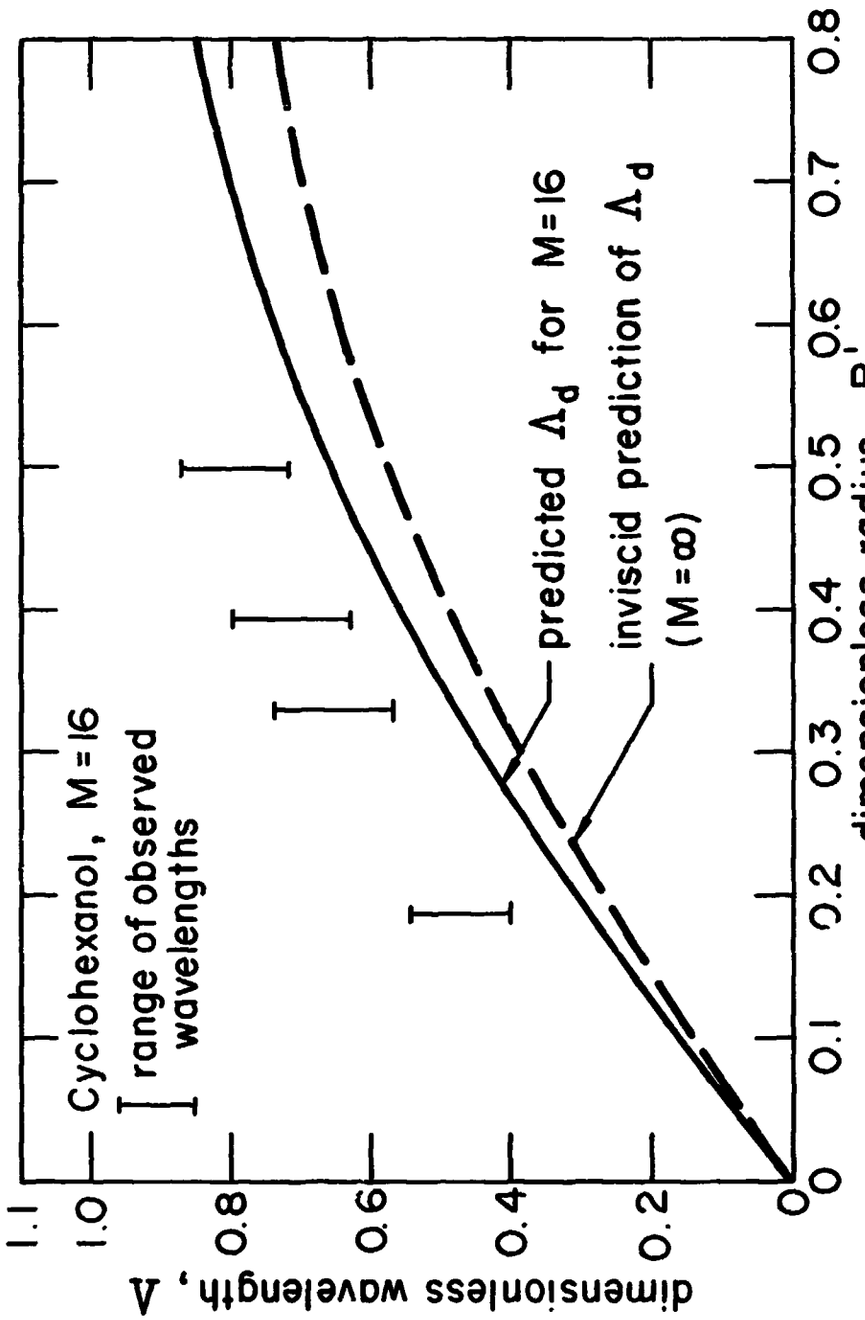

Fig. 11 Wavelengths on horizontal cylinders.

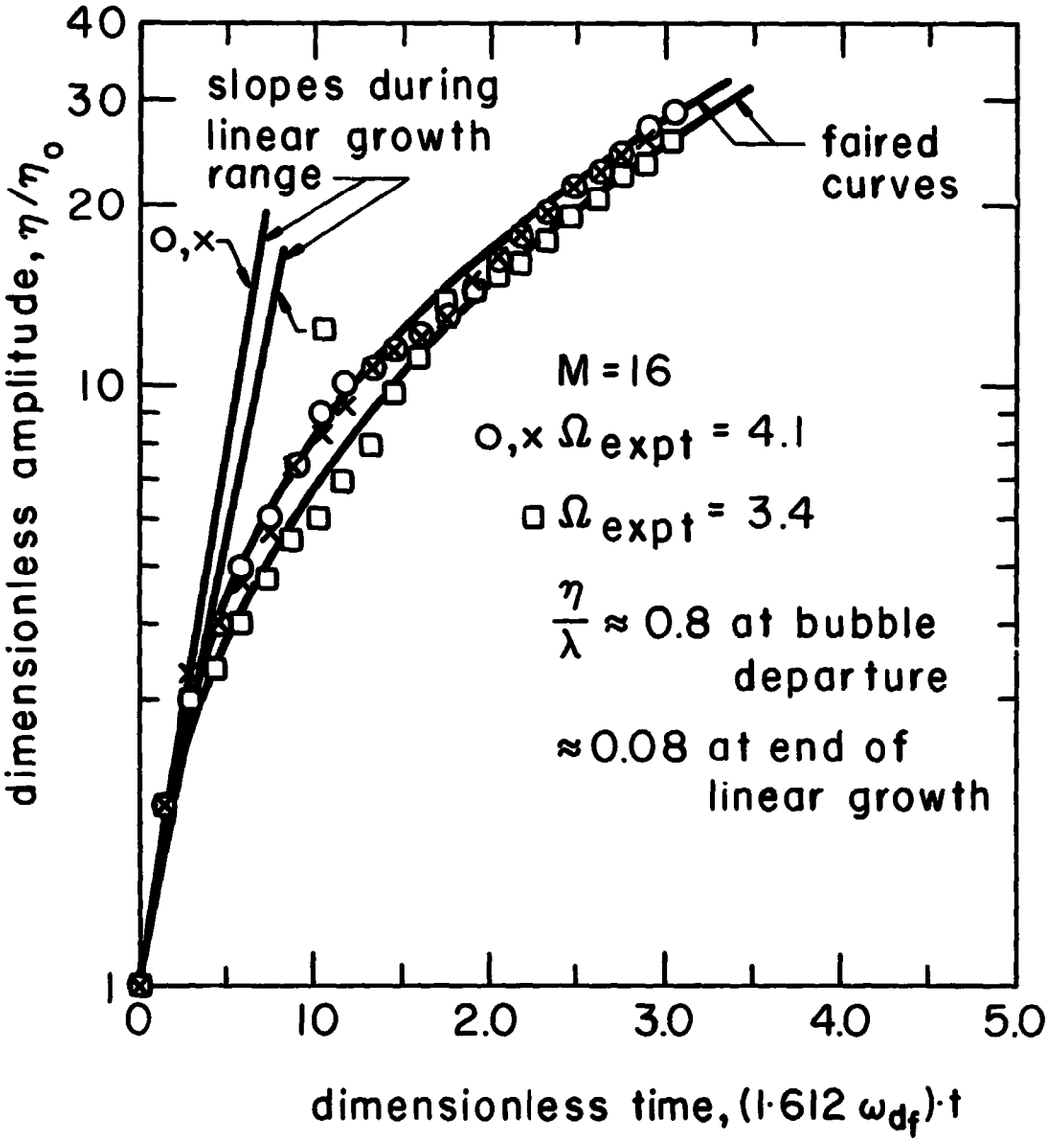

Fig. 12 Growth of waves on a 0.406 mm dia wire heater in cyclohexanol. P = 1.06 kPa, $q = 0.85 \times 10^5$ watt/meter^2, f_b = 23 bubble/sec., ω_{d_F} = 45.5 hertz, R' = 0.11, R'_c = 0.185.

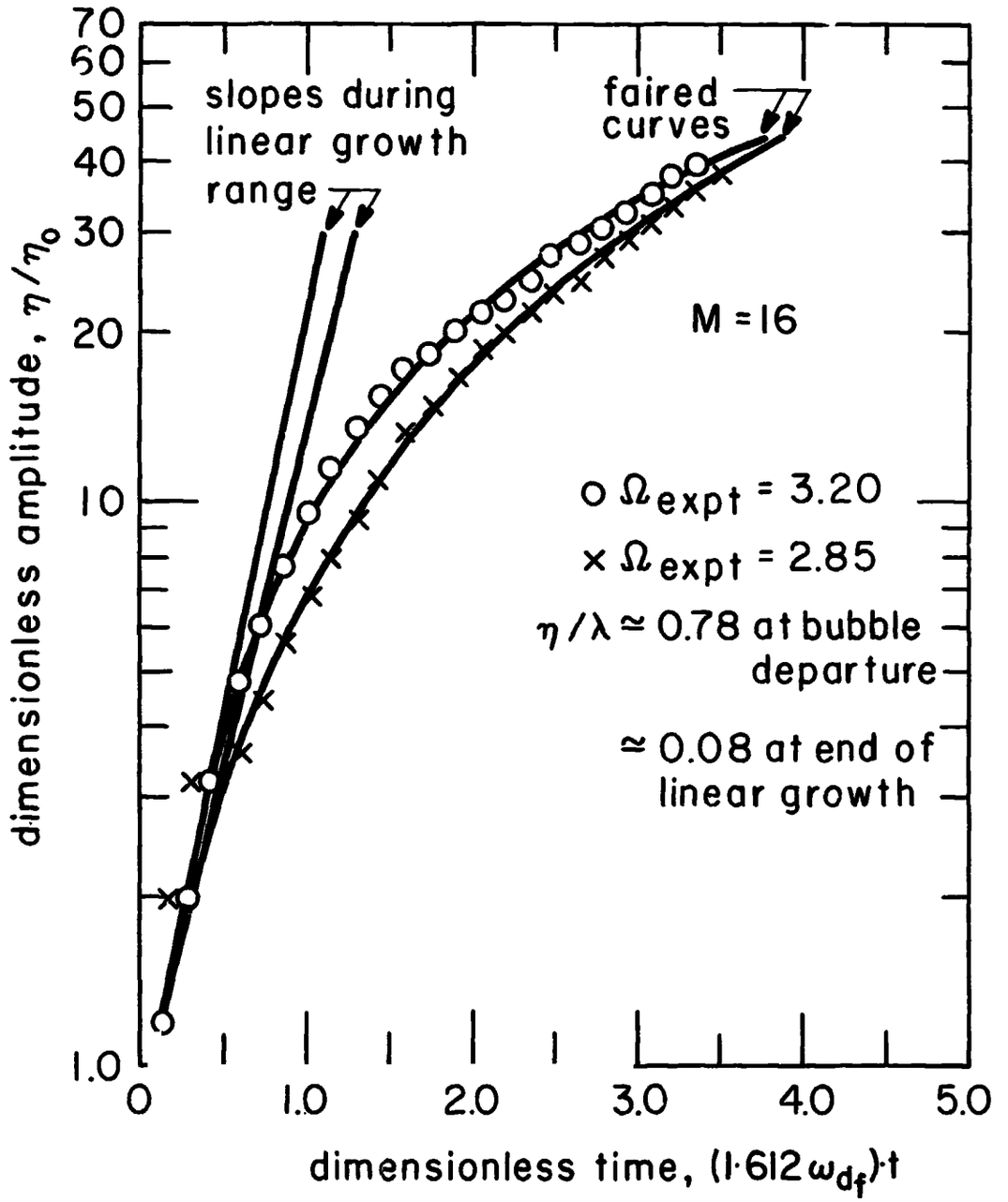

Fig. 13. Growth of waves on a 0.51mm dia wire heater in cyclohexanol. P = 1.06 k Pa, $q = 0.86 \times 10^5$ watt/meter^2, $f_b = 20$ bubble/sec, $\omega_{d_F} = 45.5$ hertz, $R' = 0.14$, $R'_C = 0.22$

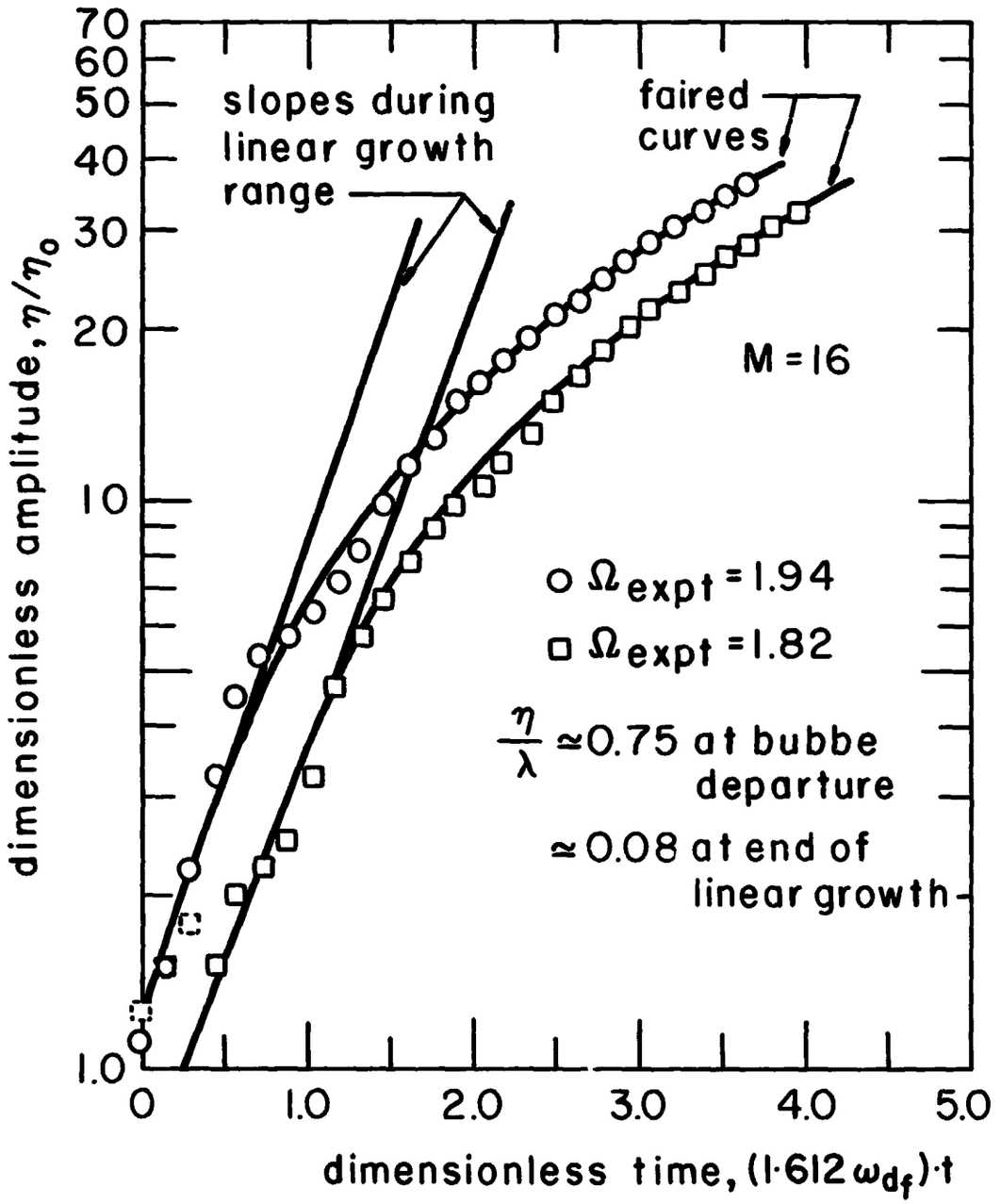

Fig. 14 Growth of waves on a 0.825 mm dia wire heater in cyclohexanol. P = 1.06 k Pa, $q = 1.01 \times 10^5$ watt/meter^2, $f_b = 18$ bubble/sec, $\omega_{d_F} = 45.5$ hertz, $R' = 0.22$, $R'_c = 0.33$

by the superposition of a disturbance evident in the wake of a departing bubble. Such a disturbance is evident in the wake of the left-hand bubble in the bottom picture in Figure 10. Data corresponding to such disturbances have been identified with dotted symbols in the wave growth rate diagrams. One may also note that the bubble grows in height to about 75 or 80 percent of the wavelength before it leaves the interface.

Having measured the frequency corresponding to a linear growth rate and the dominant wavelength, we next wish to see how well the two compare with the predicted dispersion relation. In Figures 15, 16 and 17 we trace the dispersion relations for the three dimensionless corrected radii and M=16, and we display the experimental points on them. The relation between wavelength and frequency is borne out quite well in each case. It is clear that wavelengths with frequencies slightly less than the "most susceptible" frequency can easily occur. In Figure 18, observed frequencies are plotted as a function of R_c' along with the viscous and inviscid predictions. The data fall slightly below the viscous predictions, but the inviscid theory would have predicted still higher frequencies.

Wave growth rates for M equal to 52 and 68 are plotted in Figures 19 and 20. In both cases, R_c' is 0.41. The wavelength and frequency are again consistent with the dispersion relation.

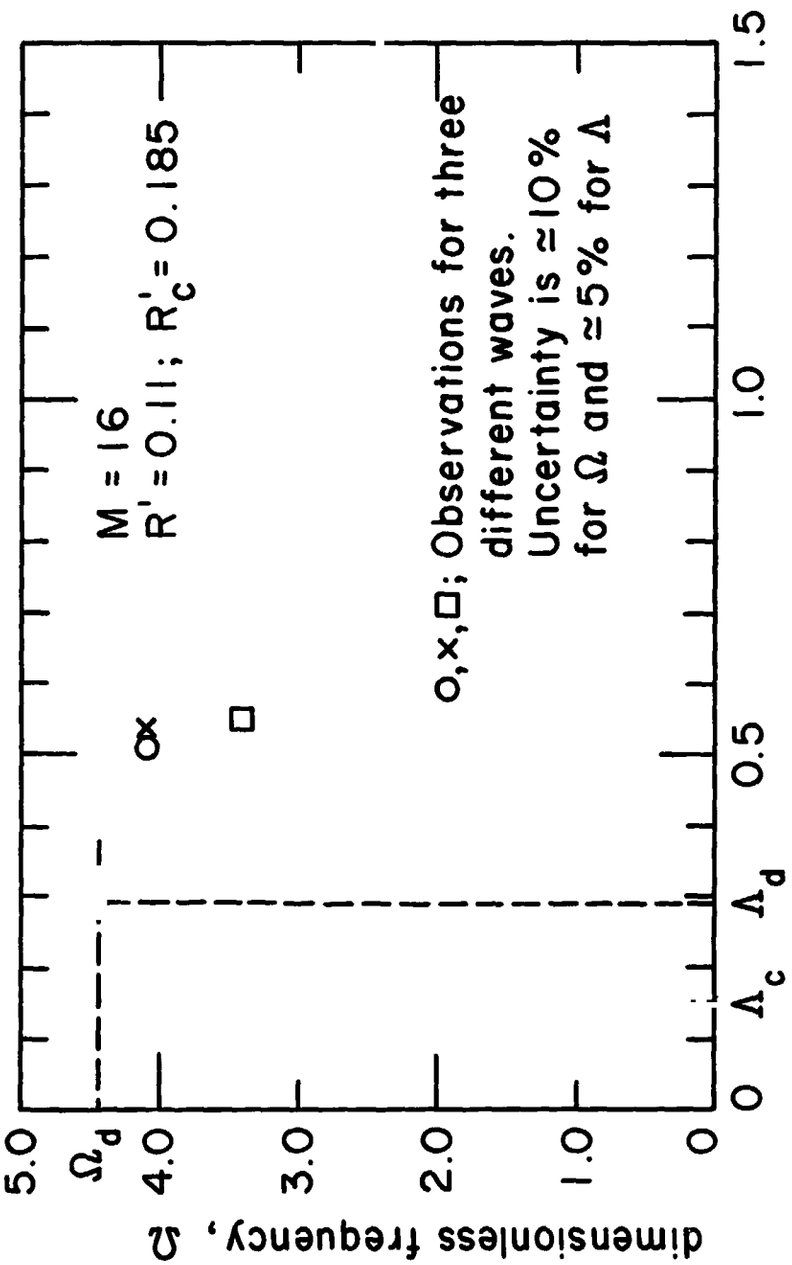

Fig. 15 Experimental verification of dispersion relation for cyclohexanol at 1.06 kPa. $q = 0.85 \times 10^5$ watt/meter^2.

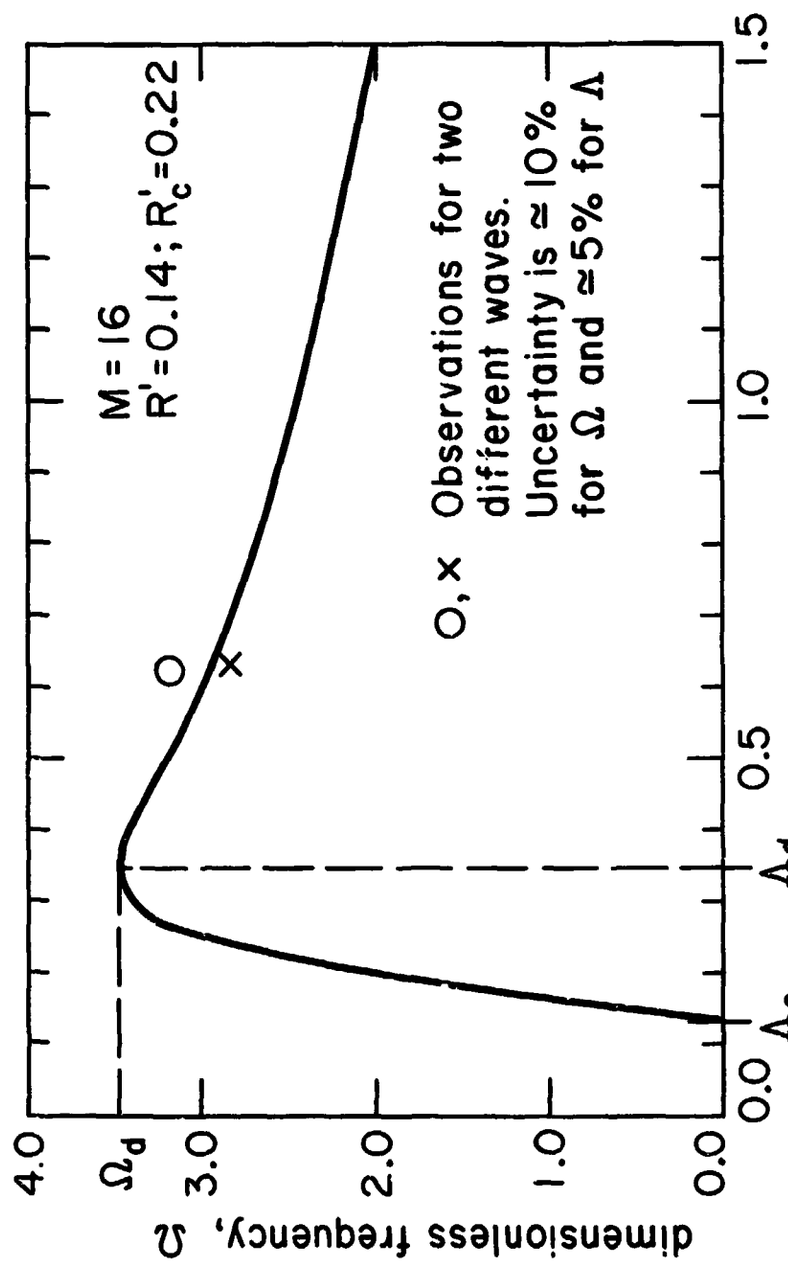

Fig. 16 Experimental verification of dispersion relation for cyclohexanol at 1.06 kPa.
$q = 0.86 \times 10^5$ watt/meter^2.

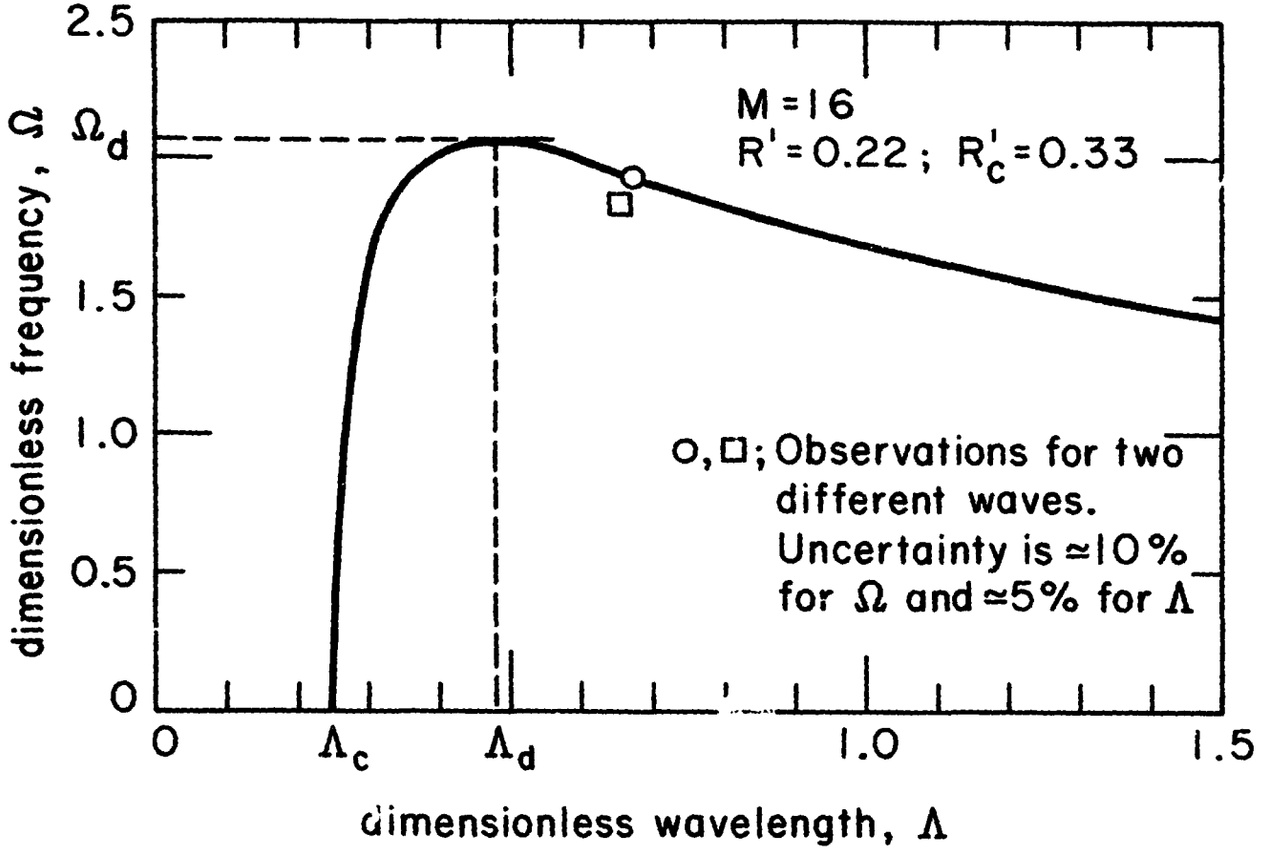

Fig. 17 Experimental verification of dispersion relation for cyclohexanol at 1.06 k Pa. $q = 1.01 \times 10^5$ watt / meter^2.

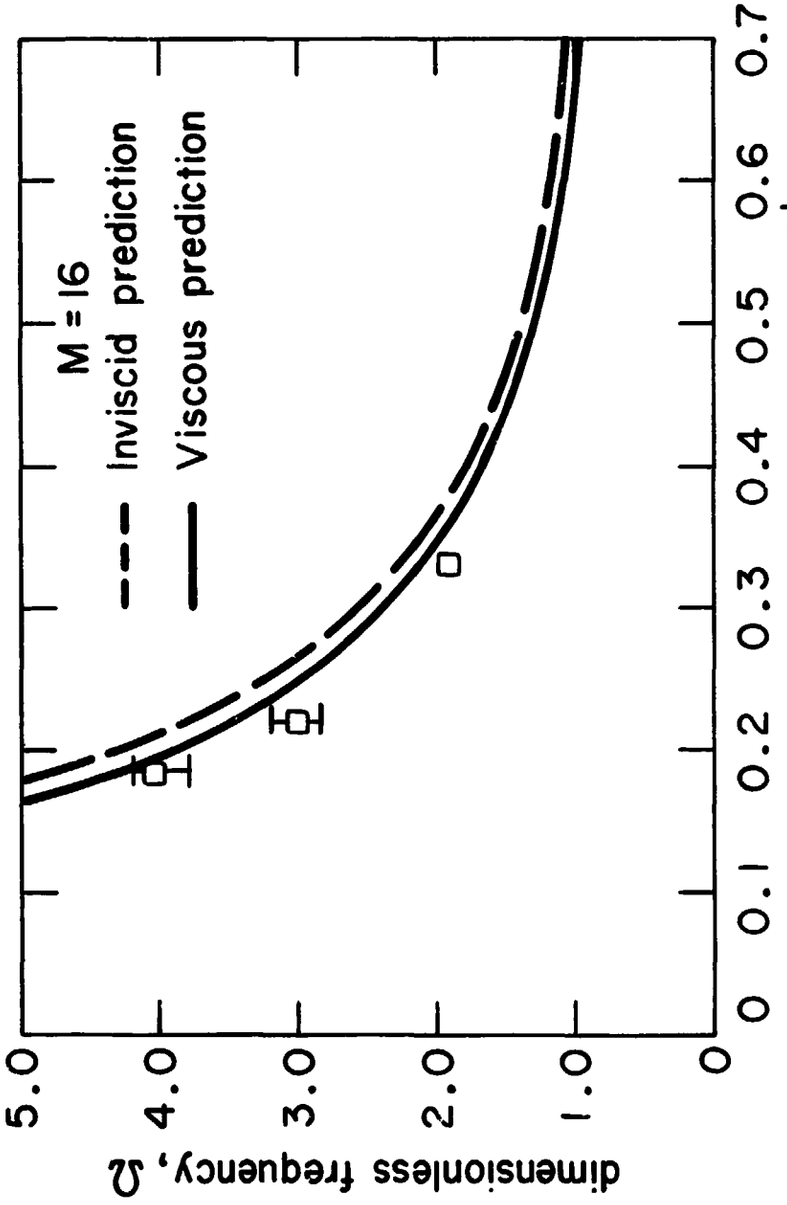

Fig. 18 Experimental observation of frequency of dominant wavelength on cylinders.

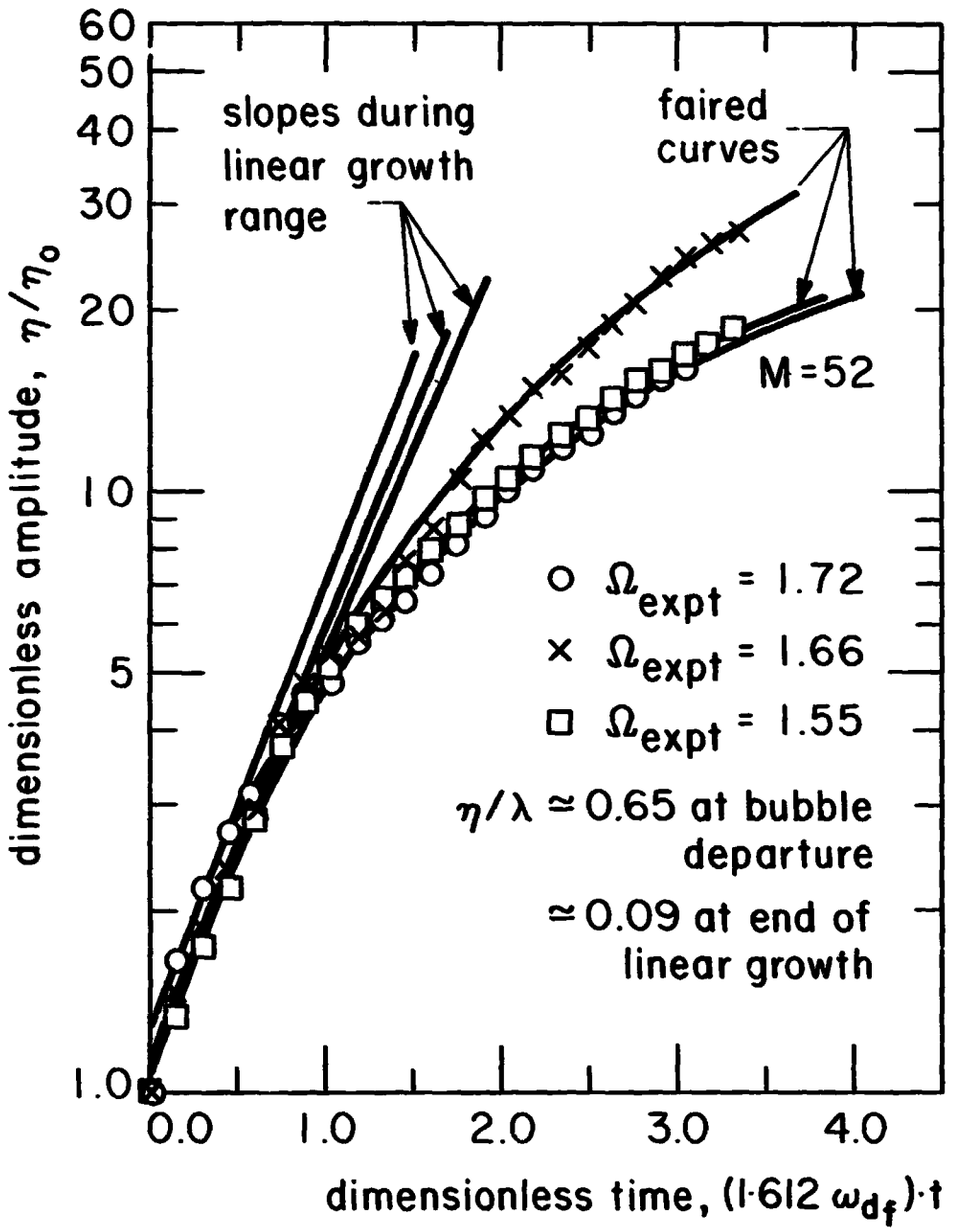

Fig. 19 Growth of waves on a 1.03 mm dia wire heater in cyclohexanol. P=4.9 kPa, $q = 0.85\times10^5$ watt/meter^2, f_b = 21 bubble/sec, ω_{d_F} = 46.3 hertz, $R' = 0.29$, $R'_c = 0.41$.

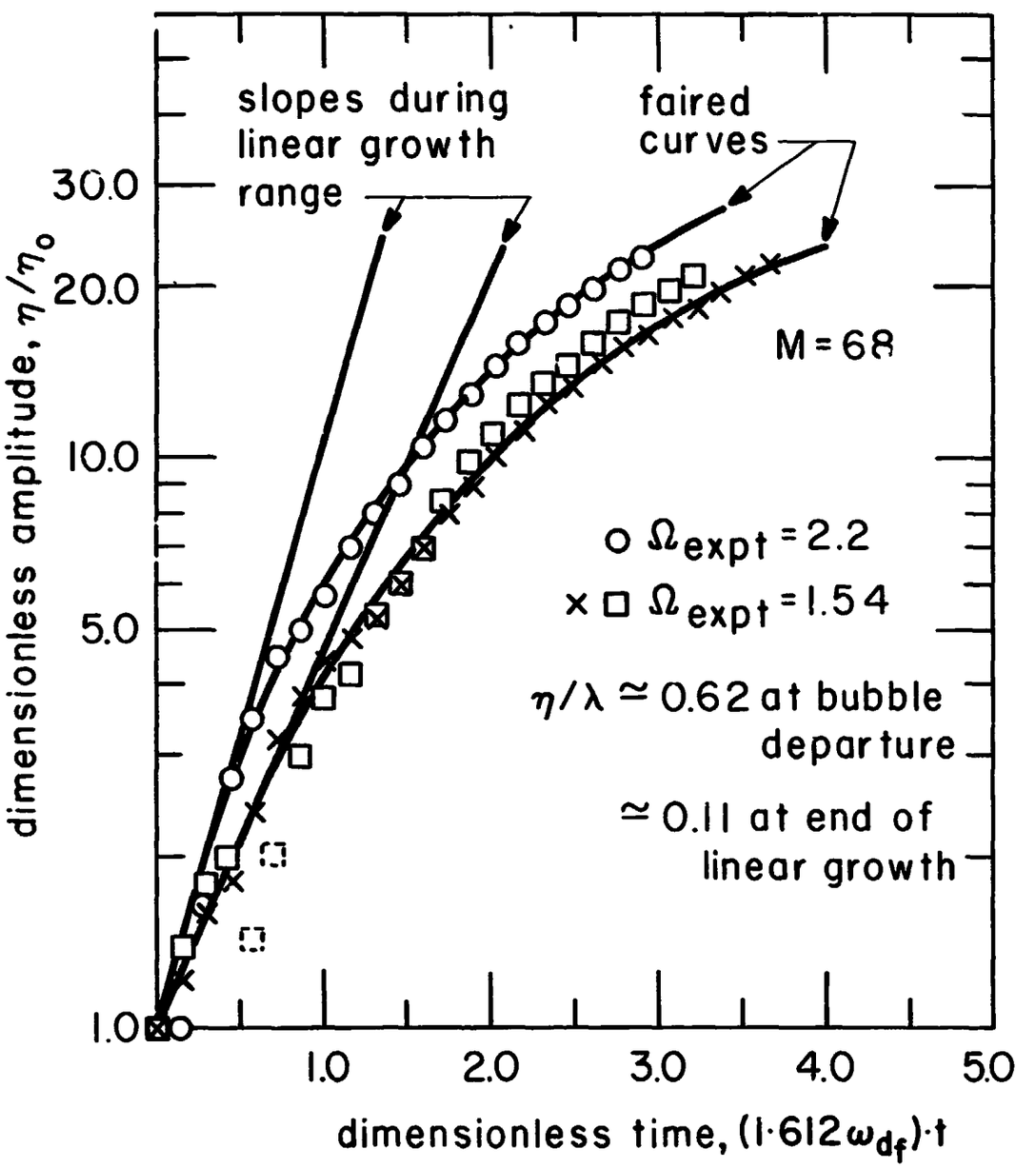

Fig. 20 Growth of waves on a 1.03 mm dia wire heater in cyclohexanol. P = 8.05 k pa, q = 0.98×10^5 watt/meter^2, f_b = 22 bubble/sec, ω_{d_F} = 46.5 hertz, R' = 0.295, R'_C = 0.41

Figures 21 and 22 show bubble growth during the film boiling of isopropanol on wires of R_c'=0.172 and 0.535 respectively. The liquid viscosity parameter has a value of 264, which means that there is very little, if any, effect of viscosity. The data presented in these figures have been reduced from high speed movies taken by Lienhard and Wong [30]. These movies were taken at 2500 ± 40 frames per second. The wave grows linearly during the first 15 percent of growth for R_c'=0.172 and the first 35 percent for R_c'=0.535. Figure 22 shows an oscillatory behavior of the interface during early growth, probably due to superimposition of a disturbance caused by the preceding departing bubble. We have attempted to ignore the disturbance again and to draw the line through the average growth curve. In Figure 23, observed frequencies for these low viscosity liquids are plotted as a function of R_c' and compared with theoretical predictions. The data tend to be low by only a small percent.

From the previous observations of growth rates, one may also note that the range of non-linear behavior starts earlier on smaller waves than it does on larger ones, and this effect seems to be enhanced by viscosity. This may be explained if one looks at the drag force experienced by a growing bubble. Keshock and Siegel [31] gave an approximate expression for the drag force as:

$$F_d = \frac{\pi}{16} C_1 \mu_f D \frac{dD}{dt} \tag{69}$$

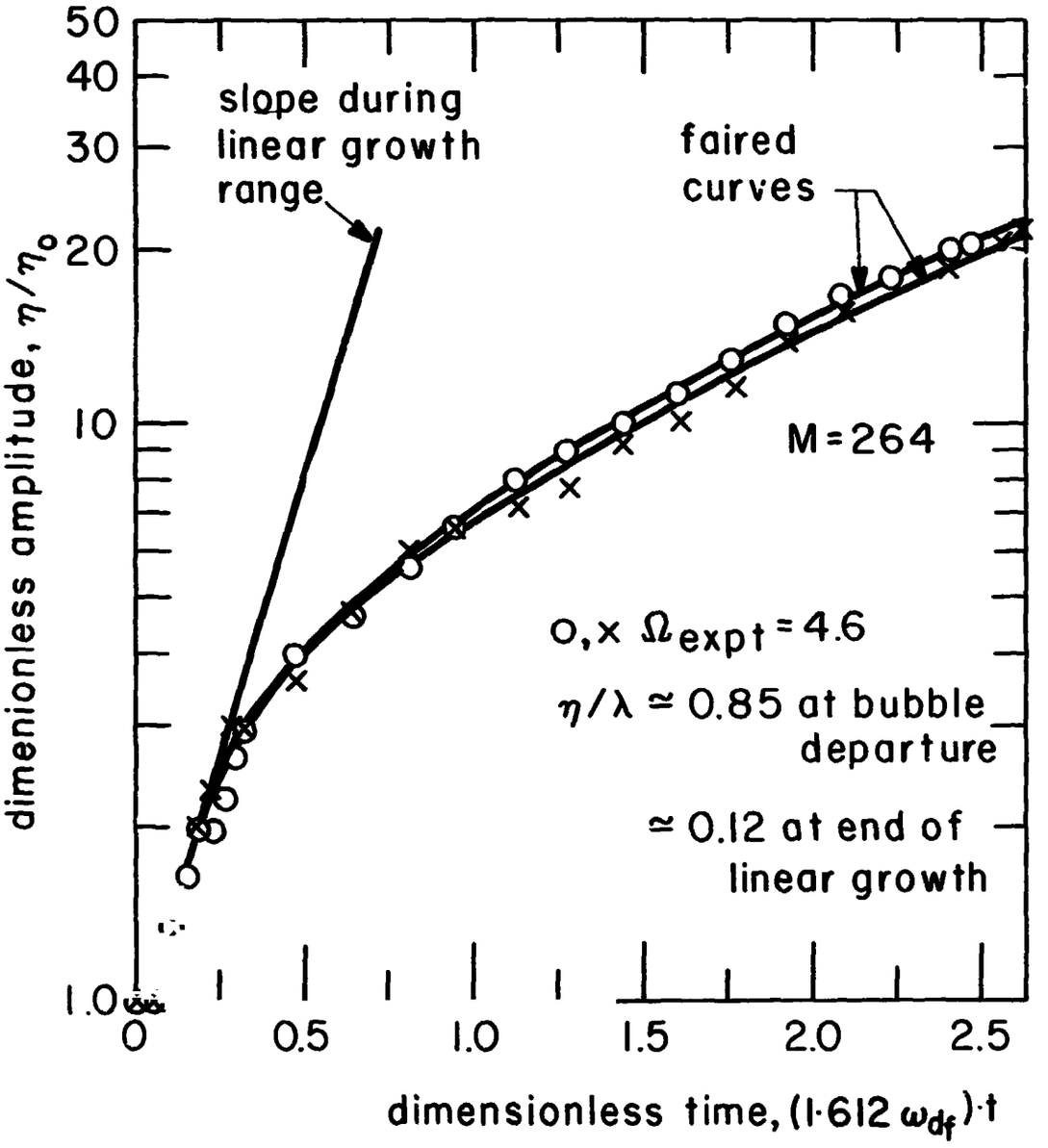

Fig. 21 Growth of waves on a 0.406 mm dia wire heater in Iso-propanol. P= 98.5 k pa, $q = 1.7 \times 10^5$ walt/meter^2, f_b = 31 bubble/sec, ω_{d_F} = 50.0 hertz, $R'_{\cdot} = 0.13$, $R'_c = 0.17$.

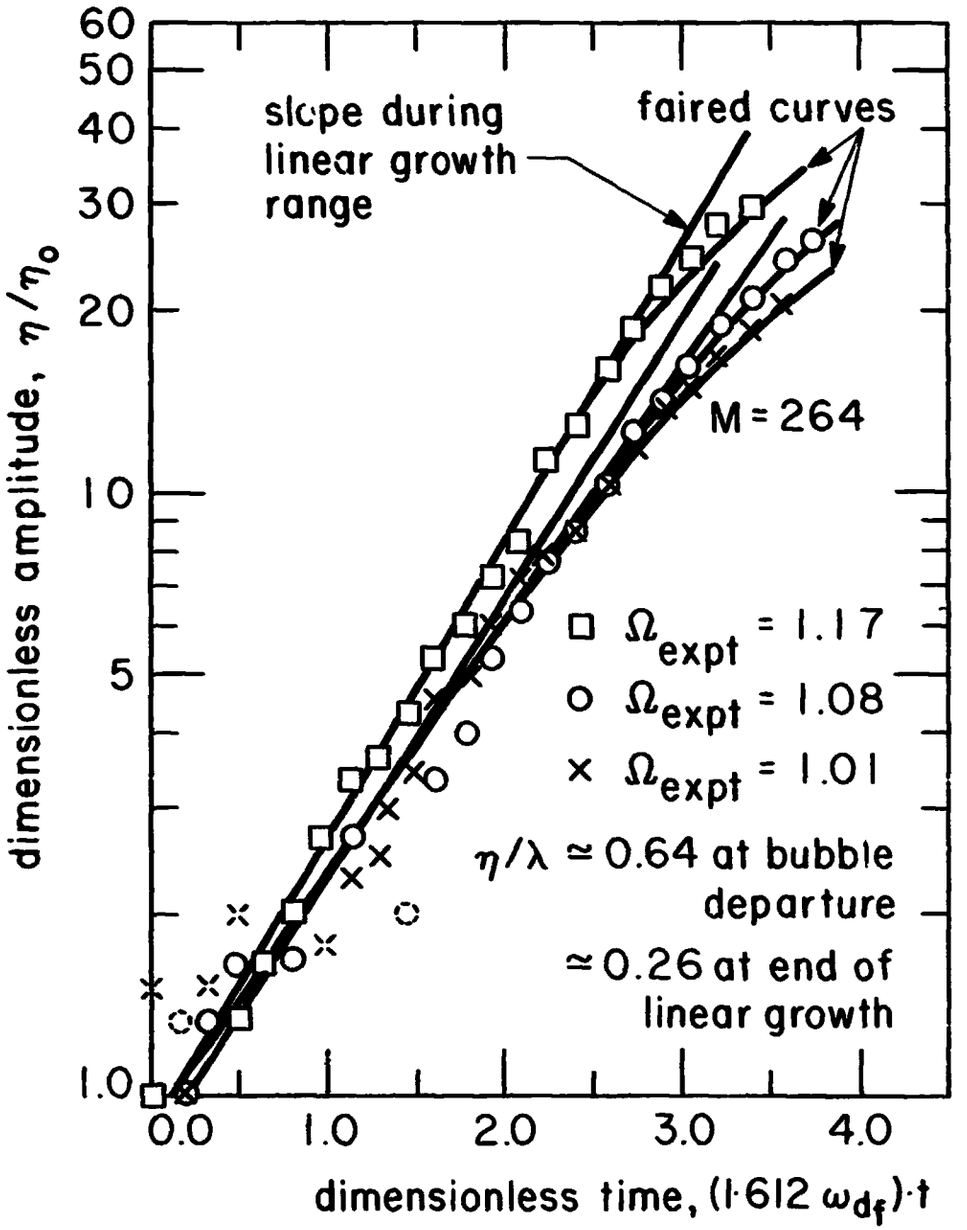

Fig. 22 Growth of waves on a 1.295 mm dia wire heater in cyclohexanol. P = 98.5 kPa, $q = 0.514 \times 10^5$ watt/meter^2, f_b = 21 bubble/sec, ω_{d_F} = 50.0 hertz, $R' = 0.425$, $R'_c = 0.54$.

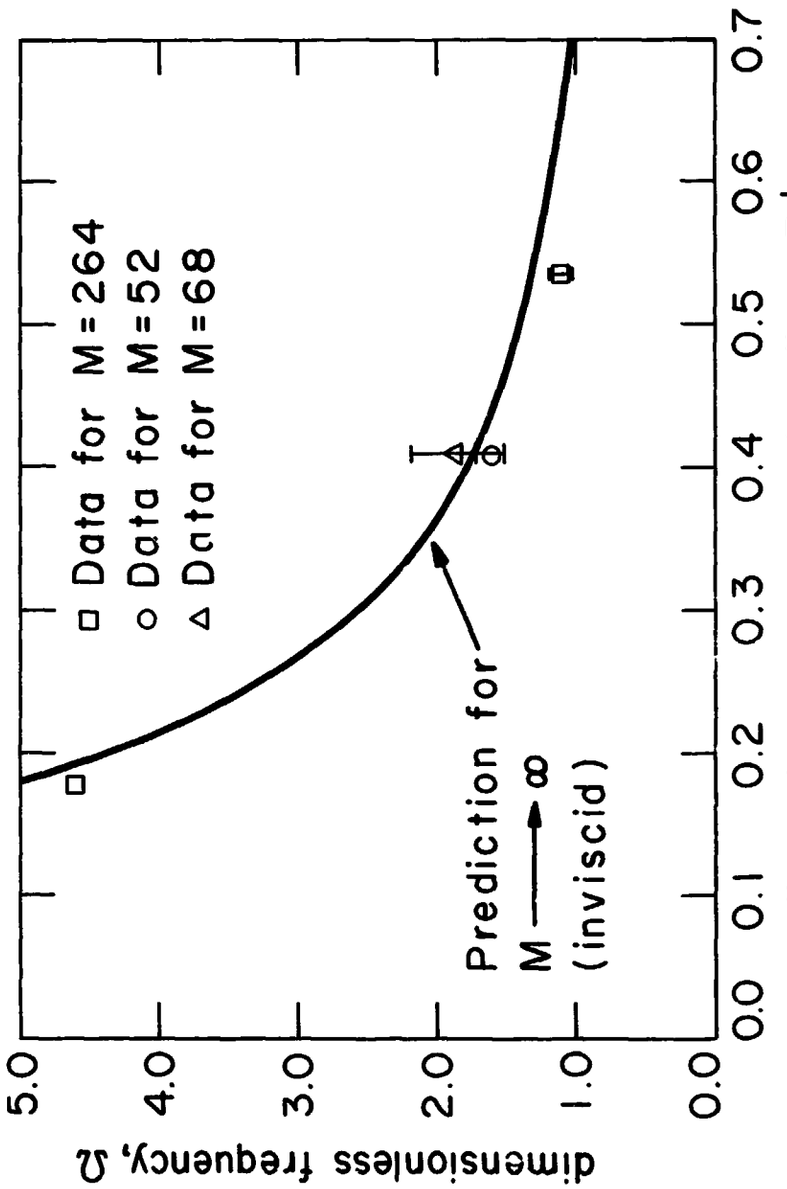

Fig. 23 Experimental observation of frequency of dominant wavelength on cylinders.

where D is an equivalent spherical diameter for the bubble and C_1 is an experimental constant. If in our case, we take η to be the equivalent diameter of the bubble, equation (67) can be written as:

$$F_d \sim \mu_f \, \eta \, \frac{d\eta}{dt} \tag{70}$$

Since $\frac{d\eta}{dt}$ is constant during linear growth it may be taken to be a function only of the dominant wavelength, i.e.,

$$\frac{d\eta}{dt} = \omega = f(\lambda) \tag{71}$$

For a particular value of η, the drag force increases with liquid viscosity and ω; but ω is higher for smaller wavelengths. Thus during early growth, small bubbles or bubbles growing in viscous liquids may experience more drag. Hence, they approach the non-linear growth regime sooner.

4. Bubble Release Frequency.

While viewing movies for the bubble growth analysis, we also noted the average time after which a bubble was released from a node. The bubble release frequency, f_b, is found by noting the number of bubbles released per second. In Figure 24 we plot the dimensionless bubble frequency as a function of observed wavelength for both the viscous and the inviscid cases. A line obeying the conditions: $f_b = 0$ at $\lambda \simeq 0$ and $df_b/d\lambda \to 0$ at $\lambda = \lambda_d$ for the

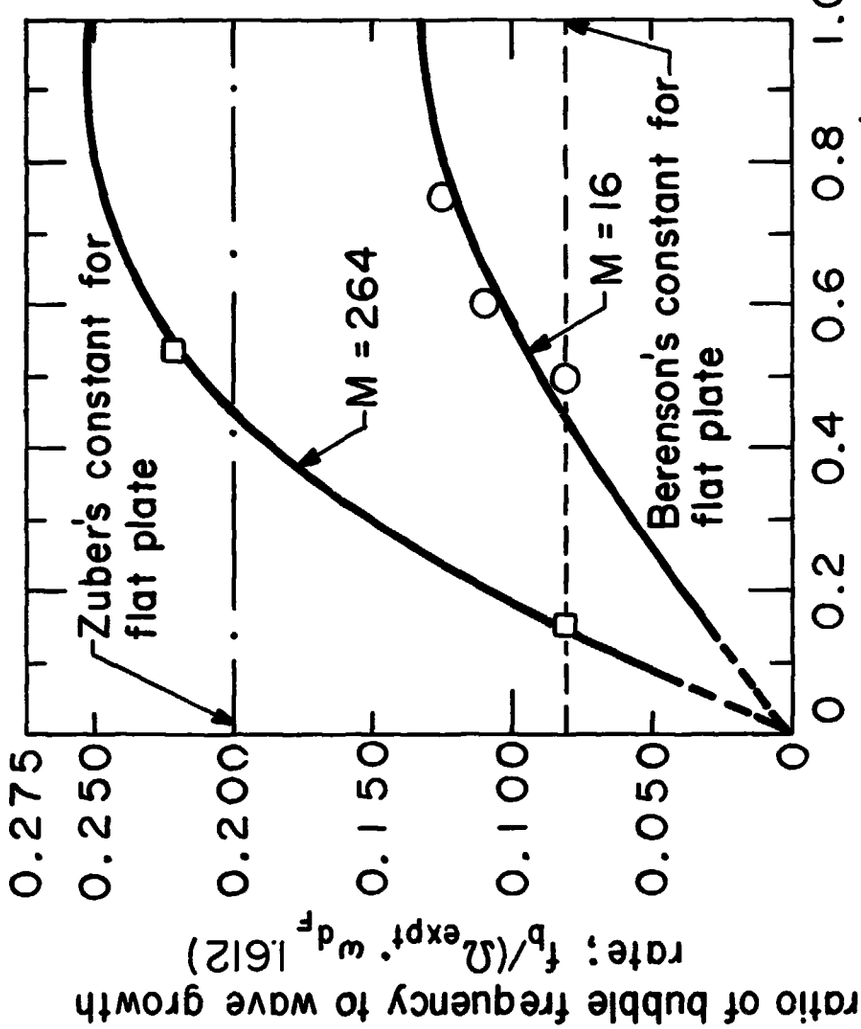

Fig. 24 Effect of viscosity and wavelength on bubble departure frequency.

flat plate, has been faired through the data.

The wavelength and liquid viscosity seem to strongly influence the ratio of the two frequencies. The "chained" line shows the value of f_b/ω_{d_F} assumed by Zuber in his prediction of the minimum heat flux on flat plates. Zuber obtained an average value for this number by averaging the growth rate over amplitude. The dotted line shows the value of f_b/ω_{d_F} as proposed by Berenson. He argued that the growth rate should be averaged over the time the bubble takes to grow to its full size and breaks off from the interface. Such an average requires full history of bubble growth. Berenson did not have this information; instead he fixed the value of f_b/ω_{d_F} empirically from the known experimental values of minimum heat flux on flat plate heaters.

Our data suggest an asymptotic value of 0.25 for $f_b/(\Omega_{expt}\omega_{d_F}1.612)$ when the liquid viscosity is small and this number decreases as liquid viscosity is increased.

5. Effect of High Volume Fluxes on the Dominant Wavelength.

In the previous sections we saw that frequently wavelengths longer than the "most susceptible" wavelength occur in real systems. These waves obeyed the dispersion relation well, though they did not assume exactly the maximum frequency. As most of our experiments were conducted at very low pressures, we pre-

sume that the longer, slower-moving waves are preferred when large volume fluxes are generated. Large volume fluxes may also be caused by high heat fluxes. On the other hand, shorter waves may be preferred when small volume fluxes occur. The film boiling studies of carbon dioxide near its critical point by Abadzic, Grigull and Goldstein [32,33] show the presence of nearly stationary waves with wavelengths close to the critical value. In this case the volume flux is quite low.

In Figure 25 we display dimensionless wavelength as a function of volume flux for horizontal cylinders. Wavelength data have been obtained both at low pressures and high heat fluxes. The coordinates have been reduced to dimensionless inviscid flat plate values so that the data obtained at different situations can be compared. A definite increase in the dominant wavelength seems to take place with volume. Photographs of the film boiling process at different heat fluxes are shown in Figure 26. The longer wavelengths at the larger volume flux in the bottom picture can easily be distinguished from the shorter wavelength in the top picture.

6. Some Remarks on the Minimum Heat Flux.

Various previous authors [18], [20] have pointed out that many physical variables, such as material of the wire, the end

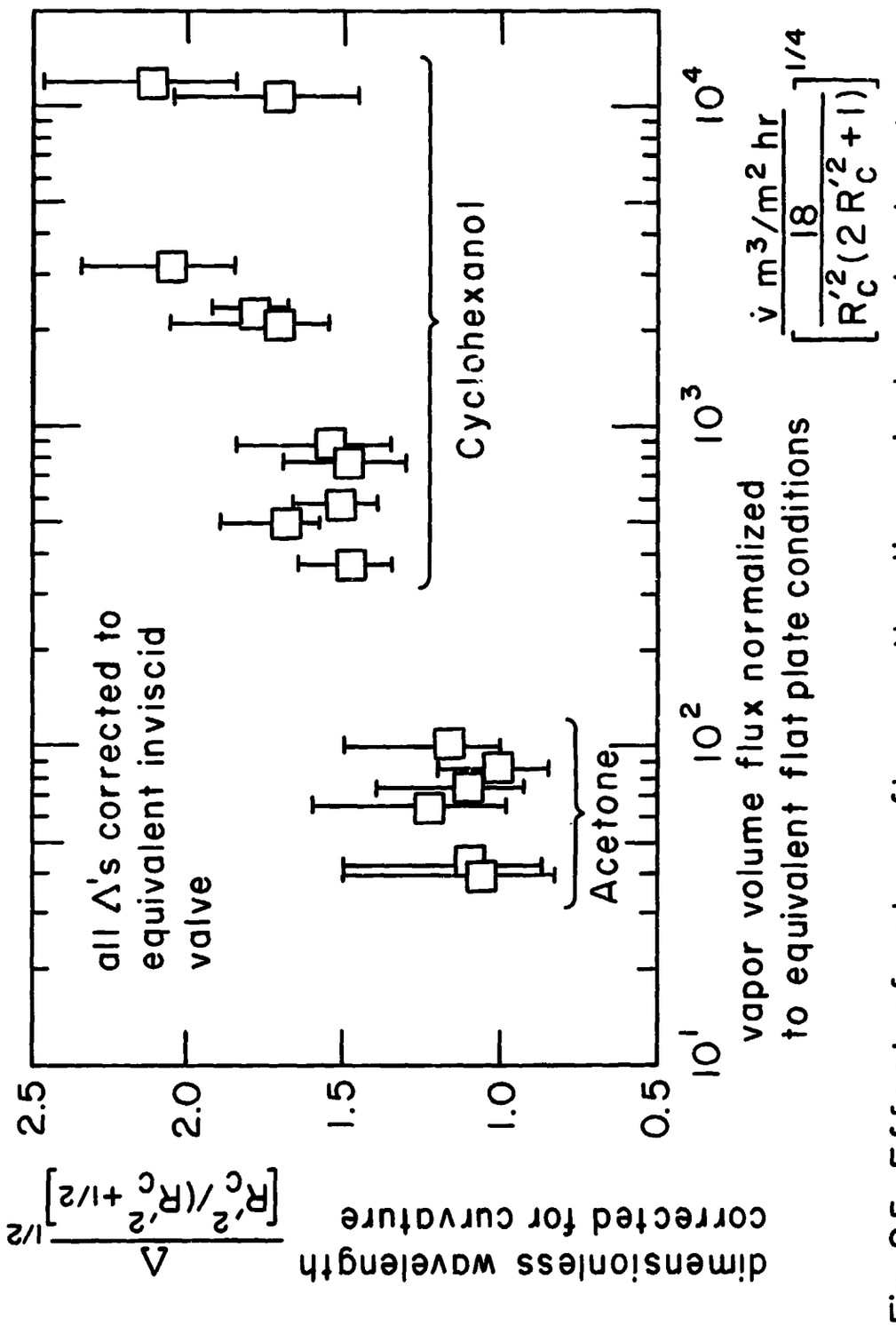

Fig. 25 Effect of volume flux on the dimensionless dominant wavelength.

$R' = 0.23$, $R'_c = 0.32$, Volume flux = 4.95×10^4 meter^3/meter^{2}hr

$R' = 0.23$, $R'_c = 0.35$, Volume flux = 8.4×10^4 meter^3/meter^{2}hr

Fig. 26. Stretching of wavelengths due to higher volume fluxes.

mountings, the material and size of the wireholders, and the way the end mountings are attached to the wire, can seriously affect the observations of minimum heat flux. Data obtained under different conditions have been found to differ with each other by as much as 100 to 200 percent. With so many variables affecting the true location of the minimum heat flux, an elaborate experimental program would be needed to provide reproducible and meaningful results. Therefore, we did not make any special effort toward measuring the minimum heat flux in the present work.

In Chapter II we made theoretical viscous predictions of the minimum heat fluxes on both flat plates and cylindrical heaters, and concluded that they should increase with viscosity. As we saw in Chapter II, the minimum heat flux depends on the product of volume of the bubbles, the number of bubbles per unit heater area, and the bubble release frequency. Bubble volume varies as dominant wavelength cubed; the area of the heater per bubble is proportional to wavelength for cylindrical heaters and to wavelength squared for flat plate heaters. Furthermore, the bubble release frequency depends mostly on the large period of time during which a bubble grows non-linearly. This information can only be obtained experimentally.

Our experimental observations show that the bubble release

frequency decreases with liquid viscosity whereas the dominant wavelength increases with it. Hence, at this time it is very difficult to say quantitatively what the net effect of viscosity is on the minimum heat flux.

Conclusions.

1. An increase of wavelength with the liquid viscosity has been measured and found to compare well with the theoretical predictions.

2. The wavelength and frequency measurements are faithful to the predicted dispersion relation.

3. A successful correlation for the vapor blanket thickness around a cylindrical heater has been established.

4. The bubble release frequency seems to depend upon both the dominant wavelength and the liquid viscosity.

5. Generation of large volume fluxes may cause wavelengths that are considerably longer than the "most susceptible" wavelength to be favored.

IV. HYDRODYNAMIC PREDICTION OF THE PEAK HEAT FLUX IN INVISCID AND VISCOUS LIQUIDS ON LARGE FLAT SURFACES

Zuber and Tribus explained that the transition from nucleate to film boiling occured when vapor jets became Helmholtz unstable and collapsed, thereby obstructing the flow of liquid toward the heater. In obtaining the expression for the critical velocity of these jets, Zuber and Tribus employed the well known results for the interfacial stability of two parallel-flowing streams of inviscid liquids. This instability is caused by pressure fluctuations and is known as Kelvin-Helmholtz instability. They also assumed that the dominant disturbance on these jets was one with wavelength equal to critical Rayleigh wavelength.

In the first part of this chapter, we will review Zuber's hydrodynamic model of peak pool boiling heat flux on very large flat horizontal surfaces and reconstruct it wherever necessary. In the latter part, we discuss the instability of gas jets when both gas and liquid are taken to be viscous and use these results to obtain expressions for the peak heat flux.

A. Peak Pool Boiling Heat Flux When Both the Liquid and Gas are Assumed Inviscid.

Near the peak heat flux the rate of evaporation is very

high. The bubble generation frequency is so large that the vapor is released in the form of jets. If U_g is the velocity of gas in vapor jets and A_j is the combined area of vapor jets supported by an area A_h of the heater, a simple energy balance at the heater surface gives:

$$q = \rho_g h_{fg} U_g A_j / A_h \tag{72}$$

The gas velocity at which these jets become Helmholtz unstable [34] is given by:

$$U_{gc} = \sqrt{\frac{2\pi\sigma}{\rho_g \lambda_H}} \tag{73}$$

in which λ_H is the dominant wavelength of the disturbance that triggers instability of the interface between gas and liquid.

Zuber also reasoned that on a horizontal surface having no geometrical features these jets locate themselves on a two dimensional square grid spaced on the Taylor unstable wavelength. His assumed vapor removal configuration is shown in Figure 27. Zuber could not decide whether the length of the dominant unstable Taylor wave should equal the critical wavelength,

$$\lambda_c = 2\pi\sqrt{\sigma/g(\rho_f - \rho_g)} \tag{74}$$

or λ_d, the wavelength which has the fastest growth rate,

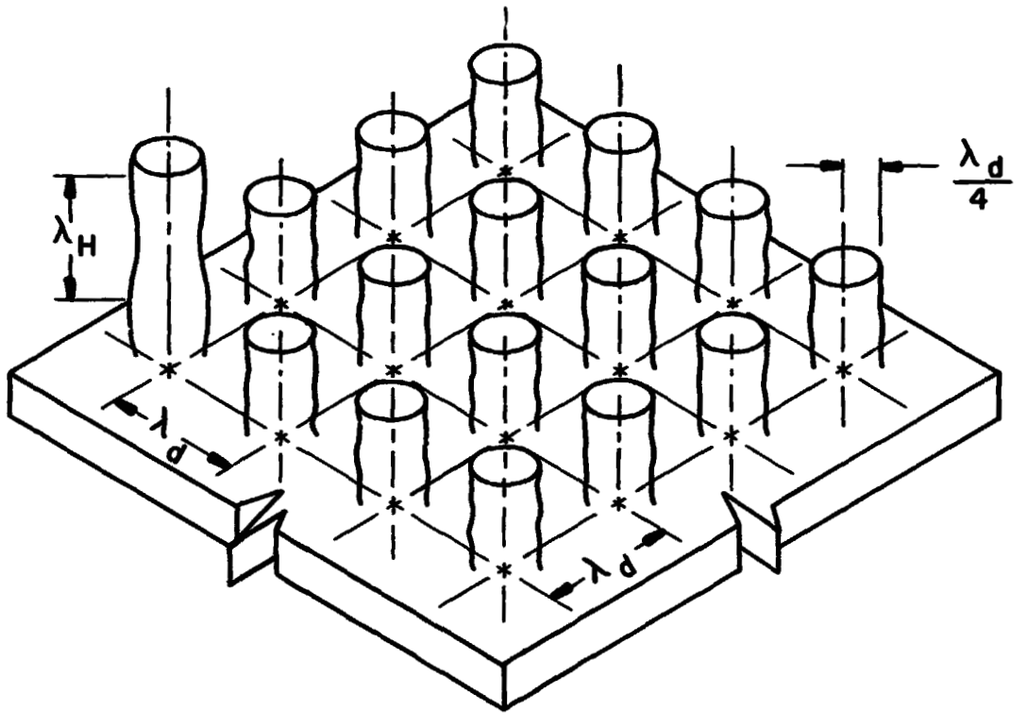

Fig. 27. Zuber's vapor removal configuration on an "infinite" flat plate.

$$\lambda_d = 2\pi \sqrt{3\sigma/g\,(\rho_f - \rho_g)} \qquad (75)$$

However, later studies of film boiling on cylinders [17,'20] and our observations in the preceding chapter have conclusively shown that the dominant wavelength is close to λ_d the "most susceptible" Taylor wavelength.

Zuber assumed that the diameter of a vapor jet was half of the spacing between the jets. Wong [17] substantiated this assumption by noting that the bubble diameter was half of the spacing between adjacent bubbles in film boiling on cylinders. Thus the ratio of area of the vapor jets to the area of heater is a constant:

$$\frac{A_j}{A_h} = \frac{\pi\left(\frac{\lambda}{4}\right)^2}{\lambda^2} = \frac{\pi}{16} \qquad (76)$$

The wavelength, λ_H, was assumed by Zuber to be the critical Rayleigh unstable wavelength(see,e.g.,[34] page 473 or [35]):

$$\lambda_H = 2\pi(\lambda_d \text{ or } \lambda_c)/4 \qquad (77)$$

Substituting equations (73) through (75) in equation (72) we get:

$$q_{max} = \frac{\pi}{24}\sqrt{\rho_g}\left[\sigma g(\rho_f - \rho_g)\right]^{1/4} h_{fg}\left[1.196 \text{ or } 0.909\right] \qquad (78)$$

depending on whether the correct wavelength was λ_c or λ_d. Instead, Zuber took the constant in the second square bracket to

be unity, which is a good mean value, and obtained equation (6) for peak heat flux on a flat plate.

Subsequent successful hydrodynamic predictions of the peak heat flux on cylinders [12], spheres [36] and on horizontally and vertically oriented ribbons [37] have assumed that the Taylor wave fixing the location of jets on the heater is also the "most susceptible" disturbance in the jets. The Rayleigh wavelength $2\pi\lambda_d/4$ is longer than the "most susceptible" Taylor wavelength λ_d. The photographic observations of references [12] and [36] show that the vapor jets on large wires and spheres are too blunt to have collapsed by virtue of longer Rayleigh wavelength $2\pi\lambda_d/4$. While the longer wave needs some distance along the jet axis to develop, the shorter Taylor wavelength, λ_d, is already developed at the onset and is picked up by the jet. Thus if we propose that this wavelength, λ_d, is also the dominant wavelength in vapor jets on a flat plate, Zuber's equation (78) reduces to

$$\left(q_{max_F}\right)_{inviscid} = 1.14\,\frac{\pi}{24}\left[\sqrt{\rho_g}\,h_{fg}\,\sqrt[4]{\sigma g(\rho_f-\rho_g)}\right] \qquad (79)$$

$$= 1.14\,q_{max_Z}$$

Equation (79) predicts 14% higher peak heat flux on an "infinite" flat plate than that predicted by Zuber's equation (6).

B. Peak Pool Boiling Heat Flux When Both the Liquid and Gas are Assumed Viscous

In this section we develop an expression for the critical velocity of the gas at which the jets become unstable in a viscous liquid and use this in conjunction with equation (72) to find the peak heat flux.

The assumed configuration of the gas jet and the liquid column, along with the respective velocity profiles, is shown in Figure 28. The inviscid model is also included in the figure for the sake of comparison. We will carry out a plane two-dimensional analysis,however we will take the effect of transverse curvature of the vapor jet into account.

1. Velocity Profile for the Primary Flow in the Gas Jet and Liquid Column.

Let U_g denote the velocity of the gas and let U_f be the velocity of the liquid. At the interface, the gas will tend to drag the liquid upward but it has to do so against the force of gravity. The gravity force is much larger than the interfacial drag in all the situations we are going to consider, hence we assume a zero velocity at the interface. The gravity force is balanced by drag and the reaction against the liquid at the heater surface. This suggests a Poiseuille flow for the gas jet and we accordingly take a velocity distribution for the gas as:

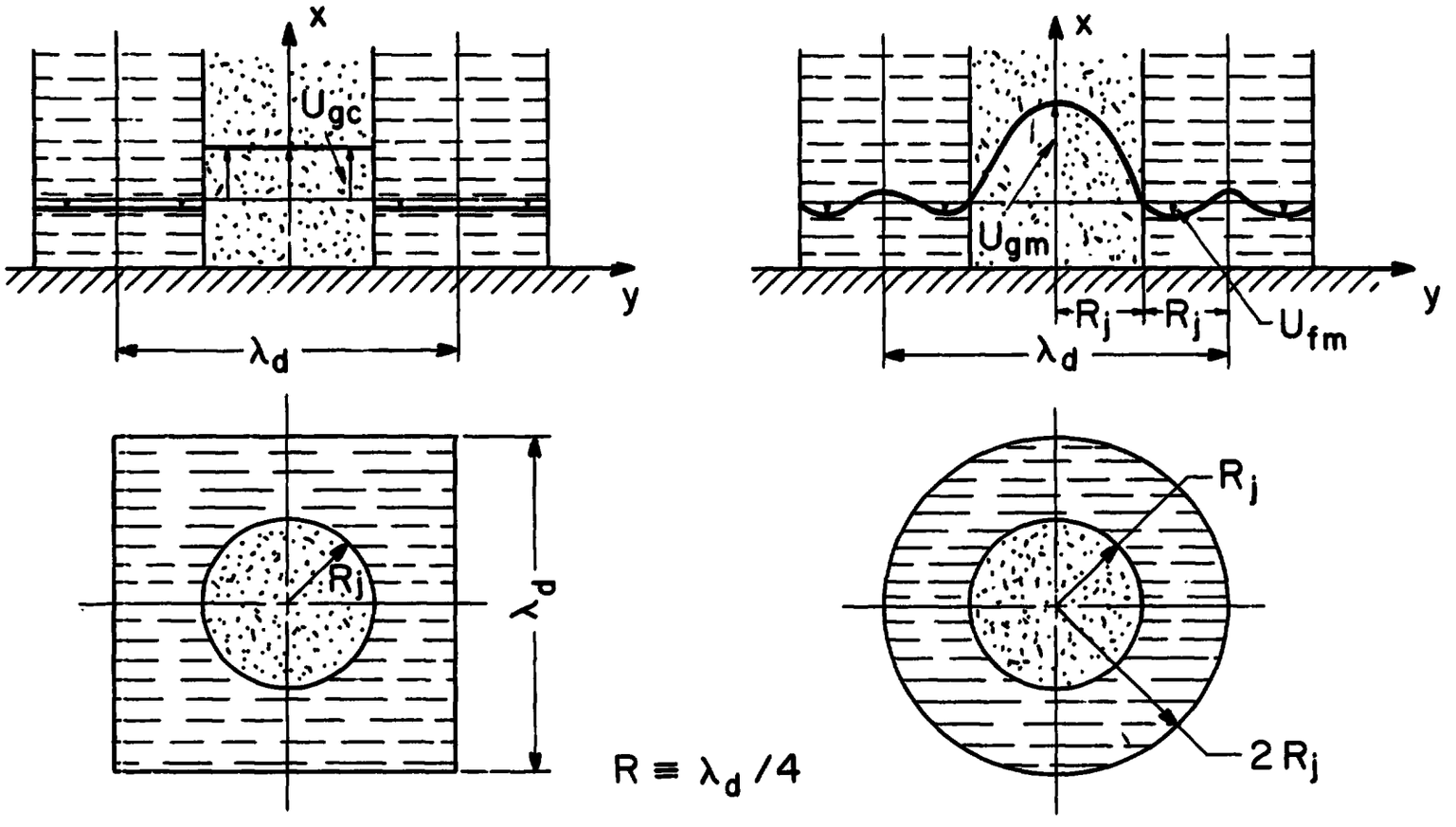

Fig. 28 Assumed theoretical models of boiling near the peak heat flux.

$$U_g = U_{gm} - U_{gm} y^2/R_j^2 \tag{80}$$

where,

$$R_j = \lambda_d/4 \tag{81}$$

The liquid velocity profile has to satisfy the following conditions:

(i) The velocity at the interface is zero

$$U_f = 0 \qquad \text{at} \qquad y = R_j$$

(ii) The first derivative of velocity vanishes at the middle of the liquid column

$$(U_f)_y = 0 \qquad \text{at} \qquad y = 2R_j$$

(iii) The shear stress at the interface from both the gas and the liquid side is the same

$$\mu_f (U_f)_y = \mu_g (U_g)_y \qquad \text{at} \qquad y = R_j$$

(iv) Conservation of mass: The net rate of downward flow of liquid is consistant with the amount of vapor generated.

$$\int_o^{2\pi} \int_o^{R_j} \rho_g U_g \, y \, dy \, d\theta = \int_o^{2\pi} \int_{R_j}^{2R_j} \rho_f U_f \, y \, dy \, d\theta$$

A velocity profile satisfying the above conditions and having symmetry about x-axis can be written as:

$$U_f = U_{gm} \left\{ \left[\frac{107}{54} \frac{\mu_g}{\mu_f} - \frac{11}{81} \frac{\rho_g}{\rho_f} \right] - \left[\frac{168}{54} \frac{\mu_g}{\mu_f} - \frac{24}{81} \frac{\rho_g}{\rho_f} \right] y^2/R_j^2 \right.$$

$$\left. + \left[\frac{69}{54} \frac{\mu_g}{\mu_f} - \frac{15}{81} \frac{\rho_g}{\rho_f} \right] y^4/R_j^4 - \left[\frac{8}{54} \frac{\mu_g}{\mu_f} - \frac{2}{81} \frac{\rho_g}{\rho_f} \right] y^6/R_j^6 \right\} \tag{82}$$

The maximum downward liquid velocity occurs at $y = 1.28\, R_j$ and may be written as:

$$U_{fm} = -U_{gm} \left[\frac{19.21}{54} \frac{\mu_g}{\mu_f} + \frac{3.14}{81} \frac{\rho_g}{\rho_f} \right] \qquad (83)$$

Equation (82) for the liquid profile gives a downward flow of liquid near the gas jet and a slight upward flow in the middle. This suggests a recirculation of liquid in the liquid column. At this point we do not wish to go into details of the liquid motion apart from saying that near the peak heat flux the vapor generation process is very violent and this type of motion of the liquid is possible.

2. Formulation of the Stability Problem.

To study the stability of the interface, we superimpose the perturbation components of velocity and pressure on the mean flow of gas. Let u_g and v_g be the perturbation components of velocity in the x and y directions and p_g be the perturbation pressure. If P_g is the mean pressure in the gas jet at any cross-section, we may write

$$\tilde{u} = U_g + u_g \qquad \tilde{v} = v_g \qquad \text{and} \qquad \tilde{p} = P_g + p_g$$

From now on for convenience of typing we do not use the subscript g to denote the physical variables of the gas. The continuity equation and equation of motion for the perturbed flow on the

gas side can be written as:

$$u_x + v_y = 0 \tag{84}$$

$$u_t + Uu_x + U_y v = -\frac{1}{\rho} p_x + \mu(u_{xx} + u_{yy}) \tag{85}$$

$$v_t + Uv_x = -\frac{1}{\rho} p_y + \mu(v_{xx} + v_{yy}) \tag{86}$$

where we have neglected the product of any two small quantities and have utilized the fact that the mean flow satisfies the Navier-Stokes equations independently. Various conditions these equations have to satisfy are:

(i) The v component of velocity vanishes at the axis of symmetry, i.e. at y = 0

$$v = 0 \quad \text{at} \quad y = 0 \tag{87}$$

(ii) The first derivative of the u component of velocity vanishes at the axis of symmetry

$$u_y = 0 \quad \text{at} \quad y = 0 \tag{88}$$

(iii) The continuity of normal stress at the interface

$$-p + 2\mu v_y - \sigma\eta/2R_j^2 - \sigma\eta_{xx} = -p_f \quad \text{at} \quad y = R_j \tag{89}$$

In the above equation $\eta(x,t)$ is the displacement of the interface from the mean position

(iv) The continuity of tangential stress at the interface

$$\mu(u_y + v_x) = \tau_f \quad \text{at} \quad y = R_j \tag{90}$$

(v) The kinematic condition at the interface can be written as

$$\eta_t = v \quad \text{at} \quad y = R_j \tag{91}$$

Next, all the variables are made dimensionless by choosing the radius of the jet, R_j, and a characteristic velocity, U_o, as

units of length and velocity, respectively. The characteristic velocity, U_o, may be taken as the maximum downward velocity of the liquid. Keeping the same symbol as for the original physical quantity, the dimensionless form of these variables is:

$$u = u/U_o \qquad v = v/U_o \qquad p = p/\rho U_o^2$$

$$x = x/R_j \qquad y = y/R_j \qquad t = tU_o/R_j$$

$$U = U/U_o \qquad \eta = \eta/R_j \qquad \tau = \tau/\rho U_o^2$$

Substituting these quantities into equations (84) through (90) we get:

$$u_x + v_y = 0 \tag{84a}$$

$$u_t + Uu_x + U_y v = -p_x + R_e^{-1}(u_{xx} + u_{yy}) \tag{85a}$$

$$v_t + Uv_x = -p_y + R_e^{-1}(v_{xx} + v_{yy}) \tag{86a}$$

The various boundary conditions become:

$$v = 0 \quad \text{at} \quad y = 0 \tag{87a}$$

$$u_y = 0 \quad \text{at} \quad y = 0 \tag{88a}$$

$$p - 2R_e^{-1} v_y + \sigma\eta_{xx}/(\rho U_o^2 R_j) + \sigma\eta/(2\rho U_o^2 R_j) = p_f \quad \text{at} \quad y = 1 \tag{89a}$$

$$u_y + v_x = R_e \tau_f \quad \text{at} \quad y = 1 \tag{90a}$$

where

$$R_e \equiv \frac{U_o R_j \rho}{\mu} \tag{92}$$

3. Introduction of Perturbation Stream Function.

We assume that the gas-liquid interface has the following two dimensional wave form:

$$\eta = \eta_o \, e^{i(kx-\omega t)} \tag{93}$$

In the dimensionless form this becomes

$$\eta = \eta_o \, e^{i\alpha(x-ct)} \tag{93a}$$

where α is the dimensionless wave number, kR_j, and c is the dimensionless wave velocity ω/kU_o. The symbol c denotes a complex number such that the imaginary part represents the growth rate of the disturbance. Now we define a perturbation stream function

$$\Psi = \eta_o F(y) e^{i\alpha(x - ct)} \tag{94}$$

such that

$$u = \Psi_y = F^I \eta \tag{95}$$

$$v = -\Psi_x = -i\alpha F\eta \tag{96}$$

Substituting these definitions of η, u and v from equations (93a), (95) and (96) in equations (85a) and (86a) we get:

$$-i\alpha cF^I\eta + i\alpha UF^I\eta - i\alpha U^I F\eta = -p_x + R_e^{-1}(-F^I\eta\alpha^2 + F^{III}\eta) \tag{85b}$$

$$-\alpha cF\eta + \alpha F\eta = -p_y + R_e^{-1}(i\alpha^2 F\eta - iF\eta) \tag{86b}$$

Roman superscripts denote differentiations with respect to y. Elimination of pressure from equation (85b) and (86b) gives

$$F^{IV} - 2\alpha^2 F^{II} + \alpha^4 F = i\alpha R_e\left[(U-c)(F^{II}-\alpha^2 F) - U^{II}F\right] \tag{97}$$

Equation (97) is a typical Orr-Sommerfeld equation and the boundary conditions for it are:

$$F(0) = 0 \tag{87b}$$

$$F^{II}(0) = 0 \tag{88b}$$

$$F^{III} - 3\alpha^2 F^{I} = i\alpha R_e\left[p_f/\eta + \sigma(\alpha^2 - 1/2)/(\rho U_o^2 R_j)\right] - i\alpha R_e\left[cF^{I}(1) - U^{I}F(1)\right] \quad \text{at} \quad y = 1 \tag{89b}$$

$$F^{II} + \alpha^2 F = \tau_f R_e/\eta \quad \text{at} \quad y = 1 \tag{90b}$$

The kinematic condition at the interface can be written as

$$c = F(1) \tag{91a}$$

4. Solution of Orr-Sommerfeld Equation.

Our next step is to find a solution of equation (97) with boundary conditions (87b) through (90b) for values of α close to 1 and $Re << 1$. This choice for α is made because the "most susceptible" Taylor wave is also the dominant one on the liquid vapor interface. The maximum downward liquid velocity near the peak heat flux is very small hence $Re << 1$. Thus we write

$$\alpha = 1 - \beta \quad \text{where} \quad \beta < 1 \tag{98}$$

We also assume a series form for the perturbation function, F

$$F = F_o + \beta F_1 + {}^{2}- \cdots \tag{99}$$

Substituting equations (98) and (99) for α and F in equation (97) and in the boundary conditions (87b) through (90b), and collecting terms of the order of β^o, β^1, etc., we get for terms of the order of β^o:

$$F_o^{IV} - 2F_o^{II} + F_o = 0 \tag{100}$$

The boundary conditions for equation (100) are:

$$F_o(0) = 0 \tag{101}$$

$$F_o^{II}(0) = 0 \tag{102}$$

$$F_o^{III}(1) - 3\,F_o^{I}(1) = i\,(\tilde{P}+S) \tag{103}$$

$$F_o^{II}(1) + F_o(1) = i\,\tilde{T} \tag{104}$$

For terms of the order of β^1 we get:

$$F_1^{IV} - 2F_1^{II} + F_1 = \left[(U-c)(F_o^{II} - F_o) - U^{II} F_o\right] . i R_e/\beta \tag{105}$$

The boundary conditions on equation (105) are:

$$F_1(0) = 0 \tag{106}$$

$$F_1^{II}(0) = 0 \tag{107}$$

$$F_1^{III}(1) - 3F_1^{I}(1) = -i(\tilde{P}+S) - i\left[cF_o^{I}(1) + U^{I}(1)F_o(1)\right] \tag{108}$$

$$F_1^{II}(1) + F_1(1) = 0 \tag{109}$$

In the above equations

$$\tilde{P} \equiv p_f R_e/\eta \tag{110}$$

$$S \equiv \sigma R_e/(2\rho U_o^2 R_j) \tag{111}$$

$$\tilde{T} \equiv \tau_f R_e/\eta \tag{112}$$

The solutions for F_o and F_1 can be written as follows:

$$F_o = \left[0.0434\ T - 0.2008\ i\ (\tilde{P}+S)\right](e^{y} - e^{-y}) + \left[0.0732\ T + 0.0868\ i\ (\tilde{P}+S)\right] y(e^{y} + e^{-y}) \tag{113}$$

$$F_1=\left\{(\tilde{P}+S)+c\left[0.5319\tilde{T}-0.1478i(\tilde{P}+S)\right]+U^I(1)\left[0.3279\tilde{T}-0.2041i(\tilde{P}+S)\right]\right\}$$

$$\times\left\{0.2008i\,(e^y-e^{-y})-0.0868i\,y(e^y+e^{-y})\right\}$$

$$+\left\{2(U-c)\left[0.0732T+0.0868i(\tilde{P}+S)\right]-U^{II}\left[0.0434\tilde{T}-0.2008i(\tilde{P}+S)\right]\right\}$$

$$\times\left\{y^2/8\cdot(e^y-e^{-y})\right\}\,iR_e/8$$

$$-\left\{U^{II}\left[0.0434\tilde{T}-0.2008i\,(\tilde{P}+S)\right]\right\}$$

$$\times\left\{e^y(y^3/24-y^2/8)+e^{-y}(y^3/24+y^2/8)\right\}\,iR_e/8 \qquad (114)$$

5. Kinematic Condition at the Interface.

The above functions F_o and F_1, when evaluated at the interface $y = 1+\eta \simeq 1$, become:

$$F_o(1) = 0.3279\tilde{T} - 0.2041\,i\,(\tilde{P}+S) \qquad (115)$$

$$F_1(1) = 0.2041i\left\{(\tilde{P}+S)+c\left[0.5319\tilde{T}-0.1478i(\tilde{P}+S)\right]\right.$$

$$\left.+\,U^I(1)\left[0.3279\tilde{T}-0.2041i(\tilde{P}+S)\right]\right\}$$

$$-c\left\{0.0431\tilde{T}+0.0511i(\tilde{P}+S)\right\}\,iR_e/8$$

$$-U^{II}(1)\left\{0.0056\tilde{T}-0.0258i(\tilde{P}+S)\right\}iR_e/8 \qquad (116)$$

The wave velocity, c, the perturbation pressure, $\tilde{P}$, and perturbation shear, $\tilde{T}$, are complex quantities. Writing them as the sum of real and imaginary parts, we have:

$$c = c_r + i\,c_i \qquad (117)$$

$$\tilde{P} = \tilde{P}_r + i\,\tilde{P}_i \qquad (118)$$

$$\tilde{T} = \tilde{T}_r + i\,\tilde{T}_i \qquad (119)$$

The kinematic condition (91a) at the interface can be written as:

$$c = F_o(1) + \beta F_1(1) \tag{91b}$$

Substituting equations (115) through (119) in (91b) and collecting real and imaginary parts we have,

$$\begin{aligned} c_r = {} & 0.3279\ \tilde{T}_r + 0.2041\,(1-\beta)\,\tilde{P}_i - \beta\,[0.1085(\tilde{T}_i c_r + \tilde{T}_r c_i) \\ & + 0.0302 c_i \tilde{P}_i - 0.0302 c_r(\tilde{P}_r + S) + 0.0669 U^I(1)\tilde{T}_i - 0.0416 U^I(1)(\tilde{P}_r + S)] \\ & + R_e[0.0056\ U^{II}(1)\ \tilde{T}_i - 0.0258\ U^{II}(1)\ (\tilde{P}_r + S)] \\ & + R_e[0.0431(\tilde{T}_i c_r + \tilde{T}_r c_i) - 0.0511\ c_i \tilde{P}_i + 0.0511\ c_r(\tilde{P}_r + S)] \end{aligned} \tag{120}$$

$$\begin{aligned} c_i = {} & 0.3279\,\tilde{T}_i - 0.2041\,(1-\beta)(\tilde{P}_r + S) + \beta\,[0.0652\,(\tilde{T}_r c_r - \tilde{T}_i c_i) \\ & + 0.0813\,(c_r \tilde{P}_i + c_i \tilde{P}_r) + 0.0669\ U^I(1)\,\tilde{T}_r + 0.0416\ U^I \tilde{P}_i] \\ & - R_e\,[0.0056\ U^{II}(1)\ \tilde{T}_r + 0.0258\ U^{II}(1)\ \tilde{P}_i\ ] \\ & - R_e\,[0.0431\,(\tilde{T}_r c_r - \tilde{T}_i c_i) - 0.0511\,(c_r \tilde{P}_i + c_i \tilde{P}_r)\ ] \end{aligned} \tag{121}$$

We are interested in the imaginary part of the wave velocity as it represents the rate of growth of the disturbance. For a neutral disturbance ($c_i = 0$), if we put $\beta = 0.57$ (i.e. $\alpha = \pi/2$ or $\lambda_H = \lambda_d$) and $R_e \simeq 0$ in equation (121) we get:

$$0.3279\ \tilde{T}_i - 0.3204\ (\tilde{P}_r + S) = 0 \tag{122}$$

Equation (122) when written in original variables, becomes

$$1.0234\ \frac{\tau_{fi}}{\eta} - \frac{p_{fr}}{\eta} = \frac{\sigma}{2R_j} \tag{123}$$

6. Normal and Tangential Perturbation Stresses of the Liquid.

The normal and shear stress perturbations on a rigid wavy surface (c = 0) have been given by Brooke Benjamin [38] and subsequently used by Craik [39] and Nayfeh and Saric [40] for the stability analysis of wind generated waves on thin liquid films. The stress perturbations for a boundary layer type of external flow with zero pressure gradient are given as:

$$\frac{p_{fr}}{\eta} = -\alpha \rho_f U_{fm}^2 \tag{124}$$

$$\frac{\tau_{fi}}{\eta} = -1.188\, \alpha^{5/3} \rho_f U_{fm}^2 \left\{ \mu_f / \left[\rho_f U_f^I(1) R_j^2 \right] \right\}^{1/3} \tag{125}$$

The liquid velocity profile in our case is more diffuse and has a negative pressure gradient in the direction of flow. This flow situation could be treated independently but that would require making more assumptions and simplification than we would like to make. Thus, although the above expressions for perturbation stresses do not necessarily represent our flow configuration; still it is worthwhile to use the above results and compare the final expression for the peak heat flux with experimental data. Using equations (124) and (125) in (123), we have:

$$U_{fm}^2 \left[1 - 1.63 \left\{ \mu_f / \left[U_f^I(1) R_j^2 \right] \right\}^{1/3} \right] = \sigma / (\rho R_j \rho_f) \tag{126}$$

7. Peak Heat Flux Prediction.

Substituting for $R_j (= \lambda_d/4)$ and for U_{fm} from equation (83) in

equation (126) and dividing throughout by U_{gc}^2 as given by equation (73) we obtain

$$\left(\frac{U_{gm}}{U_{gc}}\right)^2\left[19.21\mu_g/(54\mu_f)+3.14\rho_g/(18\rho_f)\right]$$

$$\times\left\{1-1.01\left[\mu_f/\mu_g\cdot(\rho_g/\rho_f)^{1/2}\cdot U_{gc}/(U_{gm}\cdot M\Lambda_d)\right]^{1/3}\right\}$$

$$=2\rho_g/(\pi^2\rho_f\Lambda_d) \qquad (127)$$

On the left hand side of equation (127), the second term in the first square bracket is much smaller than the first term at pressures much less than the critical pressure, and can be neglected. Now for the peak heat flux we write an energy balance equation similar to equation (72).

$$q_{max_F} = \rho_g h_{fg} (U_{gm}/2)\cdot(\pi/16) \qquad (128)$$

The use of equation (128) in conjunction with equation (79) in equation (127) gives

$$\frac{(q_{max_F})}{(q_{max_F})_{inviscid}} = \frac{0.633\ V}{M\Lambda_d^{1/2}\left\{1-0.807\left[\frac{V}{M^2\Lambda_d}\ \frac{(q_{max_F})_{inviscid}}{(q_{max_F})}\right]^{\frac{1}{3}}\right\}^{\frac{1}{2}}} \qquad (129)$$

where M and Λ are the same as defined in Chapter II and V is the product of a gas viscosity parameter similar to M and the square root of the ratio of gas and liquid densities.

$$V \equiv \frac{\rho_g^{1/2} \rho_f^{1/2} \sigma^{3/4}}{\mu_g \cdot g^{1/4} (\rho_f - \rho_g)^{3/4}} \tag{130}$$

Equation (129) is plotted in Figure 29 with M and V as independent variable. For a particular fluid, to every value of M, there is a unique value of V. We also trace such a curve for cyclohexanol in Figure 29. The effect of liquid viscosity is to significantly increase the peak heat flux.

Conclusions.

1. An improved prediction for the peak heat flux for nearly inviscid liquids on large horizontal heaters has been suggested.

2. A theoretical analysis for the instability of gas jets in viscous liquids has been done and an expression for the peak heat flux is obtained as a function of liquid viscosity, gas viscosity and density ratio of gas and liquid.

3. Liquid viscosity seems to strongly increase the peak heat flux.

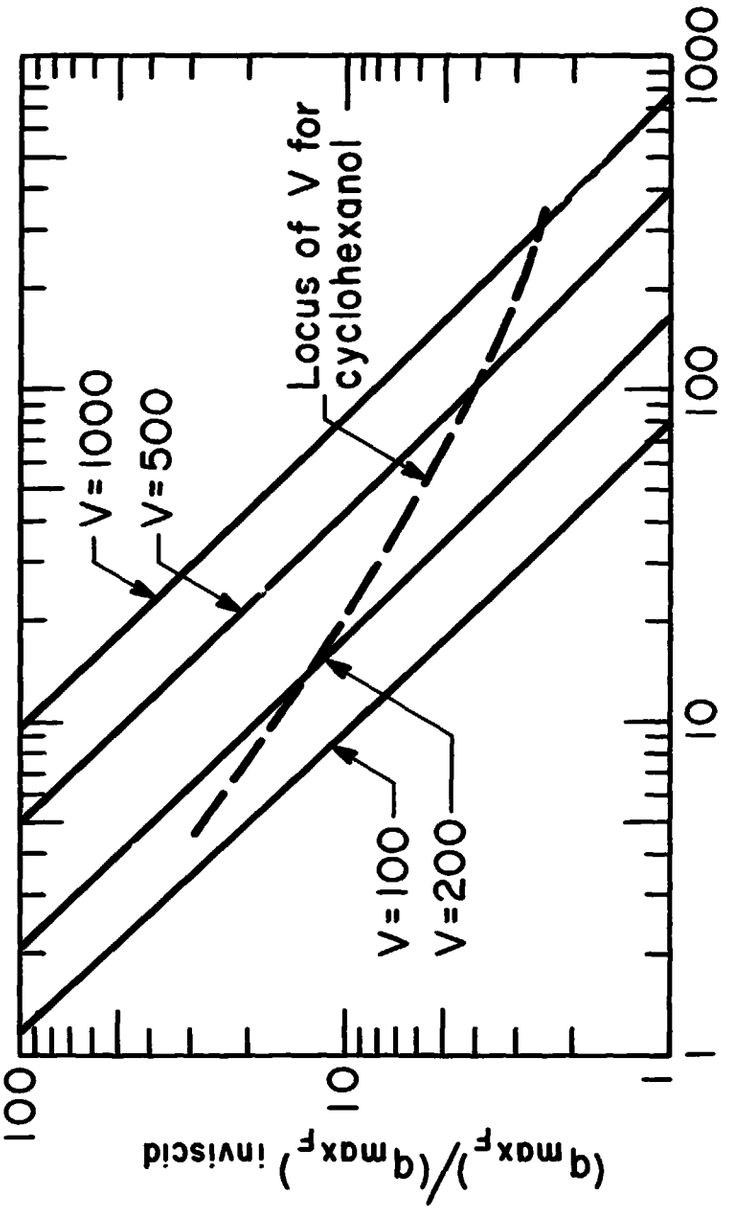

Fig. 29 Variation of dimensionless peak heat flux with M for various values of V at earth normal gravity.

V. OBSERVATIONS OF THE PEAK HEAT FLUX FOR VISCOUS AND INVISCID LIQUIDS ON AN "INFINITE" FLAT PLATE

A program for the experimental determination of the peak heat flux on an infinite flat plate, both at earth normal gravity and at elevated gravities, was carried out. By an "infinite" flat plate, we mean one with dimensions much larger than the "most susceptible" wavelength, λ_d, and one with side walls to avoid any inflow of liquid from the sides. The flat plate we used accommodated more than three wavelengths for the alcohols, and about two for water, at earth normal gravity; while these numbers increased as $g^{1/2}$ at higher gravities. The observations were made for both viscous and nearly-inviscid liquids. Reagent grade liquids used were: acetone (CH_3COCH_3), benzene (C_6H_6), isopropanol ($CH_3CHOH\ CH_3$), methanol (CH_3OH), distilled water and cyclohexanol ($CH_2(CH_2)_4\ CHOH$).

A. Description of the Experiment.

1. Apparatus.

The flat plate heater and its auxilliary apparatus consisted of a heater, a heater support, an emergency shut-off mechanism and a reflux condenser. We designed and fabricated each of these

elements because commercial models which satisfied our requirements were not commonly available. Hence we will describe each of them individually.

(a) Heater -- The flat plate heater had to fulfill the following requirements.

The maximum available power without overtaxing the existing supply line was 6 kilowatts. This meant that a maximum current of 51 amps could be drawn at 110 volts. The heater surface area and the heating elements had to be designed for this power density.

The heater was to be capable of operating at either earth normal gravity or adaptable to the centrifuge facility for studies at elevated gravities. The space available between the centrifuge arm and the side wall limited the maximum height to less than 25 cm.

To act as an "infinite" flat plate the dimensions of the heater surface had to be much larger than the "most susceptible" Taylor wavelength. This was necessary to allow enough jets on the surface and hence to reduce the end effects.

The heater design also had to provide one-dimensional heat flow to the surface, since two dimensional heat flow would complicate the interpretation of results.

Apart from being a good conductor of heat, the heater material had to be one which would not react with the test liquids.

With these restrictions in mind the heater was made of pure copper with a circular bell shaped configuration. The heater has a diameter of 6.45 cm at the boiling surface; 10.16 cm at the butt end, and a height of 10.8 cm. A pyrex glass jar allowing a liquid head of about 6 cm sits on the heater surface and is positioned with the help of two stainless steel flanges. Stainless steel has a much lower thermal conductivity than copper and hence will have a very small cooling effect on the edges of the boiling surface. The total height of the heater with the glass jar is about 19 cm and it has a final weight of 5 kg. Figure 30 shows a sectioned view of the heater.

The lower portion of the heater contains a central fin and two circular rings for transferring heat from the resistance heating wire to the main body. Each of the circular rings and central fin has square threads machined on its surface to support the heating wire. To dissipate 6kw of power, 4 meters of 1.62mm dia. nichrome wire was used. These dimensions for the wire were chosen so as to minimize the heat input density for the maximum available surface area. The wire was covered with a fiberglass sleeve to provide electrical insulation from the main body of the heater. A thick layer of Sauereisen cement was applied on the outside surface to give additional support to the wire so that it could not leave the grooves during thermal

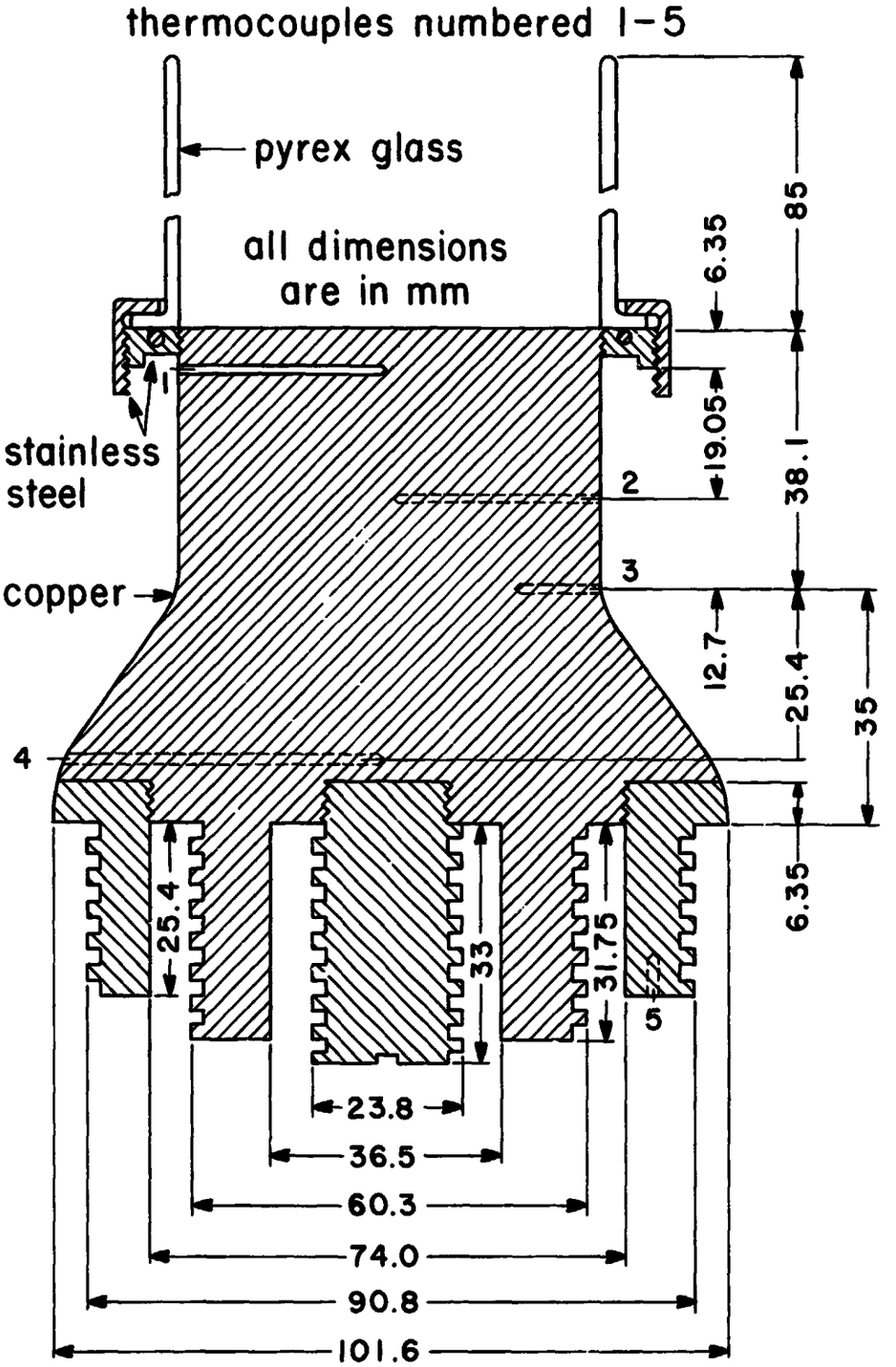

Fig. 30 Sectioned view of the flat plate heater.

expansion. Being a bad conductor of heat, Sauereisen cement also helps in reducing heat loss from the surface.

To monitor the temperature in various parts of the heater body, five 1.2mm diameter holes were drilled. The respective positions of the holes and their orientation about the heater axis are marked in Figure 31. Two-hole alumina insulator tubes carrying iron constantan thermocouples were pressed into these holes. Each of the thermocouple wires measured 0.26mm in diameter and had a spark welded junction. The top two thermocouples are used to determine the heat flux to the boiling surface. A third thermocouple is used for a countercheck on the heat flux calculations and a fourth thermocouple to show whether steady state conditions are reached. The thermocouple in the heater base is used to monitor the temperature for an emergency shut-off mechanism.

(b) Heater Support -- A support for the heater is necessary for its operation on the ground as well as in the centrifuge. Apart from being safe, the heater support had to be light in weight and able to function conveniently and efficiently in the small space available in the centrifuge.

Figure 32 shows the heater support. It has two straps with a flat base welded inbetween. The material of the support is cold-rolled steel. The straps are 6.25cm wide and have a

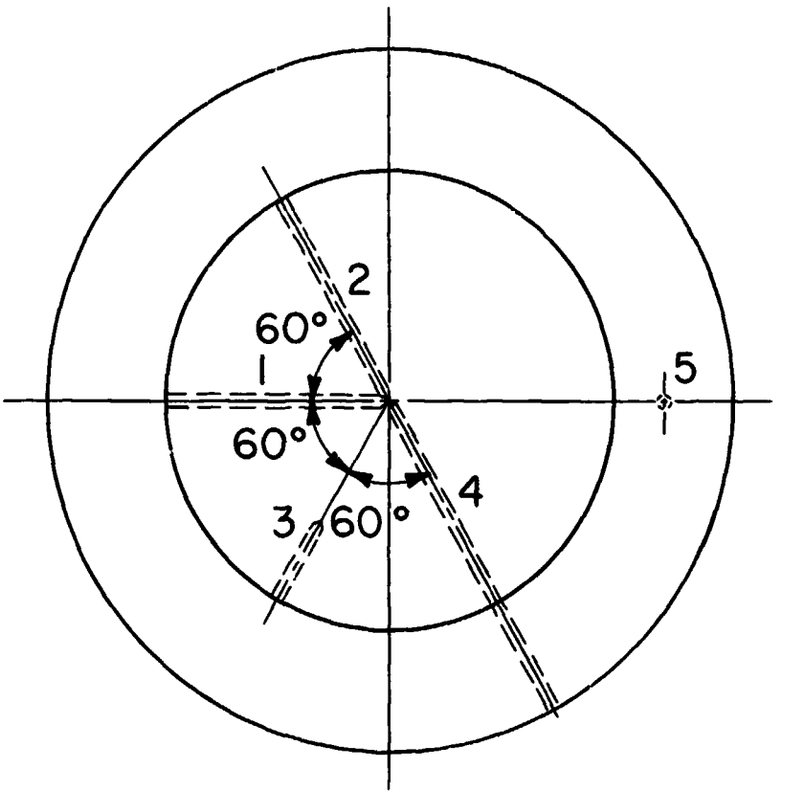

Thermocouples have been designated with numbers from 1 to 5.

Fig. 31. Orientation of thermocouples about heater axis.

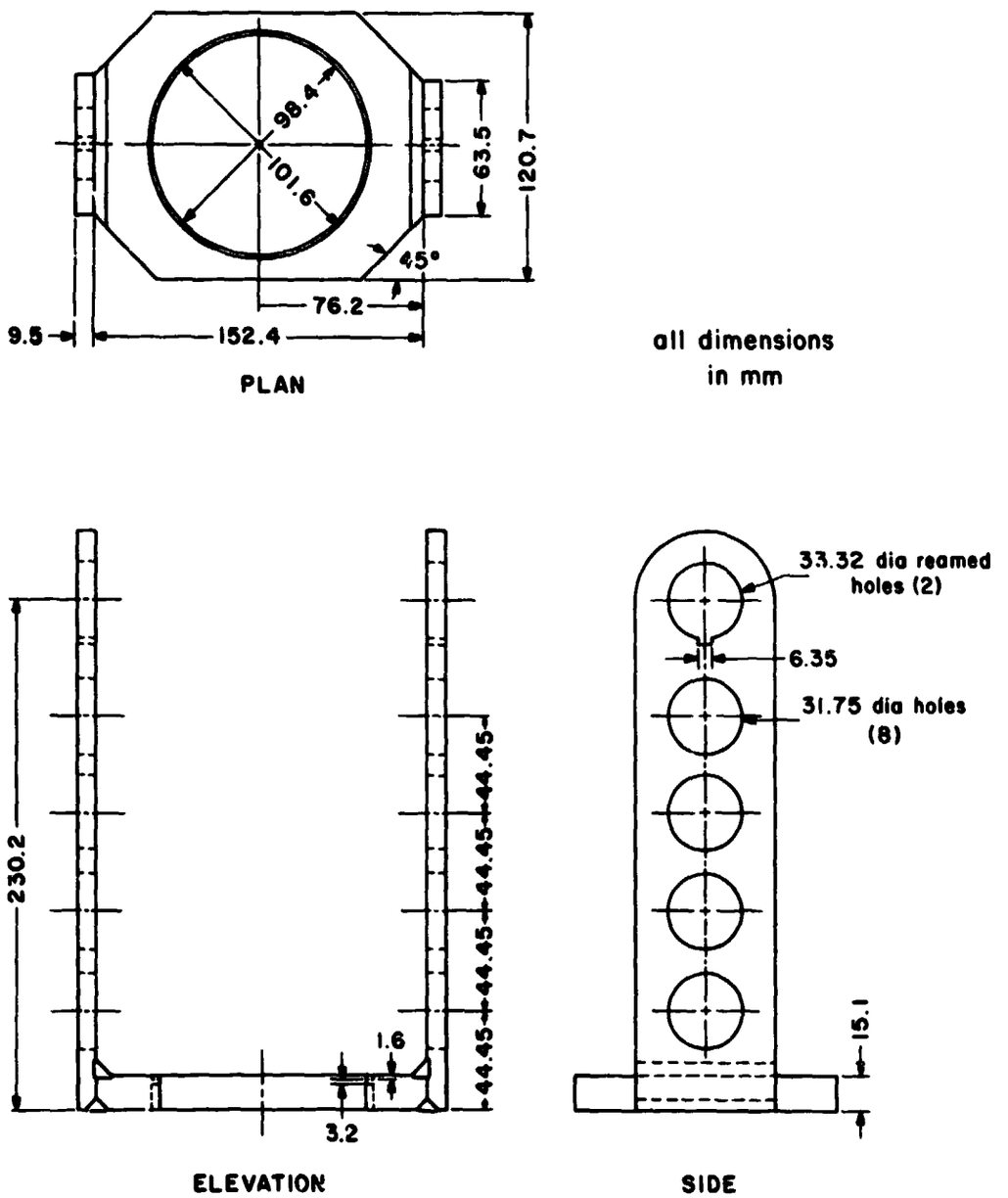

Fig. 32. Heater support.

thickness of 0.95 cm. The strap cross-section was designed to accommodate the bearing force encountered at 100g and to incorporate a liberal safety factor. To reduce the weight of the support, four large holes 3.18 cm in diameter were bored into each of the straps.

A 1.51cm thick plate with a hole to clear the outer ring of heater wire, and a shoulder to support the heater at the butt end, was used as a base of the heater support. An asbestos sleeve was placed between the butt end of the heater and shoulder in the base plate to reduce conductive heat loss from the heater to the support. The lower portion of the heater and the resistance wire were finally covered with a shroud made of a thin sheet of brass to avoid heat convection to the atmosphere. This heat loss could have been significant when the heater is operating in the centrifuge.

(c) Emergency Automatic Shut-Off Mechanism — As a large amount of heat is being dissipated over a small area, the temperature at the butt end will be rather high. The nichrome resistance wire selected for heating purposes melts at about 1200 K, therefore, we limit our operating temperature at the fin end to about 900K. While operating the flat plate heater close to the critical heat flux, one may overshoot the actual maximum and thus partially insulate the boiling surface. During this period,

power is continuously being supplied and it may cause a rapid build up of temperature in the body.

To know the approximate time in which the butt end temperature will reach a maximum safe temperature, a one-dimensional Schmidt plot was drawn. The Schmidt plot was based on a 20% excess power supply. The solution indicates that only 20 seconds are needed to reach the specified maximum temperature. This work was done by Eugene Davis, who was working on the project as an engineering aide. Details are given in his laboratory report [41].

Thus for safe operation of the heater, the power input must be terminated quickly. To avoid any delay that may be caused by manual observation, it is necessary that some automatic arrangement should be provided for shutting off the power.

The output voltage of an iron constanton thermocouple is amplified and sent to a Silicon Controlled Rectifier (SCR). When the voltage arriving at the SCR reaches a certain preset value, a make-and-break switch is activated. It allows the additional AC power supply to continue through to a plunger solenoid, mechanically linked to the main high amperage circuit breaker. When the solenoid is energized it causes the plunger to move, which in turn pulls open the main power circuit. By turning the amplifier, the voltage arriving at the SCR can be made to just

reach the breakover value at the moment the thermocouple senses a temperature of 900K. Figure 33 shows a circuit diagram of the shut-off mechanism. A photograph is displayed in Figure 34.

(d) Reflux Condenser -- Near the peak heat flux, a tremendous amount of heat is being dissipated generating large amounts of vapor. Simple calculations show that 6 cm of liquid head may last only for about two minutes near the critical heat flux. Thus we need a very effective refluxing system to capture the vapor for reuse.

For stationary flat plate tests, a glass tube 6.35 cm in diameter carrying a helical 1.2 cm diameter copper tube was used as reflux condenser. The glass tube is 1 meter in height. The coil spacing of the copper tube is about 3 cm. The glass tube is held with rubber stoppers at the two ends which also support the copper tube. Tap water was used as the coolant.

During tests on the centrifuge, two 15 mm diameter copper tubes having fins made of tin sheet were used as a reflux condenser. The fin size is 28 x 28 x 0.35 mm and the spacing in-between fins is 5.5mm. The condenser was designed on the basis of forced convection cooling at room temperature. The two limbs of the condenser are connected together at one end to facilitate connection to a vacuum pump. One may also mention

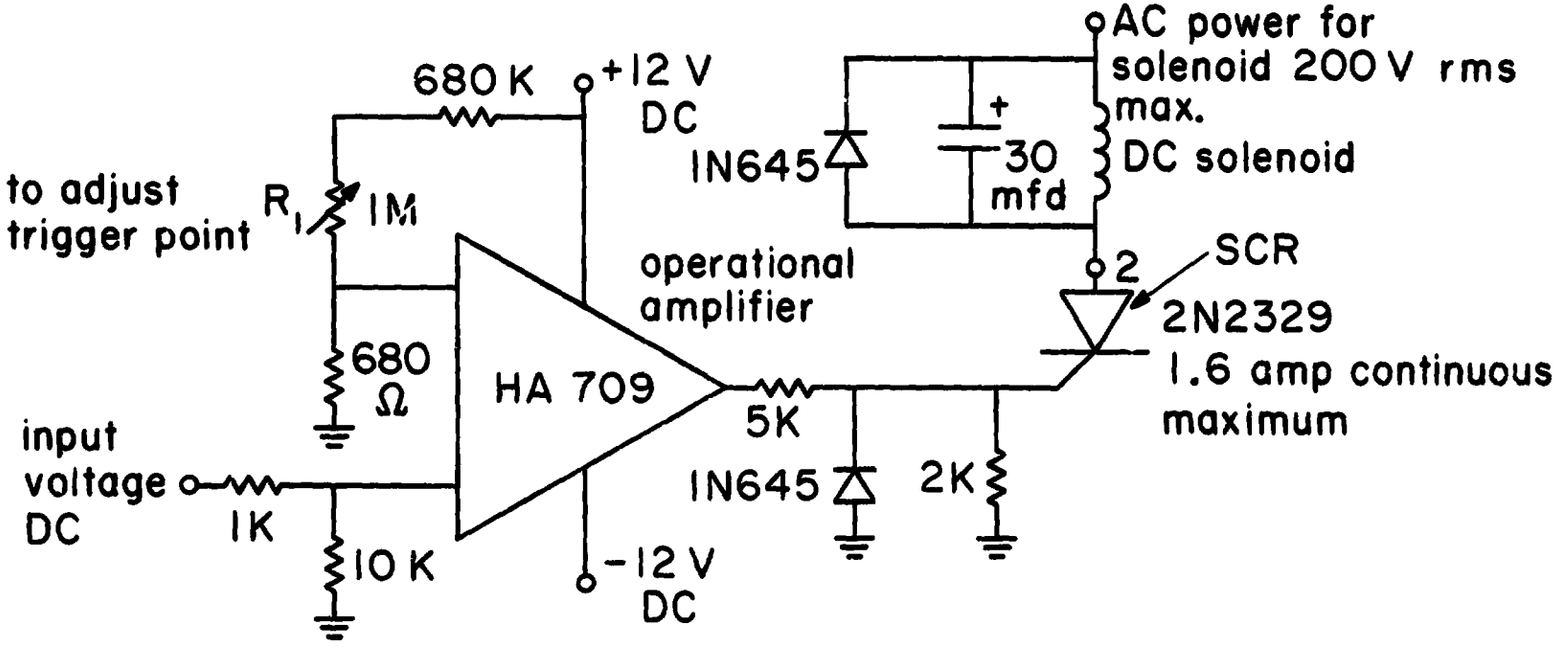

The output amplifier compares the reference voltage set at point 2 with the input voltage, using a potential divider, R_1. The SCR is off for $V_{in} < V_{ref}$ and on for $V_{in} > V_{ref}$. The input voltage at which the SCR is activated is adjustable from $\simeq 10$ mv to $\simeq 30$ mv.

Fig. 33. Circuit diagram of automatic shut-off mechanism.

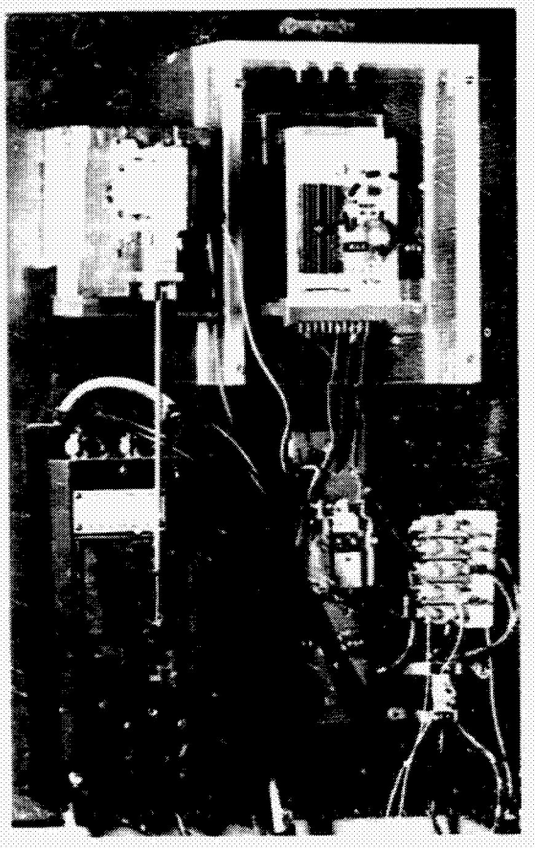

Fig. 34. Emergency shut-off mechanism.

here that the design of the reflux condenser also provided an opportunity to make a theoretical analysis of condensation under variable gravity. This information has been published in reference [42].

(e) Centrifuge Facility -- Elevated gravity tests were performed on the existing centrifuge facility at the Boiling and Phase Change Laboratory. Complete details of the centrifuge design are given in reference [21]. Figure 35 shows the centrifuge designed and built to obtain 100 times earth normal gravity at a speed of 360 rpm. When the flat plate heater is put on the centrifuge, its boiling surface is 77.7 cms from the center of rotation.

Electrical connections to the centrifuge are made through slip rings attached to the drive shaft. These include twelve circuits for power input, voltage measurement, and for thermocouples. The drive shaft also carries a tube which is connected to the vacuum pump through a stationary vacuum seal.

A strobe light is placed on a bracket attached to the stand supporting the centrifuge. It is triggered by a photo-electric pick-off which senses light reflected from a shiny metal piece attached to the centrifuge arm. Thus each revolution of the arm triggers the light only once. This causes the flat plate heater to appear stationary so one can view the boiling phenomenon.

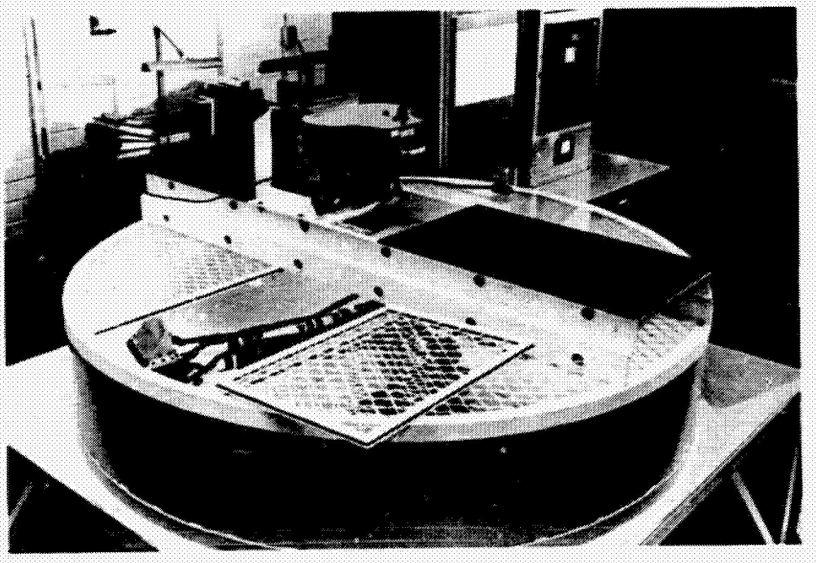

Fig. 35. Centrifuge capable of operating at 100 g

Figure 36 shows a schematic diagram of the stationary flat plate test and Figure 37 shows a photograph of the flat plate heater mounted on centrifuge.

2. Procedure.

Before each test, the boiling surface was polished with 220 grit size emery paper to remove any rust or carbon deposits formed during the previous observation. The surface was then cleaned with soap and warm water and rinsed with the test liquid. This was done to ensure that there was no uncleanliness on the surface which might affect the wettability and affect q_{max} data.

The glass jar and reflux condenser were positioned and the thermocouple and power connections were made. Before making the thermocouple connection to the SCR, a check was made to ensure that it functioned properly at the appropriate triggering voltage.

The resistance heating wire was energized and the current was gradually increased in steps. At each step the current and voltage were noted and thermocouple observations were recorded and updated until steady state was reached. It usually took about 5 minutes to reach steady state after the current was increased to the next higher value.

Various regimes of nucleate boiling (e.g. the isolated bubble regime and the transition from single bubbles to slugs and

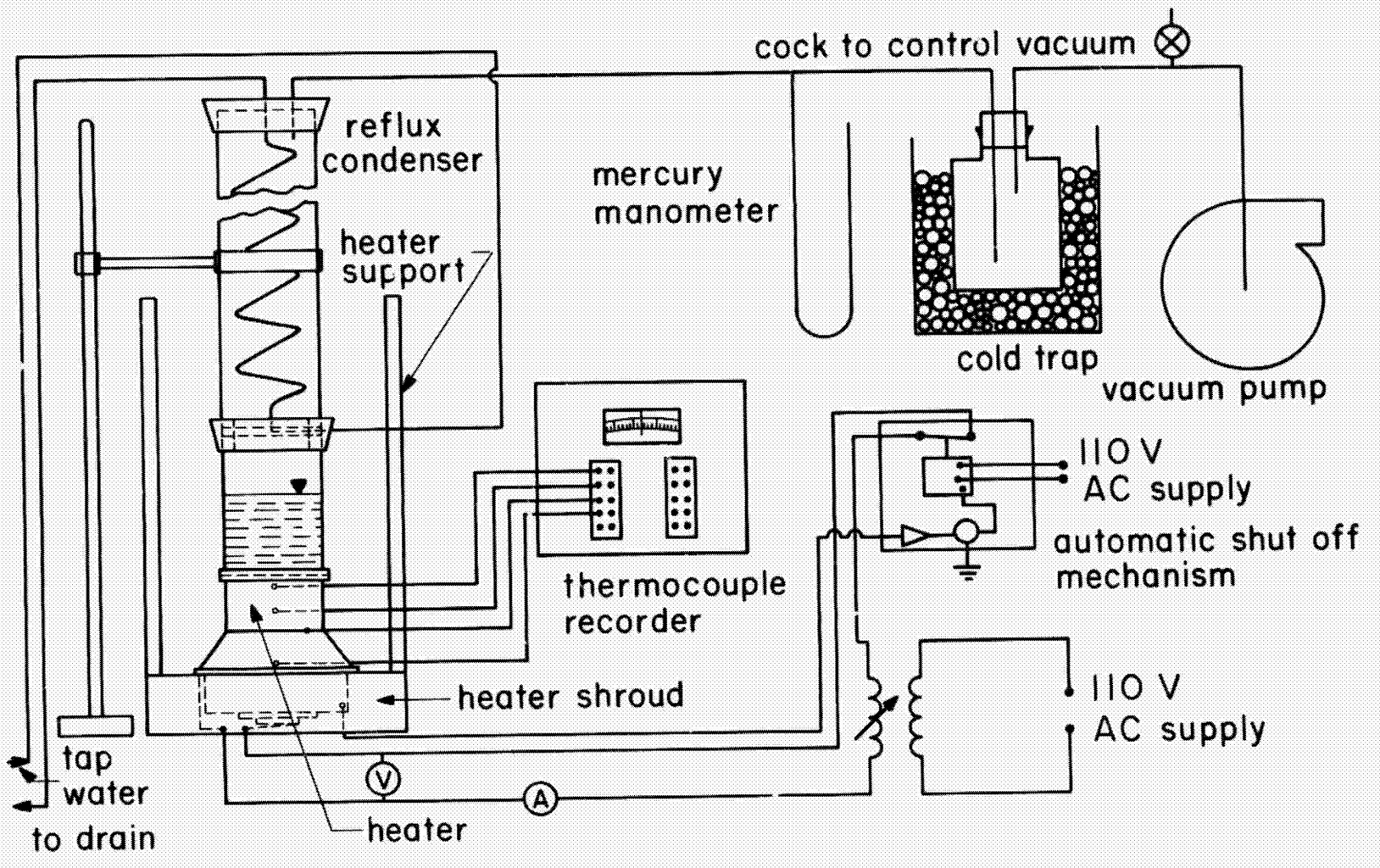

Fig. 36 Schematic diagram of stationary flat plate test.

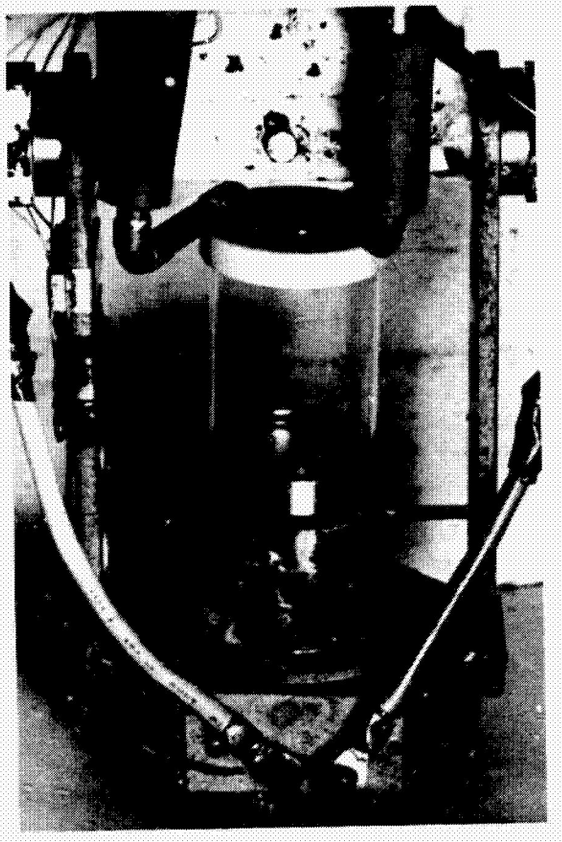

Fig. 37. Top view of the flat plate heater when mounted on the centrifuge.

columns) were easily discernable. The transition from nucleate to transitional boiling was identified by noting a slowdown of the boiling process and a sudden continuous increase in the thermocouple reading. The thermocouple reading continued to increase for a while, even after the power was removed. In most cases, the power was cut off after visual observation of the boiling transition, rather than by triggering of the automatic shut-off mechanism.

After removal of power one could also see the boiling process passing over from transitional to nucleate boiling. The peak heat flux was computed from the observations of the top two thermocouples. Observation of the third thermocouple helped in making a countercheck on the heat flux calculations. We discuss this and provide an error analysis in appendix A. The maximum probable error in q_{max} was within 7.7%.

The peak heat flux observations were made for both viscous and inviscid liquids. A few of the observations were repeated to check for reproductibility of results. Each time a new observation was made the above-mentioned procedure for cleaning the boiling surface was used and fresh test liquid was employed.

B. Discussion of Results.

1. Peak Heat Flux on "Infinite" Flat Plates for Nearly Inviscid Liquids.

Peak heat flux data from the present investigations are plotted in Figure 38. This shows data only for liquids for which liquid viscosity parameter, M, is about 400 or greater, hence the viscosity effect is negligibly small. Limited available data for clean heater surfaces and reagent grade liquids from other sources (e.g. the ethanol data of Cichelli and Bonilla [8], the carbon-tetrachloride and n-pentane data of Berenson [9], and the distilled water data of Costello et al. [13]) are also included.

The peak heat flux has been made dimensionless by dividing by Zuber's flat plate value as given by equation (6). The abscissa represents the size of the heater in terms of the number of jet spacings that can be accommodated on it. This scheme of marking the abscissa has been chosen to isolate any effect of smaller heater widths on the peak heat flux.

From Figure 38 we see that the peak heat flux data are very well represented by equation (79) which assumes an "infinite" plate model. This mode is apparently valid only for heater widths that are greater than about three times the "most susceptible" wavelength, since the distilled water data corresponding to L/λ_d close to 2 lie much below the predicted value.

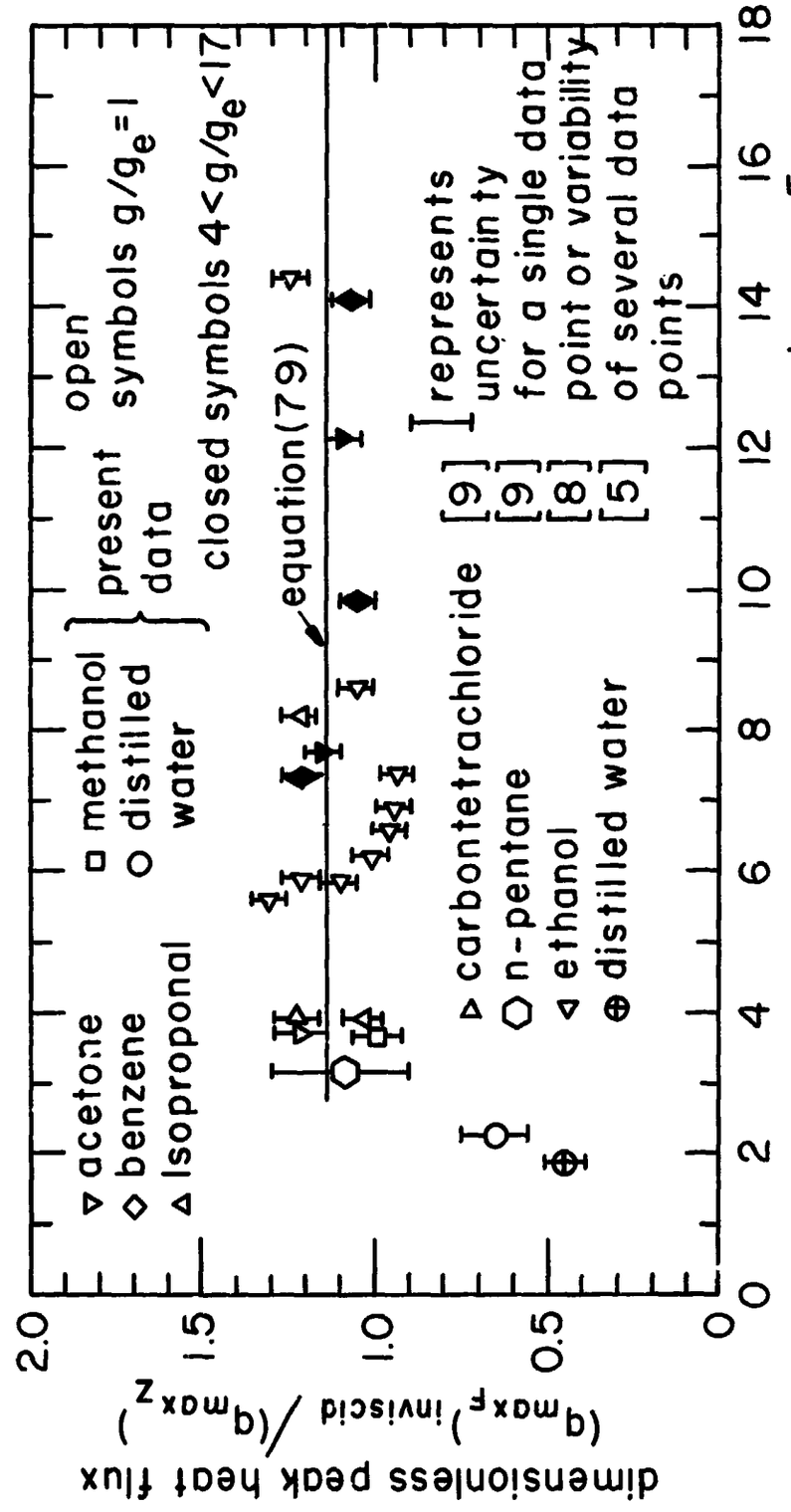

Fig. 38 Peak heat flux on broad flat plate heaters with vertical side walls.

The reason that the water data hang so low could be related to the finite size of the plate. If we look back and go through the various assumptions, the assumption most likely to be violated is that the ratio of area of the vapor jet to the area of the heater is a fixed constant (i.e. $\pi/16$). We further explore this matter next.

2. Peak Heat Flux on Finite Flat Plates for Nearly Inviscid Liquids.

In Figure 39, we again plot dimensionless peak heat flux against dimensionless heater width for a circular flat plate. This time the heat flux is based on the number of jets supported by the heater. The choice of a particular integral number of jets depends upon the size of the heater and its particular shape. A square heater, for example, will support a single jet until its width reaches almost twice the dominant wavelength. This assumes that there must be a clearance of $\lambda_d/4$ between the jet and the side wall to permit a free return of the liquid. The jets are also assumed to lie a distance λ_d apart on a square grid. It might be possible for such a square heater to accommodate 2 jets on a diagonal in the very narrow range of width: $1.707\ \lambda_d$ to $2\ \lambda_d$. However, this would be an unlikely occurrence. More likely, the four-jet grid would establish itself on a slightly shortened wavelength when the width gets close to $2\ \lambda_d$, so we discount the likelihood of a two-jet configuration.

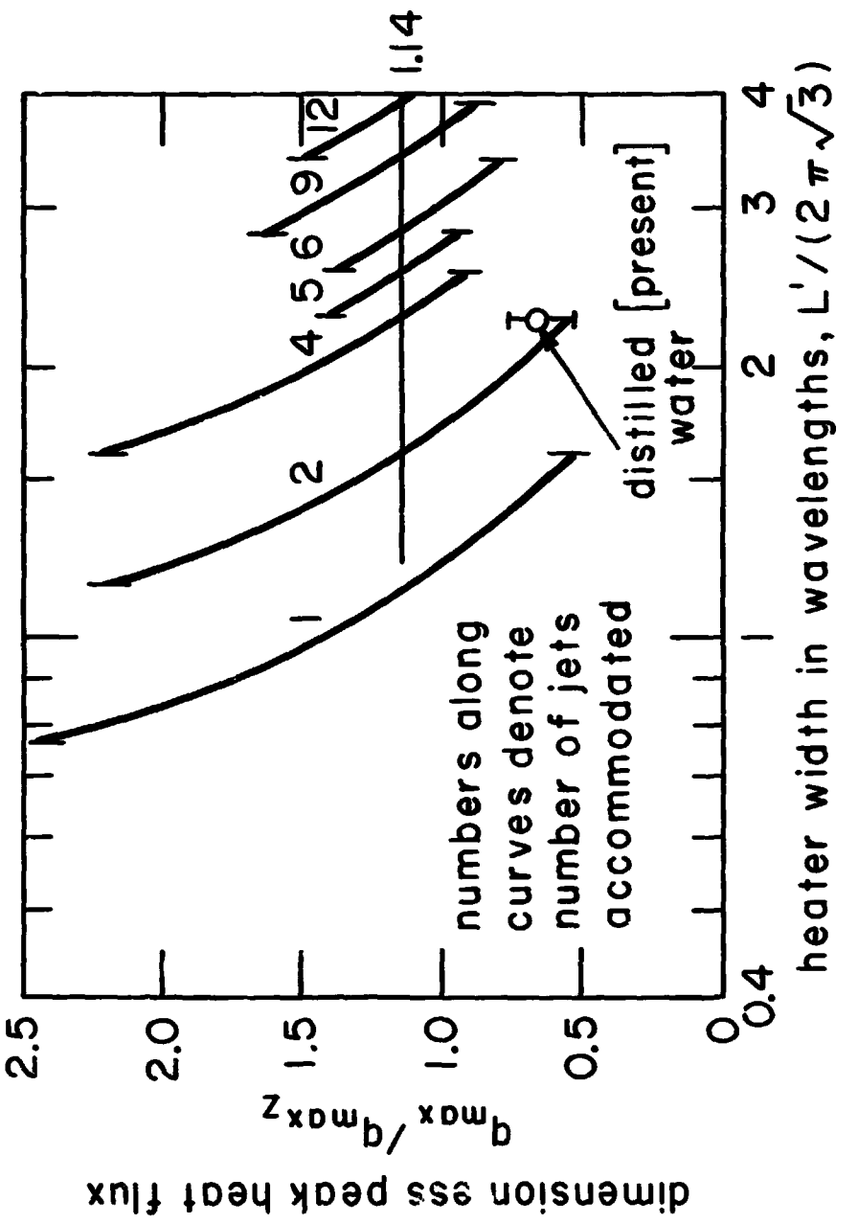

Fig. 39 Peak heat flux on a circular finite flat plate with vertical side walls.

By the same token, a circular heater will accommodate a single jet until the diameter reaches 2 λ_d. From this point up to 2.414 λ_d a two-jet configuration will be established and at 2.414 λ_d, four jets can be accommodated on the plate, and so forth.

As the number of wavelengths that can be accommodated on the heater becomes large, it becomes increasingly difficult to correctly determine the number of jets supported by the heater on account of variations in the dominant wavelength. The occurance of a wide spectrum of wavelengths close to the region of neutral stability is quite common, as we have observed during film boiling on cylinders.

The effect of these variations should be less and less significant as the number of jets becomes large. Experimental data should tend more and more to scatter about the "infinite" flat plate prediction as we have observed in Figure 38 for L/λ_d greater than 3. For smaller plates, the number of jets that can be accommodated on the heater can significantly affect the peak heat flux. Our distilled water data are very well represented by a model which assumes only two standing jets on the heater. In Figure 39 curves representing the various number of jets that we expect to occur have been terminated at heater sizes where the peak heat flux predicted by the preceeding or succeeding

curve is the same as for the "infinite" case.

To further substantiate the above observations and to exclude the possibility that the distilled water data are low because of the slightly different surface wettability character of water as argued by Costello [13], an independent study on square flat plates of different sizes and with different liquids was made by David Riherd [43]. Smooth cold-rolled nichrome ribbons, 2.29mm thick, and cut to particular sizes, were used as heaters. The ribbons were supported from below by ebonite sheet and held in brass holders. The brass holders were connected to power leads. A rectangular chimney made of tin sheet provided side walls above the heaters to avoid any inflow of liquid from the sides. A glass window in the chimney was used to observe the peak heat flux.

Riherd's data for various alcohols, and the distilled water data point of Costello for a 50.8 x 50.8 mm square plate are reproduced in Figure 40. The peak heat flux prediction based on the number of jets accommodated on the heater is also included. The one-jet model predicts the heat flux well for heater widths between one and two Taylor wavelengths. The data start deviating from the one-jet model as the plate width is decreased below one wavelength. This is not surprising. The liquid flow configuration must differ considerably from the assumed potential

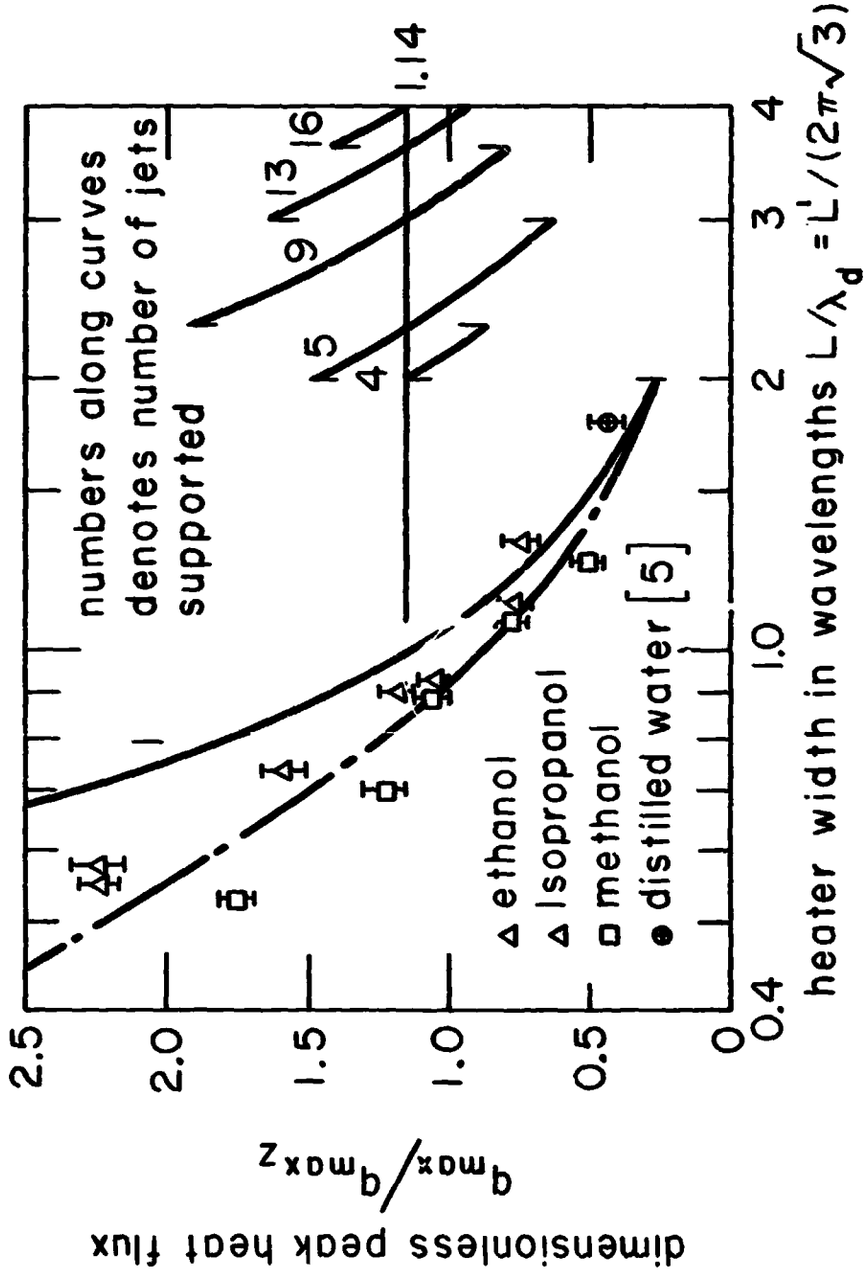

Fig. 40 Peak heat flux on a square finite flat plate with vertical side walls.

flow model as the liquid return route is squeezed into a thin annulus near the side wall.

3. Peak Heat Flux on Flat-Plate and Cylindrical Heaters when the Boiled Liquid is Viscous.

The peak heat flux for cyclohexanol on circular flat plates and on cylinders was observed both at earth normal gravity and at higher gravities. The data have been nondimensionalized by dividing them by the corresponding inviscid values.

The comparison of data for cylinders with data for flat plates is justifiable if R' is near unity, and we use data in the range $0.22 \leq R' \leq 1.24$ here. Sun and Lienhard's [12] inviscid hydrodynamic model for the peak heat flux on small cylinders assumes the gas jets are separated by λ_d. They took the jet radius to be $(R+\delta)$, where δ is the thickness of the vapor blanket surrounding the heater near the peak heat flux. While the radius of the jet decreases as $(R + \delta)$, so too does λ_H for small cylinders. The effect of a decrease in the liquid return velocity due to the smaller jet radius is nearly compensated by this shorter λ_H. Thus this model differs from our assumed flat plate model only in that the location of jets is on a line rather than on a square grid.

In Figure 41 are displayed peak heat flux data at earth normal gravity. The flat plate data for the smaller values of M have been corrected for the effect of finite plate size, since the

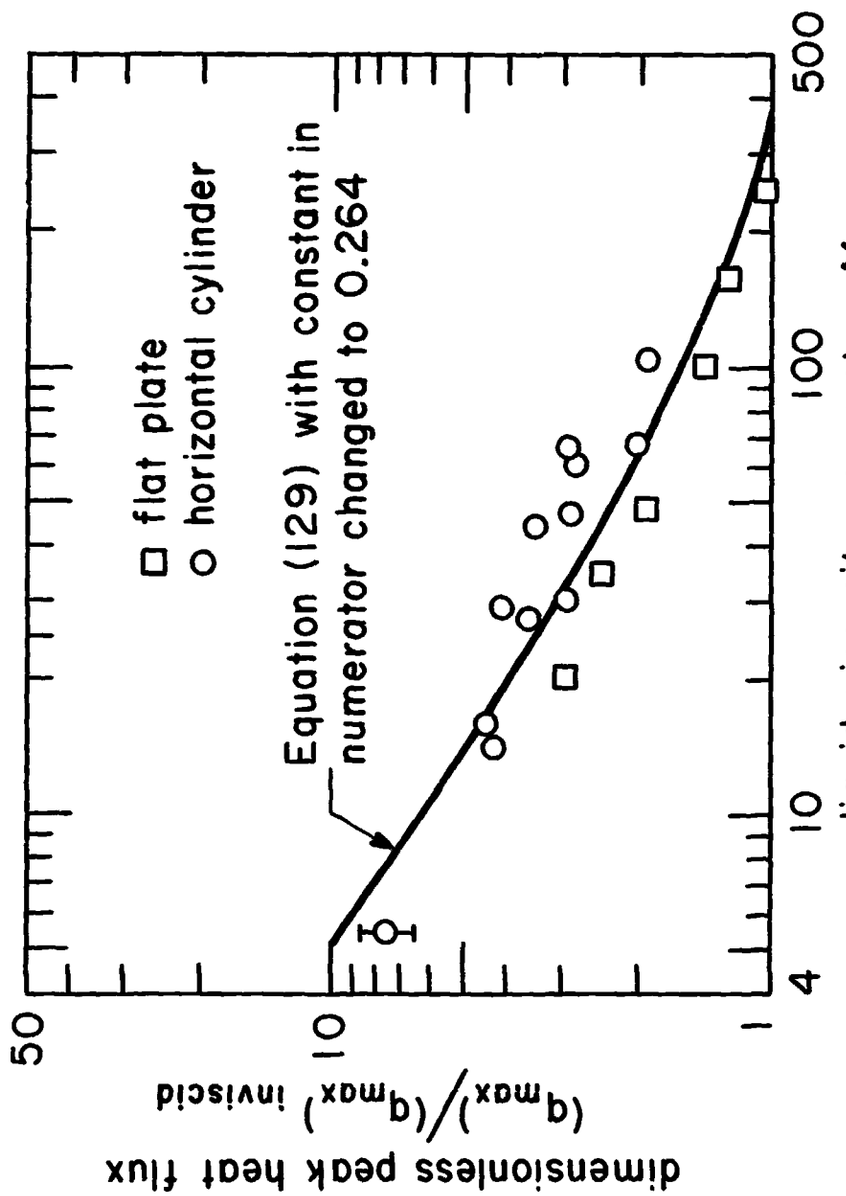

Fig. 41 Effect of liquid viscosity on peak heat flux for both flat plates and cylinders in cyclohexanol at earth normal gravity.

number of wavelengths accommodated is in the neighborhood of only 3 after a correction for the viscosity effect is made.

Now we would like to go back to Chapter IV and take a second look at our prediction equation (129). This equation was obtained with simplified boundary conditions. In the absence of an exact analysis, approximate expressions were used for the pressure and shear perturbations on a wavy surface. Thus it would be fortunate indeed if equation (129), as it is, represents the data well. We find, by comparing the experimental data (plotted in Figure 41) with the equation (129), that the predicted peak heat flux is higher than the experimental data. However, when the constant in the numerator is changed to 0.264, the prediction fits the data as well as any line could.

The functional dependence of the peak heat flux on M and V is very well brought out by equation (129). From the equations of motion, Borishanski [4] recognized that the dimensionless peak heat flux of viscous liquids should depend on three other dimensionless groups. These groups were a liquid viscosity parameter N, a ratio of the viscosities of the gas and liquid, and a ratio of the densities of gas and liquid. However,from the data for slightly viscous liquids his suggested correlation equation (3) was only dependent on N. If we return to equation (129) and rewrite it in the form

$$\frac{(q_{max_F})}{(q_{max_F})_{inviscid}} = \frac{1}{\Lambda_d^{1/2}} \frac{\mu_g}{\mu_f} \sqrt{\frac{\rho_g}{\rho_f}} \frac{(0.793 \text{ or empirical constant})}{\left\{1-0.939\left[\frac{1}{\Lambda_d M} \frac{\mu_g}{\mu_f} \sqrt{\frac{\rho_g}{\rho_f}} \frac{(q_{max_F})}{(q_{max_F})_{inviscid}}\right]^{\frac{1}{3}}\right\}^{\frac{1}{2}}} \tag{129}$$

where $\Lambda_d = f(M)$ and $M \simeq N^{1/2}$ as described in Chapter II, it contains all the groups suggested by Borishanski. Furthermore, it is much more general in nature than his equation (3). Equation (129) has been derived from purely hydrodynamic considerations.

Next we test equation (129) with high gravity data for cylindrical heaters and one high gravity data point for a flat plate heater. This plot of the peak heat flux as a function of M and V is shown in Figure 42. The corresponding predicted values of heat flux are connected by lines to the experimental points. The data seem to be well represented by equation (129); again using 0.264 for the constant in the numerator.

Conclusions.

1. The peak heat flux on an "infinite" flat plate for nearly inviscid liquids has been found to be 14% higher than predicted by Zuber.

2. The peak heat flux on a finite plate may not be represented adequately by the "infinite" flat plate model. The actual integral number of standing jets, rather than one jet per λ_d^2,

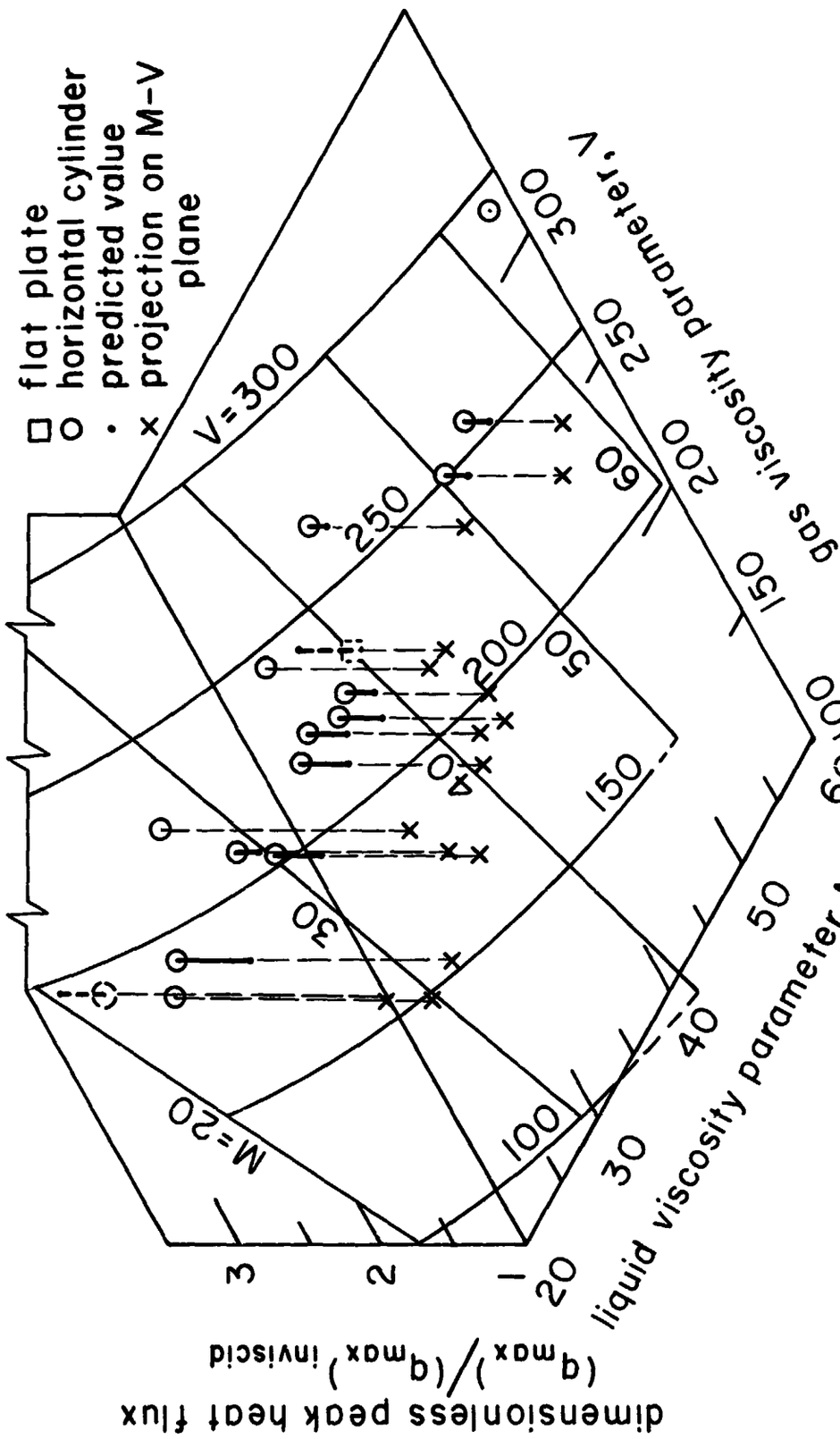

Fig. 42 Effect of liquid and gas viscosity on the peak heat flux at elevated gravities.

governs the peak heat flux on smaller plates.

3. The liquid viscosity tends to increase the peak heat flux. The data are correlated by equation (129) with the constant in numerator changed to 0.264.

VI. SUMMARY OF RESULTS

1. Liquid viscosity has been shown to increase the "most susceptible" Taylor wavelength and decrease the rate of growth of the disturbance. The results are not only applicable to film boiling but to any Taylor unstable processes. The effect of liquid viscosity becomes very significant when a liquid viscosity parameter, M, is less than 5.
2. The dominant Taylor wave during the film boiling of cyclohexanol on cylindrical heaters has been observed. Still pictures are made to measure the wavelengths and high speed motion pictures to study the wave growth rate. Data for wavelength and rate-of-growth are consistant with the theoretical dispersion relation. However, waves slightly longer than the "most susceptible" wavelength and having a slightly slower growth rate are usually preferred.
3. A correlation for the thickness of the vapor blanket surrounding a cylindrical heater has been suggested, based on available data for cyclohexanol and acetone. The data are correlated by equation (68).
4. Large vapor volume fluxes or high heat fluxes may cause the dominant wavelength in film boiling to stretch considerably from the "most susceptible" one.

5. Zuber's prediction for peak heat flux on "infinite" flat plates for nearly inviscid liquids has been slightly modified. The suggested expression is

$$(q_{max_F})_{inviscid} = 1.14\ q_{max_Z}$$

6. The peak heat flux has been observed on "infinite" flat plates at both the earth normal gravity and at higher gravities and the data have been correlated well by the above expression.

7. The effect of finite size of flat plates on the peak heat flux is discussed and some of the related controversial points resolved.

8. The stability of a gas jet in a viscous liquid has been studied. A prediction for the peak heat flux is obtained as a function of a liquid viscosity parameter, M, and a gas viscosity parameter V. The expression for the peak heat flux is given by equation (129).

9. Equation (129) succeeds in describing the peak heat flux data for cyclohexanol on cylindrical and flat plate heaters, at both earth normal and elevated gravities when the constant in the numerator is changed to 0.264.

10. The effect of liquid viscosity is to increase the peak heat flux greatly when the liquid viscosity parameter, M, is less than 200.

NOMENCLATURE

A_h	area of the heater
A_j	combined cross-sectional area of vapor jets escaping from A_h
B	ratio of viscous to surface tension force in vapor blanket, $q\mu_g/(\rho_g h^*_{fg} \sigma)$
Bo	the Bond number, ratio of buoyant to surface tension forces, $R_c^2 (\rho_f - \rho_g) g/\sigma$
c	speed of a disturbance in a liquid-vapor interface
c_v	specific heat of vapor
d_f, d_g	depth of liquid and vapor phases, respectively
f_b	number of bubbles released per second
g	acceleration due to the body force acting in a system
h_{fg}	latent heat of vaporization
h^*_{fg}	latent heat of vaporization corrected for sensible heat, $h_{fg} [1 + 0.34 c_v \Delta T/h_{fg}]^2$
h	convective heat transfer coefficient at the surface of a flat plate heater
h_w	heat transfer coefficient for film boiling on wires
k	wave number
k_g	thermal conductivity of vapor
k_n	thermal conductivity of heater material
K	dimensionless wave number, $k\sqrt{\sigma/[g(\rho_f - \rho_g)]}$
L	characteristic length of a heater

L', R'	dimensionless characteristic length of a heater, $L\sqrt{g(\rho_f - \rho_g)/\sigma}$, $R' = L'$ based on $L = R$
M	liquid viscosity parameter, defined in equation (44)
N	Borishanski number, defined in equation (4)
P	absolute pressure at the surface of a heater
$\tilde{P}$	dimensionless perturbation pressure, defined in equation (110)
P_g	pressure in a gas jet
p_f, p_g	perturbation pressure in liquid and gas, respectively
p_o	total perturbation pressure
q	heat flux
q_{max}, q_{max_F}	peak heat flux for a particular heater geometry and for an "infinite" flat plate, respectively
q_{max_Z}	Zuber's prediction as defined in equation (6) for the peak heat flux on an "infinite" flat plate
q_{min}, q_{min_F}	minimum heat flux on a cylindrical heater and on an "infinite" flat plate, respectively
R	radius of a cylindrical heater
R_c	radius of a cylindrical heater corrected for the vapor blanket thickness around it
R'_c	a dimensionless corrected radius, $R_c\sqrt{g(\rho_f - \rho_g)/\sigma}$
R_e	Reynold's number as defined in equation (65) and equation (92)
R_j	radius of gas jet
S	a dimensionless number, defined in equation (111)
T	temperature
$\tilde{T}$	dimensionless perturbation shear stress, defined in equation (112)

T_c	critical temperature of a fluid
T_s	saturation temperature of a liquid
T_w	temperature of heater wall
t	time
U_f	primary velocity of the liquid in a liquid column
U_{fm}	maximum primary downward velocity in the liquid
U_g	primary velocity of the gas in a gas jet
U_{gm}	maximum primary velocity of the gas
u_f, u_g	perturbation velocity of liquid and gas, respectively, in the x-direction
V	dimensionless gas viscosity parameter, defined in equation (130)
$\dot{v}$	vapor volume flux
v_f, v_g	perturbation velocity of liquid and gas, respectively, in the y-direction

Greek Letters

α	dimensionless wave number as used in equation (93a)
β	a number less than one
Γ	dimensionless density, $(\rho_f - \rho_g) / (\rho_f + \rho_g)$
δ	thickness of the vapor blanket on a cylindrical heater near the peak heat flux
Δ	dimensionless vapor blanket thickness in film boiling, d_g/R
ΔT	temperature difference between a heater wall and a liquid

η	ordinate of an interface measured from its mean position
Λ	dimensionless wavelength, $(\lambda/2\pi)\sqrt{g(\rho_f-\rho_g)/3\sigma}$ $= 1/K\sqrt{3}$
Λ_d	dimensionless "most susceptible" wavelength
λ	wavelength
λ_c, λ_d	the "critical" and "most susceptible" wavelengths, respectively
λ_H	Helmholtz unstable wavelength
μ_f, μ_g	viscosity of liquid and vapor, respectively
ν_f, ν_g	kinematic viscosity of liquid and vapor, respectively
ρ_f, ρ_g	density of liquid and vapor, respectively
σ	surface tension between a liquid and its vapor
τ_f, τ_g	perturbation shear stress in liquid and vapor, respectively
Φ	perturbation potential function as defined in equation (20)
Ψ	perturbation function as defined in equation (21)
$\underline{\Psi}$	perturbation stream function as defined in equation (94)
Ω	dimensionless frequency, $\omega\sqrt[4]{\sigma/g^3(\rho_f-\rho_g)}$
Ω_d	dimensionless "most susceptible" frequency
ω	angular frequency
ω_d	maximum or "most susceptible" angular frequency
ω_{d_F}	"most susceptible" angular frequency on a flat plate when both the liquid and gas are considered inviscid, $\sqrt[4]{g^3(\rho_f-\rho_g)/\sigma}/1.612$

Subscripts

expt	refers to experimental data
F	"infinite" flat plate
f	liquid
g	gas
h	heater
i	imaginary
j	jet
m or max	maximum
min	minimum
r	real

REFERENCES

1. Nukiyama, S., "The Maximum and Minimum Values of the Heat Q Transmitted from Metal to Boiling Water under Atmospheric Pressure", Trans. JSME, vol. 37, 1934, p. 367. Reprinted in Int. Jour. Heat Mass Transfer, vol. 9, 1966, pp. 1419-1433.

2. Drew, T.B. and Mueller, G., "Boiling", Trans. AIChE, vol. 33, 1937, p. 449.

3. Kutateladze, S.S.,"On the Transition to Film Boiling under Natural Convection", Kotloturbostroenie, No. 3, 1948, p. 10.

4. Borishanski, V.M., "An Equation Generalizing Experimental Data on the Cessation of Bubble Boiling in a Large Volume of Liquid", Zhurn. Tekh. Fiz., vol. 26, 1956, p. 452; translated in Soviet Physics-Technical Physics, vol. 1, p. 438.

5. Costello, C.P., Bock, C.O. and Nichols, C.C., "A Study of Induced Convective Effects on Pool Boiling Burnout," Chemical Engineering Progress Symposium Series, vol. 61, 1961, pp. 271-280.

6. Lienhard, J.H. and Keeling, K.B., Jr., "An Induced Convection Effect on the Peak Boiling Heat Flux," Jour. Heat Transfer, Trans. ASME, Series C, vol. 92, 1970, pp. 1-5.

7. Zuber, N., Tribus, M. and Westwater, J.W., "The Hydrodynamic Crisis in Pool Boiling of Saturated and Subcooled Liquids," International Developments in Heat Transfer, ASME, New York, 1963, pp. 230-235.

8. Cichelli, M.T. and Bonilla, C.F., "Heat Transfer to Liquids Boiling under Pressure," Trans. A.I.Ch.E., vol. 41, 1945, p. 755.

9. Berenson, P.J., "Transition Boiling Heat Transfer from a Horizontal Surface," Tech. Report No. 17, M.I.T. Heat Transfer Laboratory, March 1, 1960.

10. Bobrovich, G.I., Goçonin, I.I. and Kutatcladze, S.S., "Influence of Size of Heater Surface on the Peak Pool Boiling Heat Flux," Jour. App. Mech. and Tech. Phys., (ПМТФ), No. 4, 1964, pp. 137-138.

11. Lienhard, J.H. and Watanabe, K., "On Correlating the Peak and Minimum Boiling Heat Fluxes with Pressure and Heater Configuration," Jour. Heat Transfer, Trans. ASME, Series C, vol. 88, No. 1. Feb. 1966, pp. 94-100.

12. Sun, K.H. and Lienhard, J.H., "The Peak Pool Boiling Heat Flux on Horizontal Cylinders," Int. J. Heat Mass Transfer, vol. 13, 1970, pp. 1425-1439.

13. Costello, C.P. and Adams, J.M., "The Interrelation of Geometry, Orientation and Acceleration in the Peak Heat Flux Problem," Mechanical Engineering Department Report, University of Washington, Seattle, Wash., 1963.

14. Bellman, R. and Pennington, R.H., "Effects of Surface Tension and Viscosity on Taylor Instability," Quart. App. Math., vol. 12, 1954, pp. 151-162.

15. Lewis, D.J., "The Instability of Liquid Surfaces when Accelerated Perpendicular to Their Planes II," Proc. Roy. Soc. London, A-202, 1950, p. 81.

16. Allred, J.C. and Blount, G.H., "Experimental Studies of Taylor Instability," Rept. LA-1600, Los Alamos Sc. Lab. University of California, 1954.

17. Lienhard, J.H. and Wong, P.T.Y., "The Dominant Unstable Wavelength and Minimum Heat Flux During Film Boiling on a Horizontal Cylinder," Jour. Heat Transfer, Trans. ASME, Series C, vol. 86, No. 2, May 1964, pp. 220-226.

18. Kovalev, S.A., "An Investigation of Minimum Heat Fluxes in Pool Boiling of Water," Int. Jour. Heat and Mass Transfer, vol. 9, 1966, p. 219.

19. Baumeister, K.J. and Hamill, T.D., "Film Boiling from a Thin Wire as an Optimal Boundary-Value Process," ASME Paper 67-HT-62, ASME-AIChE Heat Transfer Conference, Seattle, Wash., 1967.

20. Lienhard, J.H. and Sun, K.H., "Effects of Gravity and Size Upon Film Boiling From Horizontal Cylinders," Jour. Heat Transfer, Trans. ASME, Series C, vol. 92, No. 2, 1970, pp. 292-298.

21. Lienhard, J.H. and Carter, W.M., "Gravity Boiling Studies," 1st Annual Report, Technical Report No. 1-68-ME-1, University of Kentucky, Lexington, Kentucky, 1968.

22. Taylor, G.I., "The Instability of Liquid Surfaces When Accelerated in a Direction Perpendicular to their Plane," Proc. Roy. Soc. London, A-201, 1950, p. 192.

23. Hsieh, D.Y., "Effects of Heat and Mass Transfer on Rayleigh-Taylor Instability," Jour. Basic Engineering, Trans. ASME, Series D, vol. 94, No. 1, March 1972, pp. 156-162.

24. Dhir, V. and Lienhard, J.H., discussion of "Effects of Heat and Mass Transfer on Rayleigh-Taylor Instability," by D.Y. Hsieh, Jour. Basic Engineering, Trans. ASME, Series D, vol. 94, No. 1, March 1972, pp. 161-162.

25. Numerical Analysis Library for the S/360. University Computing Center, University of Kentucky, Lexington, Ky., December 1970.

26. Breen, B.P. and Westwater, J.W., "Effects of Diameter of Horizontal Tubes on Film Boiling Heat Transfer," Chemical Engr. Prog., vol. 58, No. 7, July 1962, pp. 67-72.

27. Touloukian, Y.S. and Dewitt, D.Y., Thermal Radiative Properties of Metallic Elements and Alloys, IFI/Plenum-New York Publication.

28. Dergarabedian, P., "The Rate of Growth of Vapor Bubbles in Superheated Water," Jour. Applied Mechanics, Trans. ASME, December 1953, pp. 537-545.

29. Gubareff, G.G., Janssen, J.E. and Torborg, R.H., Thermal Radiation Properties Survey, 2nd edition, Honeywell Research Center, Minneapolis-Honeywell Regulator Company, Minneapolis, Minn., 1960.

30. Lienhard, J.H. and Wong, P.T.Y., "The Dominant Unstable Wavelength During Film Boiling," ASME/ESL Film Library.

31. Keshock, E.G. and Siegel, R., "Forces Acting on Bubbles in Nucleate Boiling Under Normal and Reduced Gravity Conditions," NASA Tech. Note TND-2299, August 1964.

32. Grigull, U. and Abadzic, E., "Heat Transfer From a Wire in the Critical Region," Proceedings of the Institution of Mechanical Engineers, vol. 182, Pt. 31, 1967-1968, pp. 52-57.

33. Abadzic, E. and Goldstein, R.J., "Film Boiling and Free Convection Heat Transfer to Carbon Dioxide Near the Critical State," International Journal of Heat and Mass Transfer, vol. 13, 1970, pp. 1163-1175.

34. Lamb, Sir H., Hydrodynamics, 6th edition, Dover, New York, 1945.

35. Dhir, V., "Some Notes on the Development of the Hydrodynamic Theory of Boiling," Tech. Report No. 19-70-ME6, University of Kentucky, Lexington, Ky., 1970.

36. Ded, J.S. and Lienhard, J.H., "The Peak Pool Boiling Heat Flux on Spheres in Saturated Liquids," AIChE Jour., vol. 18, No.2, March 1972, pp. 337-342.

37. Lienhard, J.H. and Dhir, V., "Hydrodynamic Predictions of Peak Pool Boiling Heat Fluxes from Finite Bodies," to appear in Jour. Heat Trans., Trans. ASME, (in press).

38. Brooke Benjamin T., "Shearing Flow Over a Wavy Boundary," Journal of Fluid Mechanics, voi. 6, 1959, pp. 161-205.

39. Craik, Alex D.D., "Wind Generated Waves in Thin Liquid Films," Journal of Fluid Mechanics, vol. 26, 1966, pp. 369-392.

40. Nayfeh, A.H. and Saric, W.S., "Body Force Effects on the Stability of a Liquid Film," Research Report SC-RR-70-722, Sandia Laboratories, Albuquerque, New Mexico, November 1970.

41. Davis, D.E., "The Design of a Flat Plate Heater for Pool Boiling Studies," Boiling and Phase Change Laboratory Report, University of Kentucky, Lexington, Ky., May 1970.

42. Dhir, V. and Lienhard, J.H., "Laminar Film Condensation on Plane and Axisymmetric Bodies in Nonuniform Gravity," Jour. Heat Transfer, Trans. ASME, Series C, vol. 93, No. 1, Feb. 1971, pp. 97-100.

43. Riherd, D., "Peak Pool Boiling Heat Flux or Finite Flat Plate Heaters," Special Project Report, Mechanical Engineering Department, University of Kentucky, Lexington, Ky., August 1972.

44. Eckert, E.R.G., and Drake, R.M., Jr., Heat and Mass Transfer, 2nd edition, McGraw-Hill Book Company, New York, 1959.

45. Hilpert, R., Forsch, Gebiete Engenieurw., vol. 4, 1933, p. 215.

46. Kays, W.M., Convective Heat and Mass Transfer, McGraw-Hill Book Company, New York, 1966.

47. Sun, K.H., "The Peak Pool Boiling Heat Flux on Horizontal Cylinders," M.S. Thesis, University of Kentucky, Lexington, Ky., 1969 (available as College of Engineering Bulletin No. 88, May 1969).

48. Weast, R.C., Handbook of Chemistry and Physics, college edition, The Chemical Rubber Company, Cleveland, Ohio, 1969-70.

49. Beilstein's Handbuch Der Organischen Chemie, Vierte Auflage, Band VI, Erster Teil S.1-502, System Nummer 498-510, p. 11.

50. Reid, R.C., and Sherwood, T.K., The Properties of Gases and Liquids, 2nd edition, McGraw-Hill Book Company, New York, 1966.

APPENDIX A

FLAT PLATE PEAK HEAT FLUX CALCULATIONS AND ITS ERROR ANALYSIS

Heat Flux Calculations.

The heat flux during any instant of the boiling process was evaluated by noting the readings of thermocouples 1 and 2; whereas the observation of thermocouple 3 provided a counter-check. We again mark the locations of thermocouples 1,2 and 3 below in Fig. 43 for convenience. All distances are marked in millimeters.

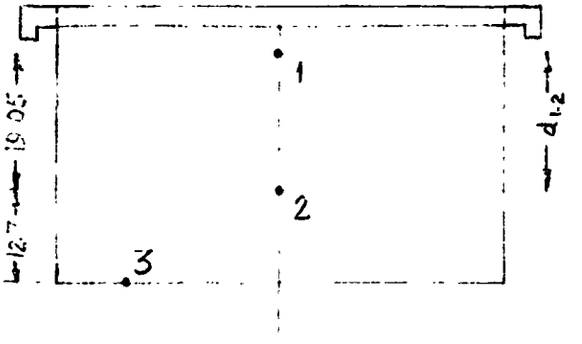

Fig. 43. Location of thermocouples used for heat flux calculations.

For steady state heat conduction in the axial direction, Fourier's law can be written as:

$$q = -k_h \frac{dT}{dx} \qquad \text{Watts/m}^2 \qquad \text{(A1)}$$

Assuming that the cross-sectional area is constant and the conductivity of copper near 100°C is given by [44]:

$$k_h(T) = 378.9 - 0.052\,(T-100) \text{ Watts/in K} \qquad (A2)$$

the integration of equation (A1) between 2 and 1 gives:

$$q_{1-2}\, d_{1-2} = (T_2-T_1)\left\{378.9 - .052\left[\frac{(T_1+T_2)}{2} - 100\right]\right\} \qquad (A3)$$

or

$$q_{1-2} = (T_2-T_1)\left\{19890 - 2.73\left[\frac{(T_1+T_2)}{2} - 100\right]\right\} \qquad (A3a)$$

Similarly, the heat flux between locations (2) and (3) can be written as

$$q_{2-3} = (T_3-T_2)\left\{29835 - 4.10\left[\frac{(T_3+T_2)}{2} - 100\right]\right\} \qquad (A4)$$

For all the observations the contribution of the term in square brackets was less than 1.5%.

Error Analysis.

The total error in finding the peak heat flux consists of three different parts and we discuss each of them under a separate subtitle.

(i) The Natural Convection Heat Loss.

This heat loss can affect the observations two ways:

(a) By giving a radial temperature gradient in the heater body: To know this we evaluate the Biot num-

ber or the ratio of internal to external resistance.

For stationary tests, the average natural convective heat transfer coefficient from the heater surface may be taken approximately to be 11 watts/(m^2K). The heat transfer coefficient has been calculated by assuming a mean temperature along the heater wall and neglecting any curvature effect of the heater. Now

$$Bi = \frac{hL}{k_h} \simeq \frac{11 \times 0.03225}{378.9} = 0.0009$$

During the centrifuge tests, heat transfer from the outer surface of heater takes place due to forced convection. Experimental data for heat transfer from a cylinder when the flow of air is normal to its axis have been obtained by R. Hilpert [45]. Using his correlation for heat transfer coefficient as given by Kays [46], the Biot number for this situation may be written as:

$$Bi = \frac{25.7 \times 0.03225}{378.9} = 0.0022$$

The Biot number in both cases is very small, implying thereby the outer surface of the heater is nearly insulated and there is a negligible heat flow in the radial direction. Hence our assumption of purely axial heat flow is realistic.

(b) By convective heat loss from the outer surface of the heater between the top thermocouple and the boiling face: Energy transferred from the main heater body to the stainless

steel flange is eventually lost to the atmosphere through natural convection. This heat loss will be considerably less than the direct heat loss from the copper surface of the heater. Assuming that the heat transfer coefficient is no greater than 25.7 watts/m^2K and the temperature difference between heater surface and ambient air is 125K, we obtain 0.014×10^5 watts/m^2 for the radial heat loss between the top thermocouple and the boiling face. This loss is less than 1% of the lowest heat flux observed.

(ii) The Error Caused by Measurements:

The heat flux measurements depend on three variables: the thermal conductivity of copper, k_h, the difference between observations of thermocouples 1 and 2, $(T_2 - T_1)$, and the distance between the two thermocouples, d_{1-2}. The dependence of q upon these variables is given by:

$$q = k_h \frac{(T_2 - T_1)}{d_{1-2}} \qquad \text{(A3)}$$

The error in the peak heat flux is the combination of the errors in these variables. To analyze the combined effect, we differentiate equation (A3) and divide by q. Hence,

$$\frac{\Delta q}{q} = \frac{\Delta k}{k} + \frac{\Delta(T_2-T_1)}{(T_2-T_1)} - \frac{\Delta(d_{1-2})}{d_{1-2}} \qquad \text{(A5)}$$

The probable error in the measurement of q is:

$$\frac{\Delta q}{q} = \sqrt{\left(\frac{\Delta k}{k}\right)^2 + \left(\frac{\Delta(T_2-T_1)}{(T_2-T_1)}\right)^2 + \left(\frac{\Delta(d_{1-2})}{d_{1-2}}\right)^2} \qquad (A6)$$

The error $\frac{\Delta k}{k}$ can arise from the difference between actual conductivity of heater block and the one used in calculations. This error should not exceed 1%.

The thermocouple temperatures were read on a potentiometer calibrated to read the temperature directly. As we are interested in the difference of the two thermocouple readings, any error in the recorder is cancelled out. The only major error is the inaccuracy in reading the scale. The maximum value of this error is 6% for the smallest temperature difference observed.

The error in the location of the two thermocouples should not be greater than 1%.

(iii) The Error Due to Occurrence of the Peak Heat Flux Before the Steady State Thermocouple Observations are Made.

The main power to the heater was increased in steps, waiting each time for steady state to be established. In some of the observations, the peak heat flux was observed just after the power input to the heater was increased. In such a situation, it was difficult to make an accurate reading of the

thermocouple while the temperature was still rising. The maximum error from this procedure is 4-1/2%.

The probable error of q_{max} can be determined by taking the root mean square of all the errors involved.

$$\frac{\Delta q_{max}}{q_{max}} = \sqrt{(\text{convective error})^2 + (\text{measurement error})^2 + (\text{error caused by power input in steps})^2}$$

$$= \sqrt{(1)^2 + \left[(1)^2 + (6)^2 + (1)^2\right] + (4.5)^2} = 7.7\%$$

APPENDIX B

PHYSICAL PROPERTIES OF CYCLOHEXANOL

To compare the viscous theoretical predictions of the Taylor waves with the experimental observations, various physical properties of cyclohexanol are needed. The peak heat flux calculations also make use of some of these properties. Vapor phase properties are needed in the formulation of a correlation for the vapor blanket thickness. Properties of other test liquids, e.g. methanol, acetone, benzene, and iso-propanol, have been carefully plotted by Sun [47]. We frequently made use of this source in this study.

The liquid density, ρ_f, surface tension, σ, and vapor pressure of cyclohexanol are plotted as a function of temperature in Figures 44, 45 and 46. These properties have been obtained from references [48] and [49]. The Clausius-Clapeyron equation was used for interpolation of vapor pressure data. Viscosity of the liquid phase was measured experimentally with a Brookfield Syncro-electric Viscometer in the temperature range of 296K to 335K. These measurements differed a little from the reported values. Nevertheless, a mean curve through our experimental data and the data reported in [49] has been chosen. Figure 47

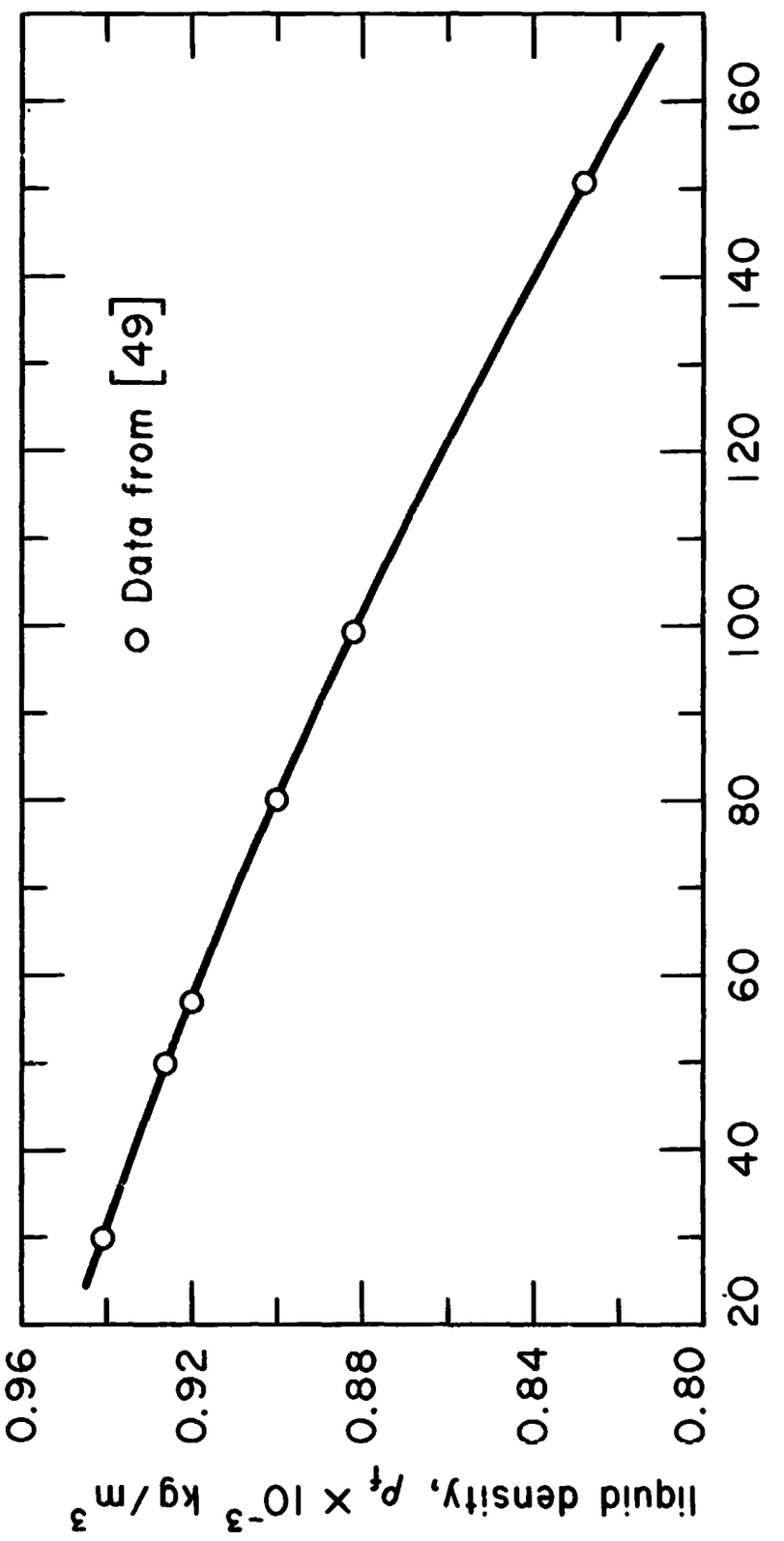

Fig. 44. Liquid density of cyclohexanol as a function of temperature.

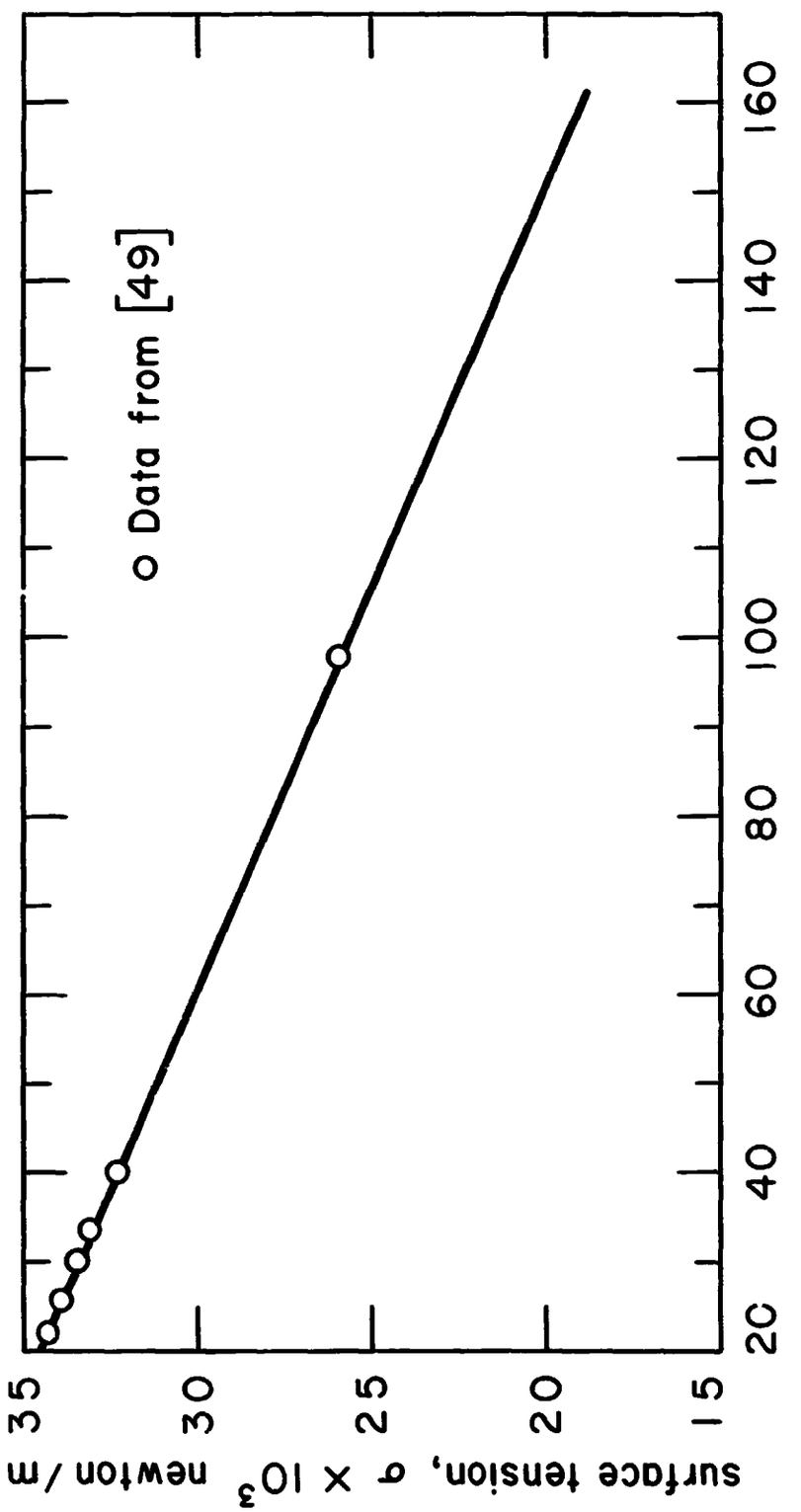

Fig. 45. Surface tension as a function of temperature.

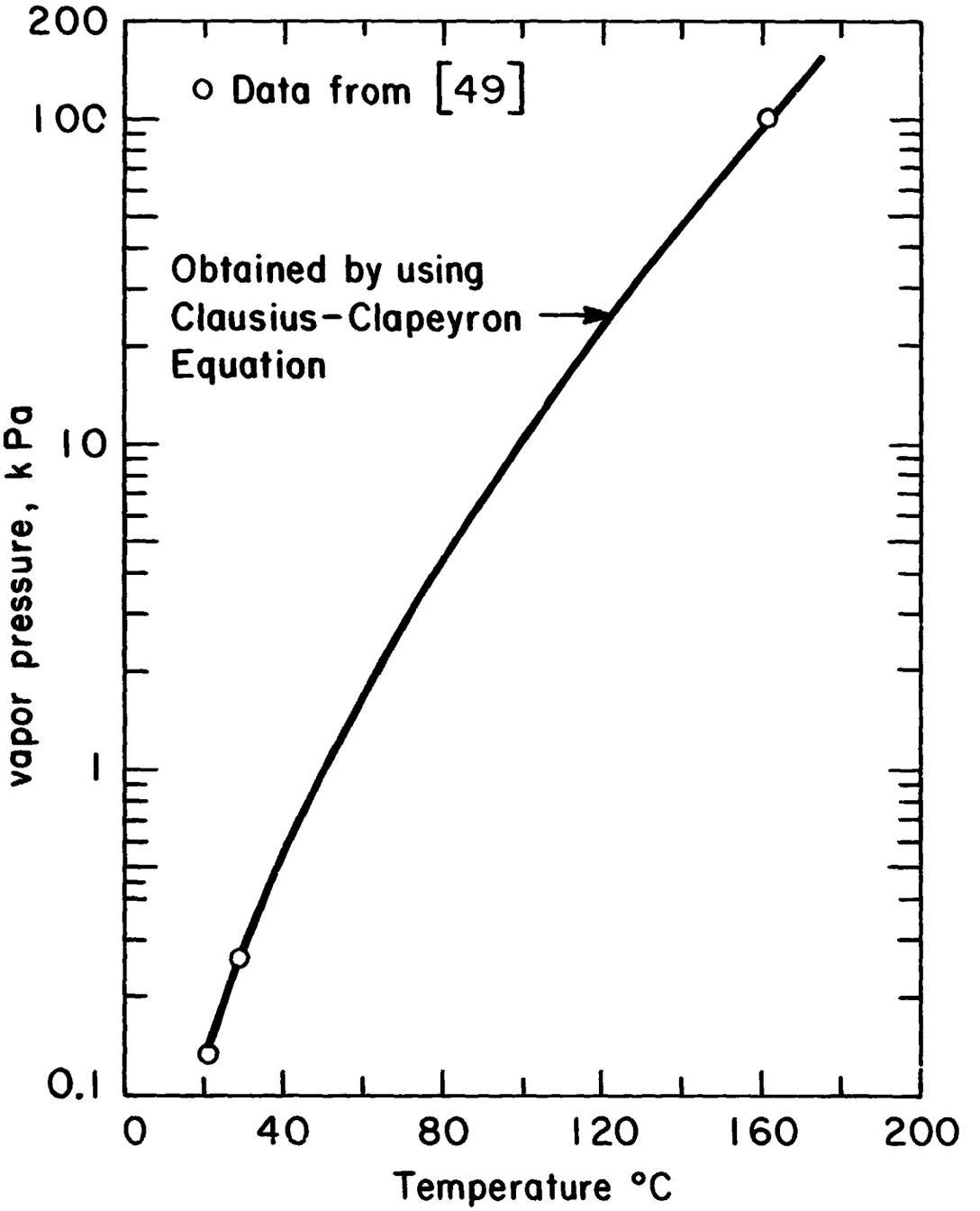

Fig. 46. Vapor pressure of cyclohexanol as a function of temperature.

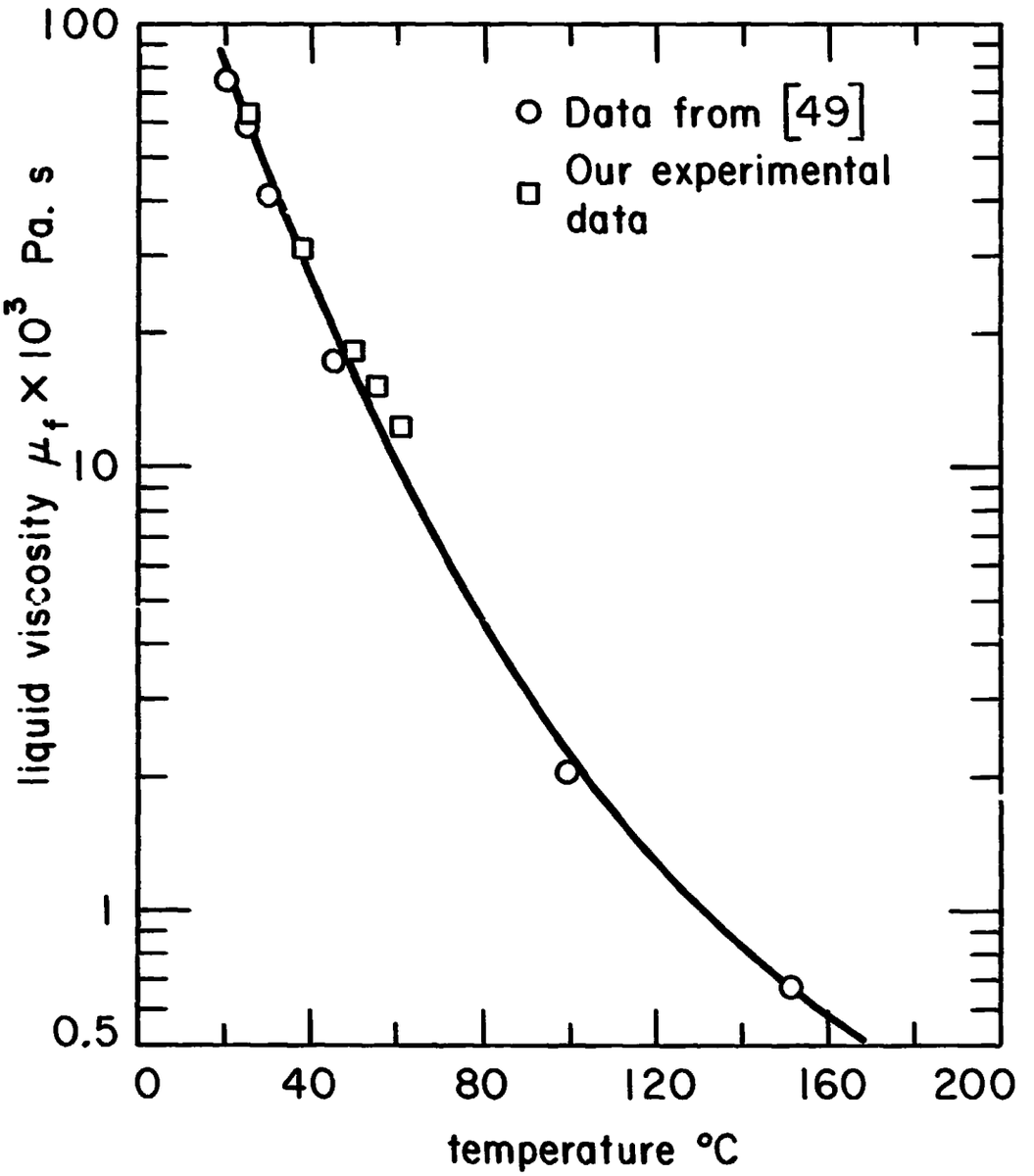

Fig. 47. Viscosity of cyclohexanol as a function of temperature.

shows such a plot for the viscosity of cyclohexanol as a function of temperature. The liquid viscosity parameter, M, which is nearly equal to the square root of the Borishanski Number, N, is plotted as a function of temperature in Figure 48.

The latent heat of vaporization, h_{fg}, at various temperatures has been calculated by using Watson's relation:

$$\frac{h_{fg_1}}{h_{fg_2}} = \left[\frac{\left(1-\frac{T_1}{T_c}\right)}{\left(1-\frac{T_2}{T_c}\right)}\right]^{0.38}$$

h_{fg} at the normal boiling point is obtained from reference [49]. We plot the latent heat as a function of temperature in Figure 49. The vapor density ρ_g at the saturation temperature is calculated by using the ideal gas law:

$$\rho_g = P/(RT)$$

The compressibility factor, $Z \equiv P/\rho_g RT$, has been assumed to be unity; which is a very good approximation at low pressures. Figure 50 shows a plot of the vapor density.

To obtain the vapor viscosity, use has been made of the corresponding state method of Stiel and Thodos. The vapor specific heat has been obtained by using Rihani and Doraiswamy's method. These methods are treated quite well in reference [50]. Figures 51 and 52, respectively, show viscosity and specific heat

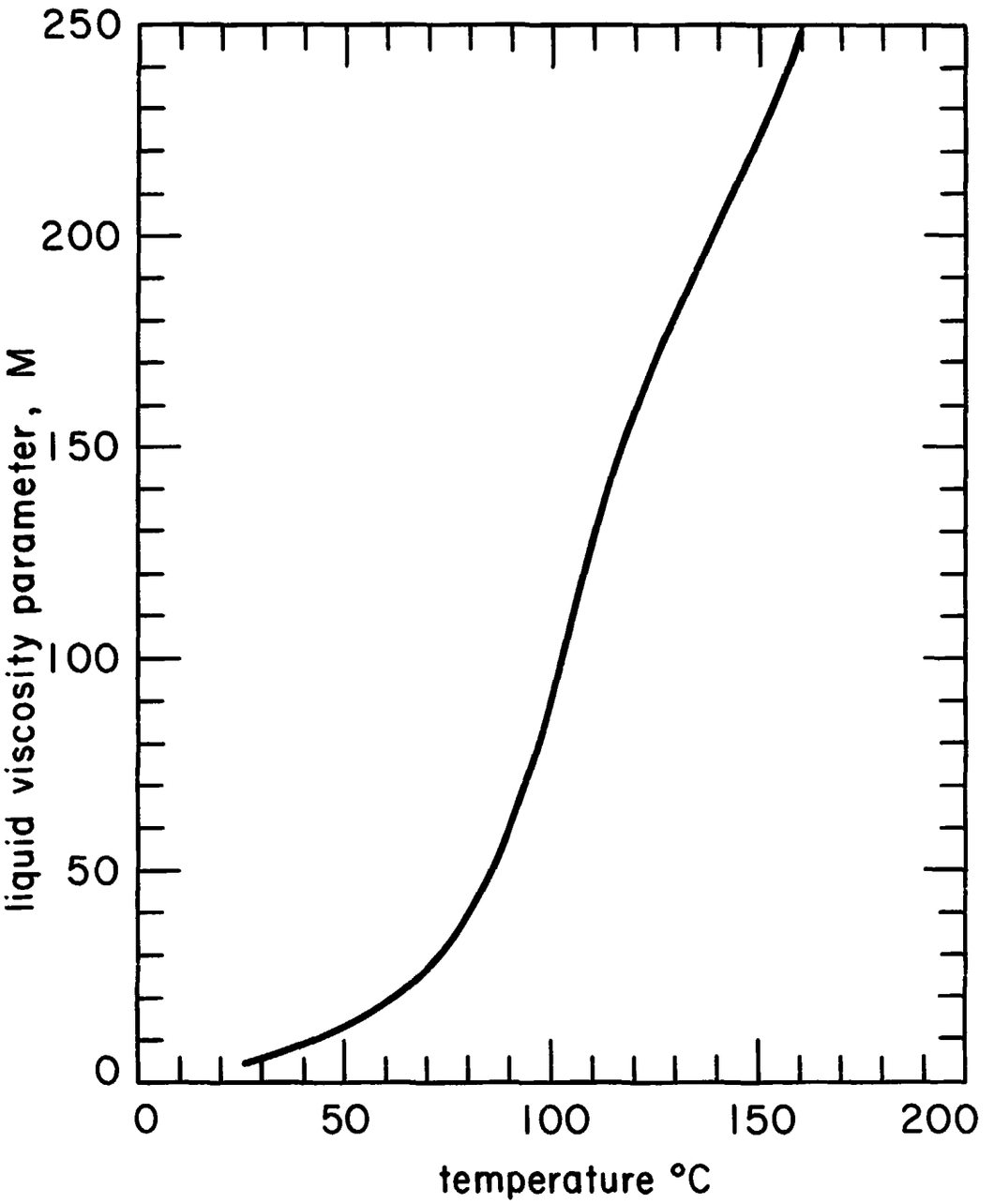

Fig. 48. Variation of liquid viscosity parameter, M, for cyclohexanol with temperature at earth normal gravity.

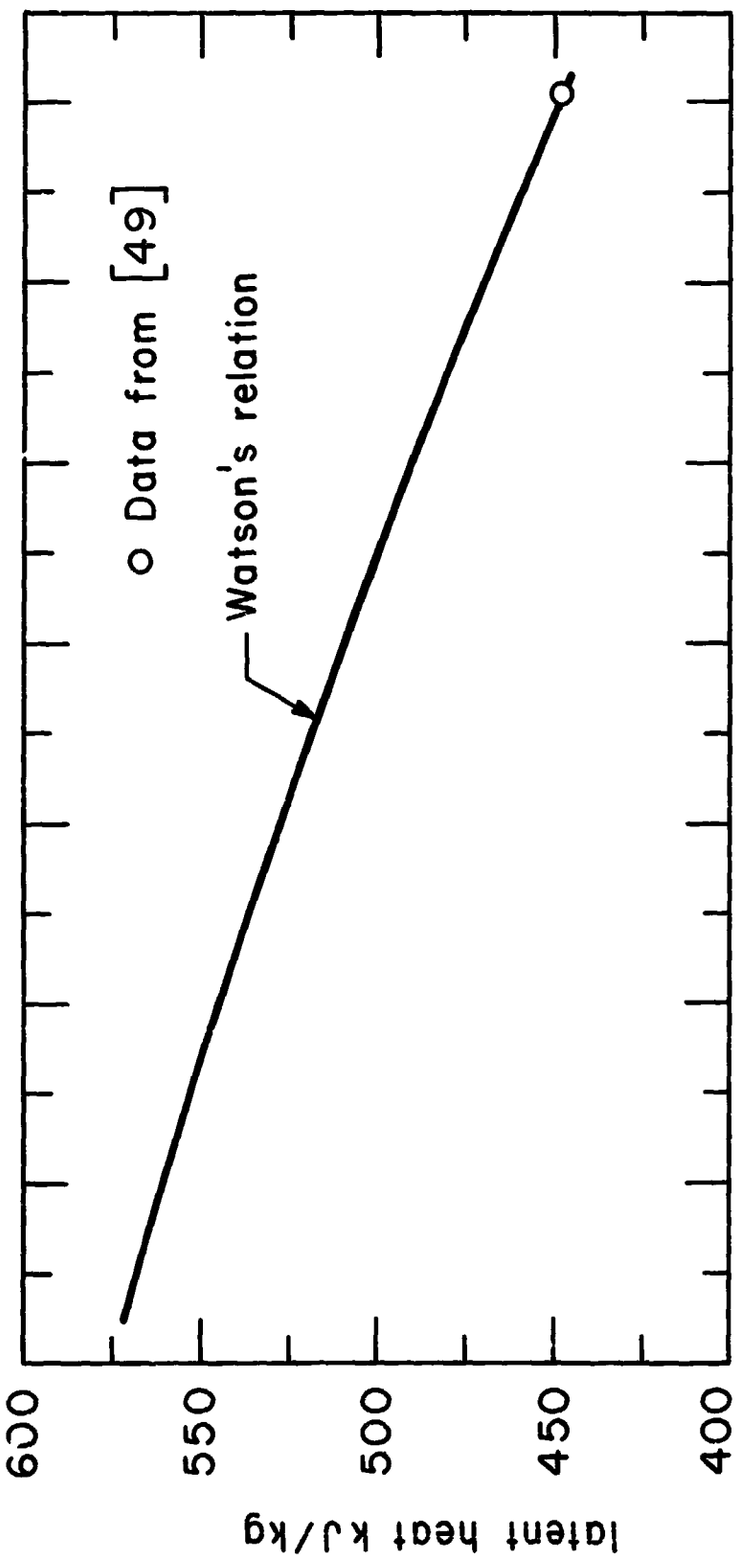

Fig. 49. Latent heat of vaporization of cyclohexanol as a function of temperature.

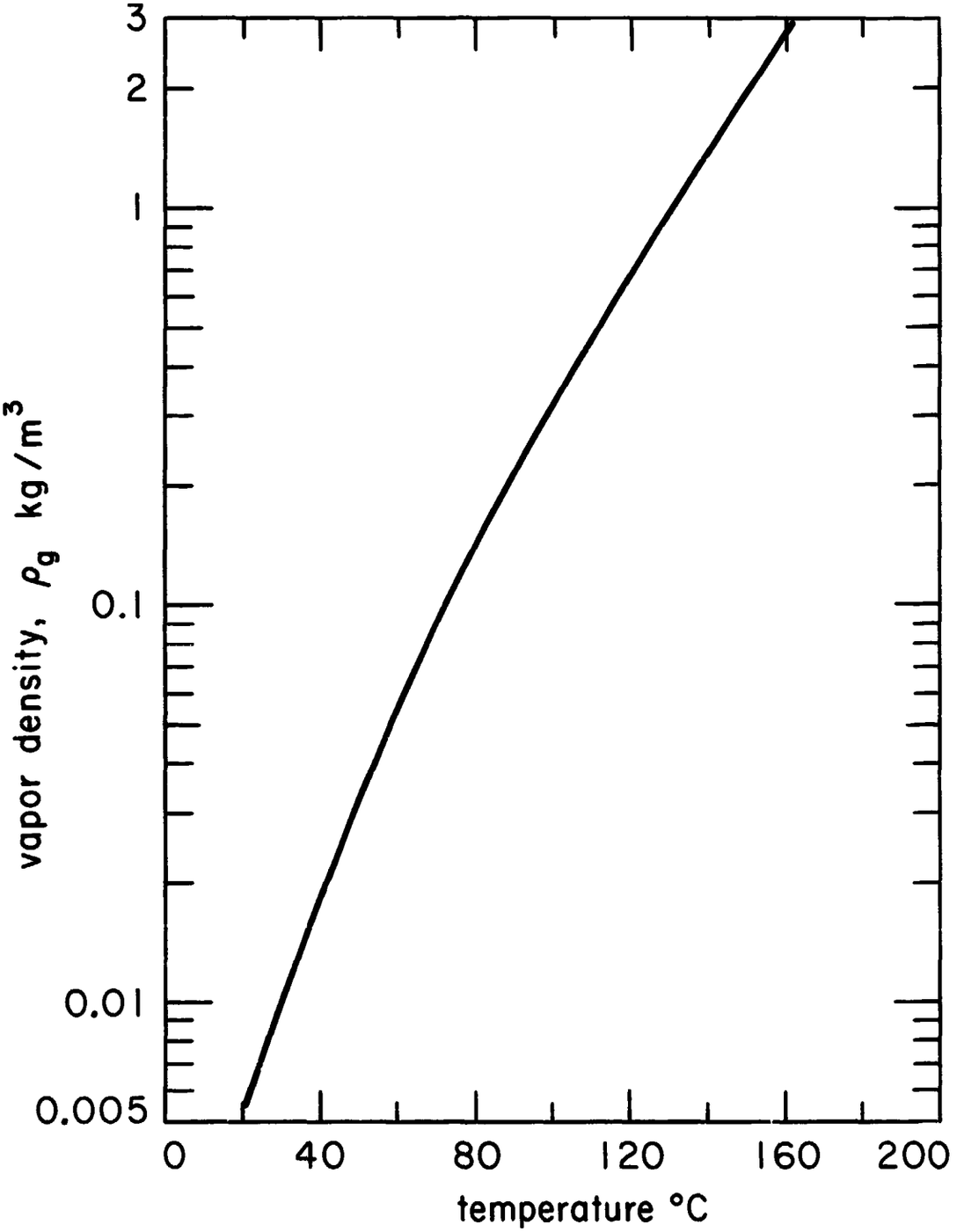

Fig. 50. Vapor density of cyclohexanol as a function of temperature.

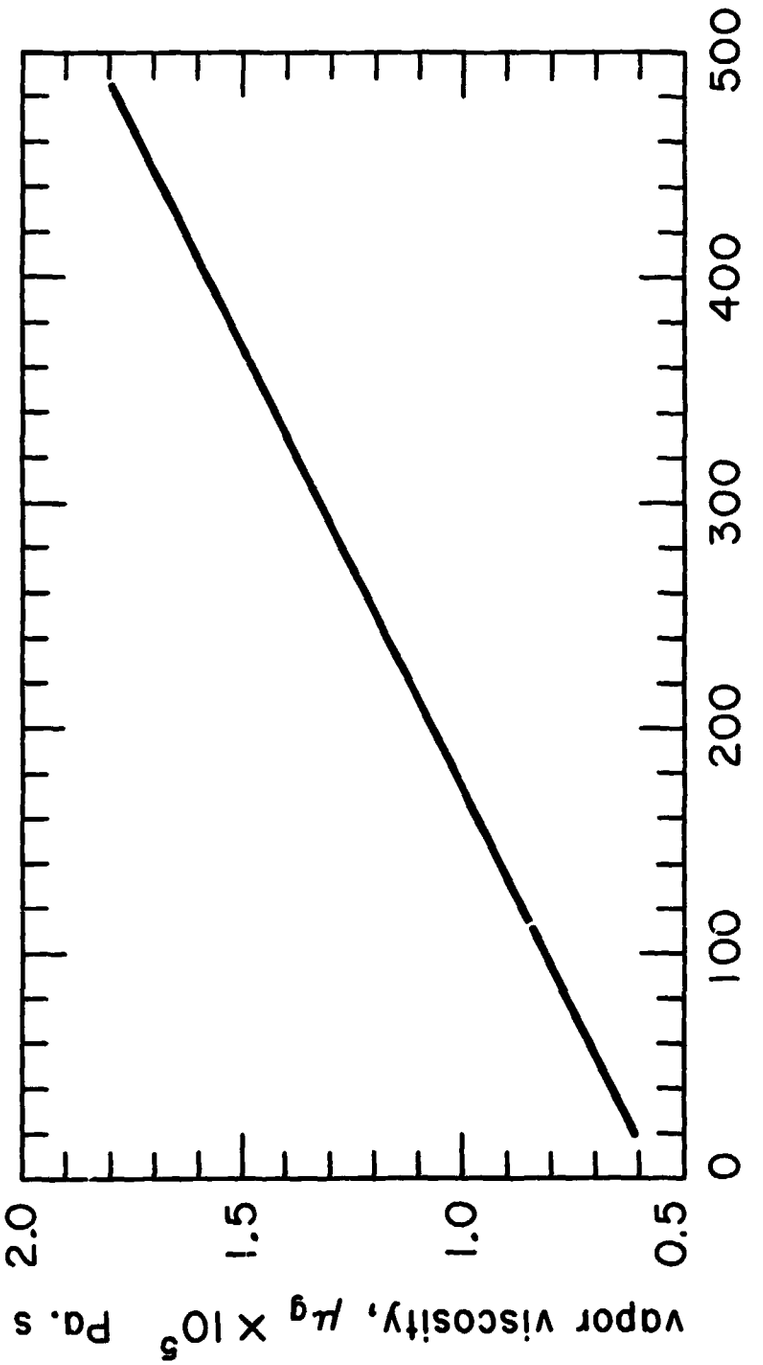

Fig. 51 Viscosity of cyclohexanol vapor as a function of temperature.

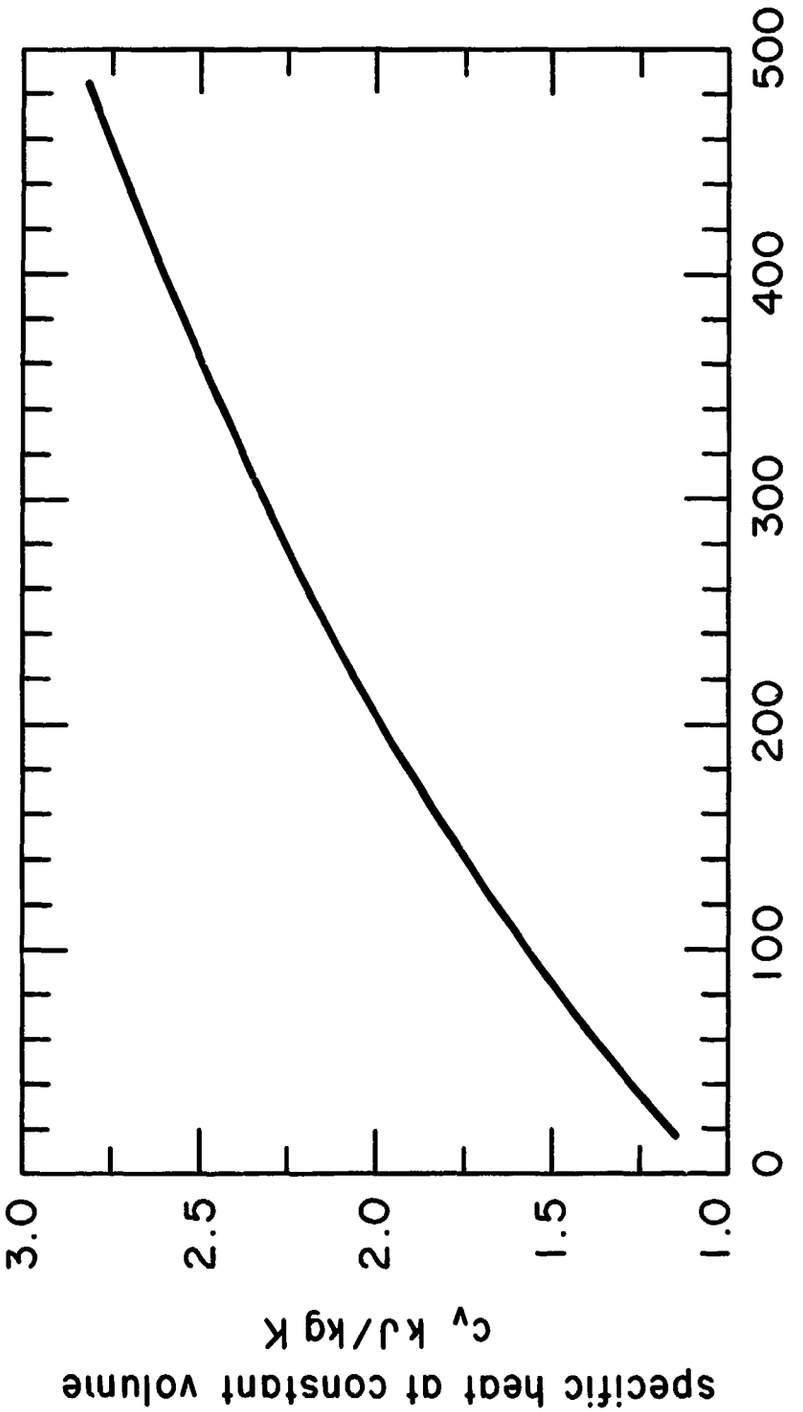

Fig. 52. Specific heat at constant volume of cyclohexanol vapor as a function of temperature.

as a function of temperature. The gas viscosity parameter, V, for cyclohexanol at earth normal gravity has been plotted as a function of temperature in Figure 53.

The liquid viscosity parameter, M, and the gas viscosity parameter, V, have been evaluated at earth normal gravity. These values can be corrected to gravity of interest by dividing by $\sqrt[4]{\text{gravity of interest/ earth normal gravity.}}$

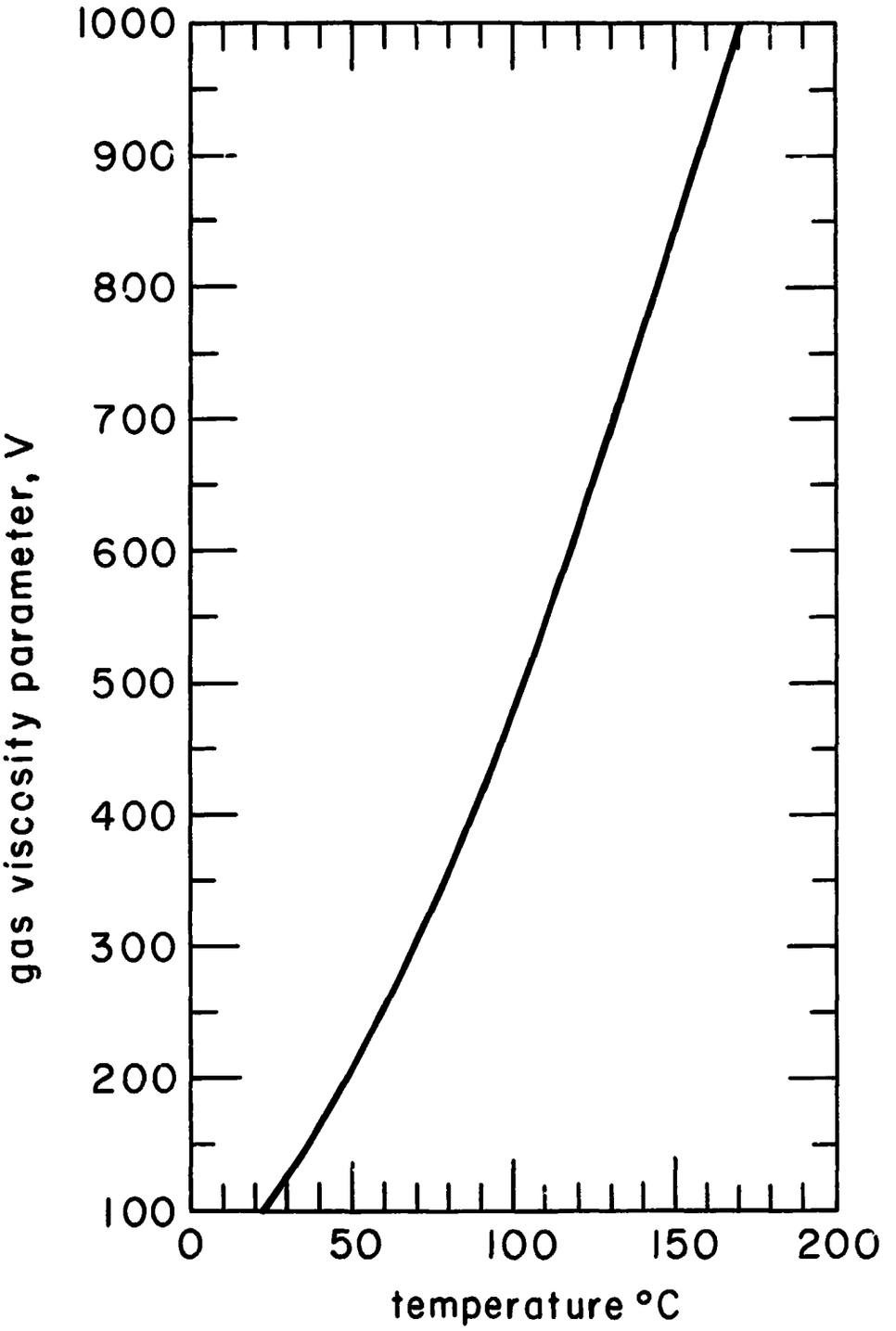

Fig. 53. Variation of gas viscosity parameter, V, for cyclohexanol with temperature at earth normal gravity.

APPENDIX C

TABULATION OF DATA

The data have been divided into three parts. The first part contains wavelength measurements. The second, vapor blanket thickness, and the third part, peak heat flux observations.

In all cases, while evaluating pressure, a correction was made for the liquid head acting on the heater surface. This correction is quite significant at very low pressures and at high gravities.

For the peak heat flux observations in the centrifuge, the frictional head loss in the condenser and other tubing between the boiling surface and manometer was also taken into account.

TABLE 1

Wavelength Data of Cyclohexanol for Horizontal Cylindrical Heaters at Earth Normal Gravity

R (mm)	R'	P (kPa)	M	$q \times 10^{-5}$ $\left(\frac{W}{m^2}\right)$	Observed Wavelength (minimum-maximum)	
					λ(mm)	Λ
0.4128	0.216	0.296	5.4	0.93	10.41-11.93	0.50-0.58
↓	↓			0.96	11.93-13.97	0.58-0.67
0.4128	0.216	0.296	5.4	1.16	11.18-15.75	0.54-0.76
0.5144	0.268			0.74	12.70-14.22	0.61-0.68
				0.81	12.70-15.24	0.61-0.73
				0.82	14.22-16.76	0.68-0.80
				0.88	12.70-13.32	0.61-0.64
				0.95	13.46-16.00	0.65-0.77
				1.00	14.98-17.53	0.72-0.84
0.6540	0.343			0.69	13.97-17.02	0.67-0.82
				0.75	12.70-17.78	0.61-0.86
				0.82	14.48-18.54	6.70-0.89
				0.84	13.97-18.54	0.67-0.89
0.8000	0.433			0.50	15.49-20.57	0.75-0.99
↓	↓	↓	↓	0.69	20.06-21.08	0.96-1.01
0.4128	0.224	1.06	16	1.11	11.93-13.72	0.59-0.68
↓	↓			1.43	13.72-14.48	0.68-0.72
0.5144	0.278			0.67	13.46-16.76	0.67-0.83
↓	↓			0.62	13.46-16.76	0.67-0.83
0.6540	0.354	↓	↓	0.72	15.24-18.54	0.75-0.92

TABLE 2

Vapor Blanket Thickness Data for Horizontal

Cylindrical Heaters at Earth Normal Gravity

R (mm)	R'	$q \times 10^{-5}$ $\left(\frac{W}{m^2}\right)$	$\frac{q\mu_g}{\rho_g h^* \sigma} \times 10^4$	$\frac{qR}{\mu_g h^*_{fg}}$	Observed Vapor Blanket Thickness (minimum - maximum)	
					d_g(mm)	$\Delta = d_g/R$
Cyclohexanol						
0.2667	0.144	0.86	10	1.25	0.12-0.15	0.45-0.55
0.4128	0.216	1.16	64	3.42	0.12-0.16	0.28-0.38
↓	↓	1.70	104	5.55	0.18-0.21	0.44-0.51
↓	↓	2.12	130	6.86	0.19-0.23	0.47-0.56
↓	0.227	1.01	11.6	2.30	0.17-0.24	0.40-0.58
0.5144	0.268	0.96	53	3.60	0.13-0.17	0.26-0.34
↓	↓	1.68	92	6.00	0.21-0.26	0.41-0.51
↓	0.278	0.67	7.3	1.90	0.15-0.19	0.29-0.37
↓	0.287	0.79	3.4	2.64	0.17-0.22	0.33-0.43
↓	0.294	0.79	1.8	2.54	0.11-0.13	0.22-0.26
↓	↓	1.02	2.4	3.30	0.10-0.13	0.20-0.26
0.6540	0.343	0.84	46	3.86	0.13-0.17	0.20-0.26
↓	↓	0.92	50	4.25	0.21-0.26	0.32-0.40
Acetone [+]						
0.2667	0.161	1.04	0.36	1.44	0.04-0.05	0.15-0.19
0.3200	0.203	1.30	0.45	2.27	0.04-0.06	0.13-0.19
0.4128	0.257	1.19	0.42	2.63	0.07-0.08	0.17-0.18
0.6440	0.409	1.01	0.35	3.55	0.05-0.06	0.08-0.1
0.6540	0.458	0.88	0.31	3.10	0.07-0.10	0.11-0.16
0.8250	0.514	1.17	0.41	5.16	0.09-0.11	0.11-0.14
1.0280	0.650	1.11	0.39	6.20	0.06-0.09	0.06-0.09

[+] Data reduced from observations of Sun as reported by Lienhard and Carter [21].

TABLE 3A

Peak Heat Flux Data on Circular Flat Plate Heaters

Liquid	g/g_e	P (k Pa)	M	$\frac{L'}{2\pi\sqrt{3}}$	$q_{max} \times 10^{-5}$ $\left(\frac{W}{m^2}\right)$	$\frac{q_{max}}{(q_{max_Z})}$
Acetone	1	98.58	599	3.71	3.94	1.18
↓	1	98.93	599	3.71	4.10	1.22
↓	4.97	23.99	548	7.69	3.44	1.14
↓	12.30	25.37	548	12.07	4.19	1.07
Benzene	4.97	18.06	384	7.36	2.98	1.21
↓	8.72	24.88	410	9.85	3.31	1.05
↓	17.5	27.09	413	14.07	4.19	1.07
Iso-	1	22.75	138	3.68	2.08	0.79
propanol	↓	46.53	182	3.78	3.34	1.0
↓	↓	73.21	233	3.85	3.82	0.98
↓	↓	88.52	243	3.88	4.54	1.10
↓	↓	98.72	254	3.91	4.26	1.0
↓	4.97	18.06	83	8.2	5.39	1.51
Methanol	1	44.60	370	3.56	3.69	0.94
↓	↓	47.43	377	3.56	4.13	1.02
↓	↓	88.04	420	3.72	5.33	1.04
↓	↓	96.38	435	3.75	5.33	1.01
↓	↓	96.52	435	3.75	5.33	1.01
↓	↓	98.10	439	3.75	5.33	1.0
Distilled	1	14.48	757	2.24	3.34	0.70
Water	↓	25.37	930	2.27	4.45	0.72
↓	↓	29.51	976	2.28	4.26	0.66
↓	↓	36.54	1040	2.29	4.82	0.67
↓	↓	39.16	1060	2.29	4.54	0.62
↓	↓	42.74	1079	2.30	4.54	0.59
Cyclo-	1	1.61	20	3.23	1.67	2.50
hexanol	↓	3.62	35	3.31	1.99	2.00
↓	↓	5.66	48	3.35	2.10	1.75
↓	↓	11.73	100	3.45	2.55	1.53
↓	↓	22.52	155	3.55	2.81	1.43
↓	↓	99.50	250	3.86	5.65	1.16
↓	4.97	11.86	70	7.69	3.75	1.69
↓	8.95	7.31	38	10.11	3.53	1.69

TABLE 3B

Peak Heat Flux Data of Cyclohexanol

for Horizontal Cylindrical Heaters

R (mm)	R'	g/g_e	P (kPa)	M	V	$q_{max} \times 10^{-5}$ $\left(\frac{W}{m^2}\right)$	$\frac{q_{max}}{(q_{max})_{inviscid}}$
0.4128	0.216	1	0.30	5.4	125	3.60	8.00
0.5144	0.268	↓	0.30	5.4	125	2.72	6.43
0.6540	0.343	↓	0.30	5.4	125	2.74	6.88
0.8001	0.419	↓	0.30	5.4	125	3.31	8.60
0.5144	0.284	↓	2.68	29	312	4.60	4.15
↓	0.289	↓	5.00	44	366	4.89	3.43
↓	0.294	↓	7.72	66	425	4.79	2.88
0.6540	0.354	↓	1.06	16	233	3.18	4.50
↓	0.362	↓	2.41	27	300	3.59	3.58
↓	0.368	↓	5.47	47	375	4.00	2.90
↓	0.373	↓	7.17	61	420	4.26	2.83
0.4128	0.222	↓	0.94	14	215	3.25	4.34
↓	0.228	↓	2.76	30	317	3.37	2.87
↓	0.233	↓	7.86	67	429	3.69	2.01
↓	0.241	↓	13.31	104	500	4.29	1.92
↓	0.669	8.5	3.54	20	196	5.27	3.01
↓	0.997	18.3	5.34	23	181	6.24	2.66
↓	1.194	25.7	6.89	26	182	8.67	2.96
↓	0.680	8.3	8.00	37	247	5.48	2.23
↓	1.020	18.3	10.41	37	218	7.16	2.24
↓	1.220	25.7	11.99	36	209	8.10	2.29
↓	0.672	8.3	5.45	28	224	5.71	2.76
↓	0.998	17.8	8.00	30	205	7.00	2.50
↓	1.207	25.7	9.44	32	193	7.95	2.44
↓	0.687	8.3	10.40	44	262	5.80	2.13
↓	1.011	17.8	11.58	39	221	6.69	2.08
↓	1.220	25.7	12.82	39	209	8.10	2.19
↓	0.702	8.3	16.52	63	295	5.48	1.65
↓	1.032	17.8	17.99	55	251	7.44	1.90
↓	1.240	25.7	19.23	53	239	8.10	1.90

APPENDIX D

ON THE USE OF SI UNITS IN THIS STUDY

The international scientific and technical comrnunity is gradually accepting one common system of measures known as the International System of Units (SI) as a substitute to the various customary units. Recognizing this trend, we have presented all the results in this work in SI units. For the convenience of those who may wish to use this information in other units, a table of conversion factors from SI units to Metric or English is given below.

Quantity	SI Units	Equivalent		
		Metric Units		English Units
density	kg/m^3	1	kg/m^3	0.0624lbm/cuft
surface tension	Newton/m	1	kg/s^2	0.0685 lbf/ft
viscosity	Pa·s ($N:s/m^2$)	1 1000.0	kg/s-m centipoises	413.22 lbm/ft hr
pressure	k Pa	101.97 7.5006	kg/m^2 torrs	0.1451 psi 0.01 bars
energy flux	W/m^2	2.39×10^{-4}	$kg\text{-}cal/m^2s$	0.3171 Btu/ft^2hr
specific heat	kJ/kg·K	0.2389	$kg\text{-}cal/kg^oc$	0.2389 Btu/lbm^oF
latent heat	kJ/kg	0.2389	kg-cal/kg	0.4303 Btu/lbm